Relativistic Stellar Pulsations

Thesis by
Lee Samuel Finn

In Partial Fulfillment of the Requirements
for the Degree of
Doctor of Philosophy

California Institute of Technology
Pasadena, California

1987

(Submitted May 11, 1987)

ACKNOWLEDGEMENTS

There have been many people whose friendship or special efforts have made these last five years enjoyable ones. In fact, there have been so many that I could not hope to list them all; thus, while there will be many whose names do not appear in these acknowledgements, all should rest assured that they share the same special place in my heart.

As the first Director of the Banzai Numerical Observatory, it has been my pleasure to have had the able assistance of Chris Kochanek and John "Many Trips" Hawley. Each has made substantial efforts to relieve me of the burdens associated with maintaining our group's growing computing facilities, and for those efforts I am eternally grateful. With my departure, Chris will assume the Directorship of the Observatory much as I assumed it (reluctantly, and with a staff of zero); however, I know that he is equal to the challange.

The **T**heoretcial **A**strophysics **I**ncluding **R**elativity group (**TAPIR**) has been my home for the last five years, and it is hard to imagine a more friendly, open, and relaxed working environment. I give my warmest thanks to the faculty and staff of Tapir — Roger Blandford, Peter Goldreich, Sterl Phinney, Kip Thorne, and Pat Lyon — for their efforts toward maintaining such an atmosphere.

Especially over this last year, I have been fortunate to have been educated in the arcane and black art of scientific supercomputing by Chuck Evans and John Hawley. I could not have apprenticed myself to two finer sorcerers than John and Chuck.

I have been particularly fortunate to have cut my research teeth under the tutelage of Kip Thorne. As I try to think of all the things I have learned from watching him "do physics," and from his gentle efforts to guide my own research, I realize that I may never know the full extent of my debt to him.

For five years now, Saturday night has been Pizza night (Pizza being the generic term for any food substance consumed for Saturday dinner). I will always carry fond memories of that venerable institution and the small group of people who have formed its mainstay: Ted Allen, Gary Gutt, Jim Kaufman, and Chris Starr. Thanks, guys.

Others whose friendship has made the time pass so pleasurably are the Lura-Allen Crowd: James Theiler, Bette Korber, Chi-Bin Chien, Mark Muldoon, and Dave Wark; my friends from the days of JPL: Robyn & Jack Lutz, Jancis & Mike Martin, Debbie Hoshino and Rich Fagen; and also Eric & Lisa Grove, Dawn & Ted Meredith, Steve & Lynn Clark, John Hawley, Roger Romani, Chris Kochanek, Peter Quinn, Pat Lyon, and Donna Driscoll.

Above all, however, I must acknowledge the love, friendship, and support of two very special people: Richard and Luanne Ross. They have provided me with aid and comfort whose value is beyond measure, and it is with deepest love that I dedicate this thesis to them.

My tenure at Caltech has been supported by a Spaulding Fellowship (1982–1983), Teaching Assistantships provided by the Physics Department (1983–1985), Summer Research Assistantships provided by Kip Thorne (1984–1986), and Research Assistantships provided by Sterl Phinney (1985–1987). I gratefully acknowledge their support.

Abstract

This thesis consists of studies on the topic of relativistic stellar pulsations.

i) A new formalism for the numerical study of g-modes in neutron stars is developed. This formalism avoids pitfalls associated with previous formalisms when applied to the study of these low-frequency modes. The formalism involves a new choice of perturbation variables, the introduction of an "instantaneous gravity" approximation to the field outside the star, and an energy principle for determining gravitational radiation damping times. The formalism is used to study g-modes that arise because of chemical inhomogeneities in neutron star crusts. g-mode frequencies associated with chemical inhomogeneities are found to be much higher than those associated with finite temperature.

ii) The relativistic Cowling approximation, introduced by McDermott, Van Horn, & Scholl (1983) and analogous to the Newtonian Cowling approximation, is refined to make it more accurate in the regime of highly relativistic stars. The approximation is used to prove a host of useful theorems regarding the non-radial modes of relativistic stars.

iii) Realistic neutron stars have a solid crust, and this will seriously affect their g-modes. The first steps toward developing a theory of non-radial relativistic pulsations in stars with a solid crust is reported on here: the calculation of the shear strain and stress during a pulsation, the introduction of the shear stress into the Einstein field equations as a source and to the equations of motion as a force, and the development of a Lagrangian and variational principle for studying non-radial relativistic pulsations in stars with a solid crust.

iv) Solar five-minute oscillations are a weak source of gravitational radiation. The inner part of the solar system is actually in the transition zone of the solar oscillation gravitational field, and future space-based beam detectors might be able to measure the solar "transition-zone radiation." The transition-zone gravitational

field is explored for four relativistic gravity theories: a spin-zero theory (Nordstøm's theory), a spin-one theory (analogous to electromagnetism), a spin-two theory (general relativity), and a mixed spin-zero/spin-one theory (Jordan-Brans-Dicke theory). From the transition-zone gravitational field, it is possible to determine experimentally the spin content of relativistic gravity.

Table of Contents

Chapter 1

Introduction

This thesis is a theoretical investigation of stellar pulsations in the context of relativistic gravity. The topics addressed range from the pulsations of and gravitational radiation generation by "Newtonian" stars (stars where the Newtonian gravitational potential is everywhere small) in a small but important class of relativistic gravity theories (Chapter 6), to general features of the pulsational eigenmodes of relativistic stars in general relativity (Chapter 4), to detailed calculations of the low-frequency spectrum of neutron star models (Chapters 2 & 3). Chapter 5 of the thesis presents a Lagrangian and the resulting variational principle for the non-radial pulsations of relativistic stars with an isotropic shear modulus.

The introduction to this thesis begins with a brief HISTORICAL INTRODUCTION to the study of stellar pulsations, starting with the observational study and identification of pulsating variable stars, and concentrating in the end on the relationship of this thesis to other theoretical work in the field of relativistic stellar pulsations. A TECHNICAL INTRODUCTION then provides a brief review of the relevant theoretical underpinnings of the work presented here. Finally, the work presented in the remaining five chapters of the thesis is briefly discussed.

HISTORICAL INTRODUCTION

Pulsating stars are a sub-class of *intrinsic variable* stars, which are in turn a subclass of *variable* stars. A variable star is identified as one whose physical properties change on timescales less than or on the order of an astronomer's lifetime: *i.e.*, from milliseconds for pulsars to decades for long-term variables. The intrinsic variables are identified as those whose variability is due to internal properties of the star; thus the class of intrinsic variables excludes eclipsing binaries, or stars whose variability is due to the interaction of the star with the interstellar medium. Intrinsic variables are further divided into *eruptive* variables (*e.g.*, novae) and *pulsating* variables (*e.g.*, the Cepheids).

Variable stars play an important role in our modern understanding of the Universe: supernovae are the crucible in which the heavier elements are cooked; the *Cepheids,* in their role as the bottom rung of the cosmic distance ladder, help us to determine the age and size of the universe; and pulsars are the most stable long-term clocks available to us, have provided us with the first direct evidence for general relativistic gravitational radiation, and allow us to probe for cosmic gravitational radiation from the big bang.

For all of their importance, however, the serious observational study of pulsating variable stars began late in the history of astronomy; it was not until 1596 that the systematic study of pulsating variables began with the observations of *Mira Ceti;* and it was over 60 years before *Mira Ceti's* periodicity was firmly established (Ledoux & Walraven 1958).

Observation and classification of variable stars was initially very slow: In 1784, when the variability of δ *Cephei* was observed (the first example of the Cepheids), only 3 pulsating variables were known; and by 1844, only 10 pulsating variables had been identified. It was only after the work of Herschel and Argelander that the rate of discovery increased: by 1865, 113 pulsating variable stars had been identified (Ledoux & Walraven). As new technology (*e.g.,* differential photometry) and new science (*e.g.,* spectroscopy) were brought to bear on the problem of identification and classification of variables, the rate of discovery increased. Today, there are over 25 000 variable stars identified, and over 90% are pulsating variables (Cox 1980).

Variability has been observed in a wide range of stars; however, the single most important pulsating star, owing to both its proximity and accessibility, is the Sun. Solar pulsations were first observed by Leighton, Noyes, & Simon in 1960.

The classification of some variable stars as intrinsic, and the identification of some intrinsic variables as pulsating stars, did not occur until relatively recently. Initially, explanations of variability were purely geometrical (eclipses, precession of

ellipsoidal stars, or general recessional motion); it was not until 1878 that Ritter suggested the variability of some stars could be due to their free oscillations.

The *pulsational hypothesis* provides a simple relationship between the fundamental pulsational period and the mean density of the star; along with an independent determination of the mean density of the Cepheids, this period-density relationship was used by Shapley (1914) to argue for the pulsational hypothesis. Eddington (1918a,b) established the mathematical foundation and initiated the study of radial pulsations of stars.

The pulsational modes of a non-rotating gas star can be divided into two types: radial modes and non-radial modes. The radial modes are "breathing" modes of the star: the gas motion is purely radial. The non-radial modes (called non-radial only because they do not involve *exclusively* radial motion) encompass all of the other spheroidal pulsational modes, and may be further classified according to the spherical harmonic order of, *e.g.,* the pressure perturbation. In rotating stars, this simple classification is complicated first by Coriolis forces and second (in more rapidly rotating stars) by centrifugal forces. In the case of slowly rotating stars, however, it is possible to identify modes that would be radial if the star were non-rotating; these modes are referred to as the *quasi-radial* modes. Also, modes that would correspond to differential rotation in non-rotating stars have non-zero frequency in rotating stars (toroidal modes).

At first, the study of stellar pulsations concentrated on radial pulsations. Non-radial pulsations were studied, but the major theoretical effort was toward understanding the radial pulsations. It was not until the relatively recent (1960) discovery of solar oscillations that the major theoretical effort turned from the study of radial to non-radial pulsations. The reasons for this are two-fold: radial pulsation theory is more tractable than non-radial pulsation theory, and the variability in most stars seems to be due to radial pulsations. The Sun is a notable exception, in

that its radial and dipole modes have been particularly hard to detect, and this has stimulated work on non-radial pulsations.

At the same time that the discovery of solar oscillations was increasing the interest in non-radial stellar pulsations, the entire pulsation theory (both radial and non-radial) was being extended to encompass general relativity, thus enabling the treatment of stars where relativistic gravity plays an important role in the pulsations: white dwarfs, neutron stars, and supermassive stars.

The first step toward a relativistic theory of stellar pulsations was taken by Chandrasekhar (1964a,b) and Feynman (1964). They developed the theory of radial pulsations for relativistic stars in the framework of general relativity. Earlier work had established that a star of mass M under hydrostatic equilibrium cannot have a (Schwarzschild coordinate) radius R less than $2.25GM/c^2$ (here and henceforth, G is the Newtonian gravitational constant and c is the speed of light).[1] Chandrasekhar and Feynman showed that, owing to general relativistic effects, if the ratio of specific heats γ of the gas composing the star remains always finite, then the fundamental radial pulsational mode becomes dynamically unstable well before the mass contracts to this limiting radius: such a star perturbed from equilibrium will not pulsate, but will collapse at an exponential rate.[2] The closer γ is to 4/3, the larger the radius and the smaller the mass where the instability sets in. Since both white dwarf and neutron stars are predominantly composed of highly degenerate matter with a γ close to 4/3, the presence of this instability plays an important role in determining the maximum mass and radius of white dwarfs and neutron stars.

[1] This is the minimum radius for polytropic stars in the limit of incompressibility.

[2] The instability of the fundamental radial mode was first shown by Zel'dovich using a static analysis of the stability of a star; Chandrasekhar's action principle provided a dynamical analysis of the radial mode instability.

(The definitive analysis of the radial instability in ultrarelativistic stars was due to Ipser 1970).

The next steps toward the development of the theory of relativistic stellar pulsations were taken in the late 60s through the mid 70s by Thorne, Campolattaro, Price, Ipser, and Detweiler (Thorne & Campolattaro 1967; Price & Thorne 1969; Thorne 1969a,b; Campolattaro & Thorne 1970; Ipser & Thorne 1973; Detweiler & Ipser 1973; Detweiler 1975a,b). A general perturbation theory for the non-radial modes of non-rotating, perfect fluid relativistic spheres was developed, the gravitational radiation emitted by the pulsations was analyzed, and variational principles were developed to study the eigenfrequencies and stability of the modes. Additionally, the theory was used to explore numerically a small part of the non-radial pulsation spectrum of model neutron stars. (The non-radial pulsational spectrum is discussed in the TECHNICAL INTRODUCTION below). At the same time, the theory of radial pulsations of relativistic stars was extended to encompass the *quasi-radial* modes of slowly rotating stars (Hartle & Thorne 1969; Hartle, Thorne, & Chitre 1972).

The development of a relativistic theory of non-radial pulsations began within three years of the work on relativistic radial pulsations. It is interesting to note that the discovery of pulsars and their identification as neutron stars in the fall of 1967 occurred simultaneously and independently of the first published paper on non-radial pulsations of relativistic stars (Thorne & Campolattaro 1967). Interesting, perhaps, but not surprising: the observational discovery of neutron stars did not occur in a theoretical vacuum. Detailed hydrodynamical models were suggesting that a supernova could leave behind a neutron star remanent, neutron stars were being considered as sources of galactic X-rays, and supermassive stars were under investigation in connection with quasars (Thorne & Campolattaro).

However strongly astrophysical considerations might have motivated the development of a theory of non-radial relativistic stellar pulsations, another important motivation of an entirely different sort was also present. Any (special) relativistic theory of gravity must predict gravitational radiation, and general relativity is no exception. After much controversy and numerous false starts, the physical reality of general relativistic gravitational radiation was conclusively demonstrated (theoretically) by Bondi in 1957; however, no self-consistent calculations of the emission of gravitational radiation from a source with significant self-gravity had ever been made. The development of a theory of non-radial relativistic stellar pulsations filled this gap by providing the first rigorous calculation of emission of gravitational radiation from a strong field source. The radial theory of relativistic pulsations could not serve this purpose: since general relativity is a spin-two theory (*i.e.*, in linearized general relativity, gravity can be expressed as being due to the action of a spin-two field), only the quadrupole and higher order non-radial modes can radiate gravitationally in the limit of perturbation theory.

By 1976, observations of some pulsars had uncovered quasi-periodic micropulsations in the structure of the subpulses (Boriakoff 1976; Cordes & Hankins 1977). The millisecond timescales associated with these micropulsations are coincident with the timescales of neutron star pulsations, and this led Boriakoff to suggest that the phenomena could be related. Van Horn (1980) reiterated Boriakoff's suggestion and noted that additionally, owing to its solid crust, a neutron star would support toroidal mode oscillations with frequencies that could be related to the drifting sub-pulses observed in pulsars. In 1982, Van Horn, McDermott, & Carroll pointed toward the "ringing" phenomena observed in the flux of some X-ray burst sources, which are associated with accretion directly onto the surface of a neutron star in a close binary, as being possibly related to low-frequency pulsations of neutron stars.

As a consequence of all this activity, Glass & Lindblom (1983), and Lindblom & Detweiler (1983) published the first comprehensive survey of the fundamental radial and non-radial pulsational modes of neutron star models, examining some 13 equations of state over a wide range of central densities, and Schumaker & Thorne (1983) developed the theory of torsional oscillations of relativistic stars.

At the same time, McDermott, Van Horn, & Scholl (1983) completed an investigation into the effects of the temperature structure of realistic neutron star models on the low-frequency non-radial (g-mode) pulsation spectrum. The radially varying non-zero temperature structure of a neutron star leads to a spectrum of low-frequency non-radial modes (g-modes). Previous analyses of neutron star pulsations had concentrated on the case of zero temperature stars.

The numerical study of g-modes is fraught with difficulties (*cf.* Chapter 2), all related ultimately to the low-frequency character of the modes. In order to make their numerical study more tractable, McDermott, Van Horn, & Scholl introduced an approximation to the full theory of non-radial stellar pulsations (Thorne & Campolattaro), which permitted them to calculate the highest frequency g-modes due to the finite temperature structure of model neutron stars. Their approximation, termed the *relativistic Cowling approximation* [because it is a relativistic generalization of the Newtonian Cowling approximation (Cowling 1941)], is equivalent to the neglect of all the gravitational perturbations in the formalism of Thorne & Campolattaro.

In 1986, Finn (Chapter 2 of this thesis) reformulated the non-radial pulsations theory for relativistic stars to make advantageous use of the low-frequency character of g-modes. The resulting *slow-motion formalism* enabled him to compute the g-mode spectrum of relativistic stars without the neglect of the gravitational perturbations. Finn (1987a and Chapter 3 of this thesis) used the slow-motion

formalism to compute for zero temperature model neutron stars the influence of chemical homogeneities on the g-mode spectrum.

The Cowling approximation (Cowling 1941), upon which the relativistic Cowling approximation introduced by McDermott *et al.* is based, is a landmark work in the theory of non-radial Newtonian pulsations. Within the context of the approximation (which is simply the neglect of the perturbation to the Newtonian gravitational potential), it is possible to show rigorously that *i)* the non-radial pulsational modes form a nearly Sturm-Liouville system and, using the Sturm comparison theorem, to *ii)* classify the non-radial pulsational modes, *iii)* provide necessary and sufficient conditions for the stability of the modes, and *iv)* prove a remarkable number of powerful node theorems regarding the ordering of the mode eigenfrequencies and the number of nodes in the corresponding eigenfunctions. Finn (1987b and Chapter 4 of this thesis) has modified the relativistic Cowling approximation of McDermott *et al.* to more accurately describe the pulsations of very relativistic stars, and has used the approximation to show that the same set of theorems that were previously available only for Newtonian pulsations hold also for relativistic pulsations.

The presence of a solid crust in a neutron star not only introduces torsional modes (Schumaker & Thorne 1983), but also is expected to modify significantly the g-mode spectrum: the delicate balance of the gravitational and compressional-pressure forces in these pulsations makes the much smaller shear-modulus forces significant. Finn (Chapter 5 of this thesis) has taken the first steps toward extending the formalism for non-radial relativistic stellar pulsations to encompass relativistic stars with a crust by deriving the Lagrangian that describes the pulsations and providing a variational principle that can be used to calculate the pulsational eigenmodes of model neutron stars with a crust.

TECHNICAL INTRODUCTION

The bulk of this thesis (Chapters 2–5) deals with the general relativistic theory of stellar pulsations, originally formulated by Thorne & Campolattaro (1967). That theory is a first-order perturbation theory of the matter and gravitational (metric) field of a non-rotating, spherically symmetric, perfect fluid sphere. The perturbation theory is an extension of the Regge-Wheeler (Regge & Wheeler 1957) perturbation theory of the Schwarzschild black-hole solution for a spherically symmetric space-time without matter. This TECHNICAL INTRODUCTION provides a brief introduction to *i)* the perturbation theory of the matter and space-time containing a spherically symmetric perfect fluid sphere, and *ii)* the spectrum of non-radial pulsations of non-rotating stars.

In general relativity, gravitation is a property of the distances between points in space-time, and the natural state of motion of a particle moving between two points under only gravitational forces is that which minimizes the space-time (or *proper*) distance traveled. The *field* that describes gravitation is thus the *metric*, $\mathbf{g}$, which is just a differential measure of the distance between points. The source of the gravitational field in the Einstein field equations is the stress-energy tensor of the matter fields present. Gravitational perturbations are thus equivalently thought of as metric perturbations, and the perturbed gravitational field is just the metric perturbation. The source of the metric perturbation is the perturbation of the stress-energy tensor.

For a perfect fluid, the stress-energy tensor $\mathbf{T}$ takes on a particularly simple form:

$$\mathbf{T} = (\rho + p)\mathbf{U} \otimes \mathbf{U} - p\mathbf{g}, \tag{2.1}$$

where ρ is the energy density (including rest mass), p is the (isotropic) pressure, and $\mathbf{U}$ is the 4-momentum of the fluid. (Here and henceforth, units where $G = c = 1$

are used.) To complete the description of the unperturbed background solution upon which the Thorne-Campolattaro formalism is based, the metric describing a space-time containing a static, spherically symmetric star, is given by

$$\mathbf{g} = \exp(\nu)\mathbf{d}t^2 - \exp(\lambda)\mathbf{d}r^2 - r^2(\mathbf{d}\theta^2 + \sin^2\theta\,\mathbf{d}\phi^2), \tag{2.2}$$

where ν and λ are functions strictly of r and are given by

$$\begin{aligned} \frac{d\nu}{dr} &= 2\frac{m + 4\pi r^3 p}{r(r-2m)}, \\ \exp[\lambda(r)] &= [1 - 2m(r)/r]^{-1}, \\ m(r) &= \int_0^r dr\, 4\pi r^2 \rho \end{aligned} \tag{2.3}$$

(*cf.* Chapter 23 of Misner, Thorne, & Wheeler 1973). The differential equation for the potential ν is integrated subject to the boundary condition $\lim_{r\to\infty}\nu = 0$. For a spherically symmetric space-time, $m(r)$ can be interpreted as the mass within the coordinate radius r, and in the limit of weak fields ν is twice the Newtonian gravitational potential.

The most general metric perturbation, being a symmetric tensor in four dimension, has ten components, while the most general fluid perturbation has three components (a spatial displacement vector). Since we are interested in only first order perturbations of the spherically symmetric equilibrium background, the angular dependence of the perturbations can be resolved into spherical harmonic angular dependence, and the perturbations of each spherical harmonic order and type can be treated separately. The non-radial perturbations of a star have *even-parity:* under a spatial-coordinate inversion, the sign of the perturbations behaves as $(-1)^l$. This symmetry reduces the number of metric tensor and displacement vector components that are involved in the perturbation: only two independent components of the displacement vector and seven components of the metric tensor have this symmetry.

The metric plays a dual role in general relativity: it not only expresses the effects of gravitation, it also describes the relationship between the coordinates and distance. This relationship permits us to choose our 4 space-time coordinates to eliminate 4 of the 10 components of the general metric perturbation in the same way that we choose a gauge to eliminate a single component of the electromagnetic potential **A**.

The generator of a *coordinate gauge transformation* is a 4-vector. A general 4-vector has only three components with the $(-1)^l$ spatial coordinate inversion symmetry of a non-radial pulsation mode; consequently, only three gauge freedoms can be exploited in simplifying the metric perturbation. Regge & Wheeler (1957) chose to simplify the metric perturbation by using the coordinate gauge freedom to eliminate those three metric perturbations that behave as vectors and tensors on the sphere, and their choice has endured to this day in the theory of relativistic stellar pulsations. The final, simplified form of the perturbed metric used throughout the remainder of this thesis has the Regge-Wheeler form

$$\begin{aligned}\mathbf{g} = &\exp(\nu)(1 + H_0 Y_{lm})\mathbf{dt}^2 + \frac{dH_1}{dt} Y_{lm}(\mathbf{dt}\,\mathbf{dr} + \mathbf{dr}\,\mathbf{dt}) \\ &- \exp(\lambda)(1 - H_2 Y_{lm})\mathbf{dr}^2 - r^2(1 - K Y_{lm})(\mathbf{d\theta}^2 + \sin^2\theta\,\mathbf{d\phi}^2).\end{aligned} \tag{2.4}$$

The $(7 - 3 = 4)$ perturbation variables H_0, H_1, H_2, and K are all functions of only r and t. In the absence of anisotropic stresses, the Einstein field equations show the two metric perturbations H_0 and H_2 to be equal; accordingly, with the exception of Chapter 5, where the perturbation theory of relativistic stars with a non-zero shear modulus is discussed, we always make the substitution of H_0 for H_2.

The fluid perturbation in the Thorne-Campolattaro formalism is described by the fluid spatial-displacement vector $\vec{\xi}$; for ease of computation, the two independent components of $\vec{\xi}$ (recall the spherical harmonic symmetry of the non-radial modes)

are denoted W and V:

$$\begin{aligned} \xi^r &= \exp(-\lambda/2) W Y_{lm}/r^2, \\ \xi_\theta &= V \partial_\theta Y_{lm}, \\ \xi_\phi &= V \partial_\phi Y_{lm}. \end{aligned} \tag{2.5}$$

Like the metric perturbations, W and V are functions of only r and t.

The perturbed continuity equation together with the equation of state determines the perturbations in the energy density $\delta\rho$ and the pressure δp in terms of the metric and fluid perturbations, thus defining the source term (the perturbed stress-energy tensor) of the Einstein field equations for the metric perturbation in terms of the perturbation variables discussed above. Together with the boundary conditions, which are discussed in Chapter 2, this completes the general technical description of the Thorne-Campolattaro formalism.

Non-radial stellar pulsations can be classified into three groups, both mathematically and physically. At a given spherical harmonic order l ($l \geq 1$), ignoring the degeneracy in m, there is a single *fundamental mode,* or f-mode. In the limit of a constant density incompressible star, the f-mode is a (fluid dynamical) gravity wave on the surface of the star. The f-mode is also known as the *Kelvin mode,* because it is the only mode present in the pulsation of homogeneous incompressible fluid spheres studied by Kelvin.

While the f-mode in an incompressible star has many aspects of a surface gravity wave, Eulerian pressure perturbations (pressure perturbations at fixed r, θ, ϕ) play a significant role in determining the restoring force acting on a perturbed fluid element. In a compressible fluid star, there is an infinite spectrum of modes with higher frequency than the f-modes. In these modes the predominant restoring force is due to the Eulerian pressure perturbation; thus the modes are known as *pressure modes,* or p-modes. These modes are acoustic vibrations of the star, with small,

predominantly radial fluid motions and large Eulerian pressure perturbations. As long as the star is compressible, the p-modes are always present, and when they are present they are always stable. The initial investigations of non-radial modes of relativistic stars (*e.g.,* Thorne 1969a) concentrated on f-modes and low-order p-modes.

At lower frequencies than the f-mode there are also stable modes; however, in these modes it is not the Eulerian pressure perturbation that supplies the dominant restoring force, but rather the unperturbed gravitational field of the star acting on the Eulerian density perturbations. These modes are known as *gravity modes,* or g-modes. In a g-mode, a perturbed fluid element is nearly in pressure equilibrium with its surroundings, and so the only restoring force present is due to the gravitational force acting on the density perturbations. For this reason, the g-mode spectrum is very sensitive to the gradient of specific entropy in the star, because the specific entropy controls (in part) the relationship between pressure equilibrium and density equality. For an adiabatic pulsation, if the specific entropy gradient is positive on any radial shell of the star, then it will contain an infinite number of stable g-modes, all with frequencies lower than the f-mode frequency. If the specific entropy gradient vanishes on any radial shell, then it will contain an infinite spectrum of neutrally stable (or zero-frequency) g-modes. Finally, if the specific entropy gradient is negative on any spherical shell of the star, then it will contain an infinite spectrum of imaginary frequency modes, corresponding to convective instability. McDermott *et al.* (1983) made the first study of non-zero frequency g-modes in relativistic stars.

The specific entropy is not the entire story; in neutron stars, it is not even the most important story. In an inhomogeneous neutron star, variations in the chemical composition also play a role in determining the relationship between pressure equilibrium and density equality. In a neutron star the chemical composition changes

discontinuously in the crust, and for each discontinuity in the composition there may be a *single* g-mode (or *discontinuity mode*) that can be associated with each discontinuity, and that mode may be stable or unstable depending on whether or not the density of the fluid increases inward across the appropriate discontinuity. [The difficulty in associating a stable (or unstable) mode with a discontinuity in the density arises when there is an infinite spectrum of stable (or unstable) modes due to the presence of a specific entropy gradient.] Finn (1987a, and Chapter 3 below) provided the first study of discontinuity g-modes in relativistic stars.

Introduction to the Remaining Chapters

Chapter 2 puts the Thorne-Campolattaro theory of relativistic stellar pulsations into a new form intended to permit an accurate numerical treatment of g-mode pulsations. As mentioned previously, the low-frequency character of the g-modes causes problems when the Thorne-Campolattaro formalism is used to numerically compute the eigenmodes. The difficulties are essentially of three kinds: *i)* the perturbation variables H_0 and K become degenerate within the star in the low-frequency limit, and the small difference between them plays an important role. *ii)* The Eulerian pressure perturbation becomes vanishingly small in a g-mode pulsation and this puts constraints on the expansion of a fluid element during a pulsation. This constraint fixes the angular displacement of a fluid element in relation to the radial displacement. *iii)* The gravitational field of a relativistic star undergoing free oscillations must satisfy the Sommerfeld condition of outgoing gravitational radiation at infinity. In a numerical calculation, this condition becomes one of outgoing gravitational radiation in the wave zone, which is at a distance of roughly three or more wavelengths. As the frequency becomes small, which is the case for g-modes, the wave zone recedes farther and farther from the star, making it more and more difficult to impose the outgoing-wave boundary condition. By making use of a new

set of perturbation variables, a slow-motion approximation to the gravitational field near the relativistic star, and a conserved energy (obtained from a variational principle) for the pulsations, these difficulties are overcome and it becomes possible to compute the g-modes of relativistic stars with high accuracy.

In Chapter 3, the slow-motion formalism developed in Chapter 2 is extended and applied to the study of discontinuity modes in zero-temperature neutron stars. In a truly zero-temperature neutron star the specific entropy vanishes and the finite frequency of the g-mode pulsations are due entirely to changes in chemical composition; so, approximating a neutron star as being at zero temperature allows one to study unambiguously the character of the discontinuity eigenfunctions and frequencies. Two results of this investigation of discontinuity modes are worthy of particular note: one is the very close relationship between the discontinuity modes in a neutron star and the internal gravity waves in a discontinuously stratified incompressible fluid, leading to very simple yet very accurate formulae for the frequency and energy in the pulsations. The other is the relatively high frequency of the pulsations compared to the frequencies of the finite-temperature g-modes studied by McDermott *et al.* (1983). Consequently, in neutron stars it may be the case that the highest frequency g-modes (the ones most likely to be observationally important) are due to the discontinuities in the equation of state, not to the effects of finite temperature.

As discussed above, the Newtonian Cowling approximation permits the proof of a wide range of theorems regarding Newtonian stellar pulsations. Chapter 4 of this thesis refines the relativistic Cowling approximation of McDermott *et al.* and uses it to show that many of the same theorems that hold for Newtonian stellar pulsations hold also for pulsations of relativistic stars. Previous to the work presented in this chapter, the presence of such theorems for relativistic pulsations had been conjectured, but never proved.

At densities ranging from 10^6 g cm^{-3} to nuclear density, neutron star crusts are solid and have a non-zero shear modulus. This shear modulus allows the crust to support non-zero frequency torsional oscillations, and the theory of torsional oscillations has been developed by Schumaker & Thorne (1983). The presence of a shear modulus also modifies the character of the non-radial pulsational g-modes; Chapter 5 reports briefly on work-in-progress toward extending the theory of non-radial relativistic stellar pulsations to encompass stars that have a solid crust. The shear stress tensor (which is the new source term introduced into the Einstein field equations by the solid crust) is presented, and the Lagrangian that governs the pulsations is derived. From the Lagrangian is derived a variational principle that may be used to find the eigenmodes of the pulsations.

Chapter 6 of the thesis examines a different type of problem related to relativistic stellar pulsations: that of the gravitational field of a non-radially pulsating Newtonian star (the Sun) in relativistic gravity theories. With the exception of the Hulse-Taylor binary pulsar, tests of general relativity are confined to motion in a non-dynamical gravitational field. In order to observe directly the character of dynamical gravity, it is necessary to be far enough away from a source of gravitational radiation that the near-zone field has begun evolving into the wave-zone field. Solar p-mode oscillations with five minute periods are a source of gravitational radiation for which the Earth is in the transition zone where the near-zone gravitational field has begun evolving into the radiation-zone field. In Chapter 6 (Finn 1985), the transition-zone field is examined, and it is shown that it would be possible in principle, though difficult in practice, to determine the spin of the dynamical gravitational field from measurements made by space-based interferometers. This work complements the work of Eardley, Lee, & Lightman (1973), which examines the classification of relativistic gravity theories based on the radiation-zone field, and also

the work of Johnson *et al.* (1980), which examines the near-zone time-dependent Newtonian gravitational field of the Sun owing to solar oscillations.

REFERENCES

Bondi, H. 1957. *Nature,* **179**, 1072.

Boriakoff, V. 1976. *Astrophys. J. (Letters)* , **208**, L43.

Campolattaro, A., & Thorne, K.S. 1970. *Astrophys. J.,* **159**, 847.

Chandrasekhar, S. 1964a. *Phys. Rev. Letters,* **12**, 114.

Chandrasekhar, S. 1964b. *Astrophys. J.,* **140**, 417.

Cordes, J., & Hankins, T.H. 1977. *Astrophys. J.,* **218**, 484.

Cowling, T.G. 1941. *Mon. Not. R. astr. Soc.,* **101**, 367.

Cox, J.P. 1980. **Theory of Stellar Pulsation,** Princeton University Press, Princeton (New Jersey).

Detweiler, S.L., & Ipser, J.R. 1973. *Astrophys. J.,* **185**, 685.

Detweiler, S.L. 1975a. *Astrophys. J.,* **197**, 203.

Detweiler, S.L. 1975b. *Astrophys. J.,* **201**, 440.

Douglass, D.H. 1979. **A Close-Up of the Sun,** JPL Publication 78-70, Pasadena.

Eardley, D.M., Lee, D.L., & Lightman, A.P. 1973. *Phys. Rev.* D, **8**, 3308.

Eddington, A.S. 1918a. *Mon. Not. R. astr. Soc.,* **79**, 2.

Eddington, A.S. 1918b. *Mon. Not. R. astr. Soc.,* **79**, 177.

Feynman, R.P. 1964. Unpublished work, quoted and relied upon by Fowler & Hoyle 1964.

Finn, L.S. 1985. *Class. Quantum Grav.,* **2**, 381.

Finn, L.S. 1986. *Mon. Not. R. astr. Soc.,* **222**, 393.

Finn, L.S. 1987a. *Mon. Not. R. astr. Soc., in press.*

Finn, L.S. 1987b. Submitted to *Mon. Not. R. astr. Soc.*

Fowler, W. A., & Hoyle, F. 1964. *Astrophys. J. Suppl.,* **91**, 201.

Glass, E. N., & Lindblom, L. 1983. *Astrophys. J. Suppl.,* **53**, 93.

Hartle, J. B., & Thorne, K. S., 1969. *Astrophys. J.,* **158**, 719.

Hartle, J. B., Thorne, K. S., & Chitre, S. M. 1972. *Astrophys. J.,* **176**, 177.

Ipser, J. R. 1970. *Astrophys. Space Sci.,* **7**, 361.

Ipser, J. R., & Thorne, K. S. 1973. *Astrophys. J.,* **181**, 181.

Jackson, J. D. 1975. **Classical Electrodynamics,** John Wiley & Sons, New York.

Johnson, W. W., Winget, D. E., Douglass, D. H., & Van Horn, H. M 1980. **Nonradial and Nonlinear Stellar Pulsations, Tucson 1979,** ed. Hill, H. A., Springer-Verlag, Berlin, pp. 220–36.

Ledoux, P. & Walraven, Th. 1958. **Handbuch der Physik, 51,** ed. Flügge, S., Springer-Verlag, Berlin.

Leighton, R. B., Noyes, R. W., & Simon, G. W. 1960. *Astrophys. J.,* **135**, 474.

Lindblom, L., & Detweiler, S. L., 1983. *Astrophys. J. Suppl.,* **53**, 73.

McDermott, P. N., Van Horn, H. M., & Scholl, J. F. 1983. *Astrophys. J.,* **268**, 837.

Misner, C. A., Thorne, K. S., Wheeler, J. A. 1973. **Gravitation,** Freeman, San Francisco.

Price, R., & Thorne, K. S. 1969. *Astrophys. J.,* **155**, 163.

Regge, T. & Wheeler, J. A. 1957. *Phys. Rev.,* **108**, 1063.

Ritter, A. 1878. *Wiedemanns Ann.,* **5.**

Schumaker, B. L., & Thorne, K. S., 1983. *Mon. Not. R. astr. Soc.,* **203**, 457.

Shapley, H. 1914. *Astrophys. J.,* **40**, 448.

Thorne, K. S. 1969a. *Astrophys. J.,* **158**, 1.

Thorne, K. S. 1969b. *Astrophys. J.,* **158**, 997.

Thorne, K. S., & Campolattaro, A.,

Van Horn, H. M. 1980. *Astrophys. J.,* **236**, 899. 1967. *Astrophys. J.,* **149**, 591.

Van Horn, H. M., McDermott, P. N., & Carroll, B. W., 1982. *University of Rochester preprint.*

Chapter 2

G-Modes of Non-Radially Pulsating Stars: The Slow-Motion Formalism

Originally appeared in *Monthly Notices of the Royal Astronomical Society,* **222**, 393–416 (1986).

Abstract

A new formalism, designed explicitly for the numerical study of g-modes of non-rotating, perfect-fluid, relativistic stars, is presented. The formalism is based on the analysis of Thorne & Campolattaro (1967), but with: (*i*) a choice of perturbation variables more suited to the numerical analysis of the low-frequency g-mode pulsations, (*ii*) the introduction of an instantaneous-gravity approximation that replaces the boundary condition of outgoing gravitational radiation at infinity by a non-radiative, Newtonian-like boundary condition, and (*iii*) an energy principle for determining the damping time of a mode due to gravitational radiation. The new formalism is applied to the study of g-mode pulsations of neutron star models with a polytropic equation of state.

1. Introduction

1.1. MOTIVATION

The general relativistic theory of nonradial pulsations of perfect fluid stars was developed in the late 1960s by Thorne, Campolattaro, Price, & Ipser (see Ipser & Thorne 1973 for a complete set of references). Subsequently, in the 1970s and 80s, this formalism was refined and improved by Ipser, Detweiler, and Lindblom (see Detweiler & Lindblom 1983 for a complete set of references). This by-now standard formalism has found fairly extensive applications in numerical studies of f-modes and p-modes of neutron stars.

In 1980, Van Horn called attention to the possibility that low-frequency modes of neutron stars — g-modes and torsional modes — might be observable in radio pulsar and X-ray burster data. Unfortunately, the standard version of the formalism is not able to handle either g-modes (because of low-frequency effects that cause numerical problems) nor torsional modes (because the formalism assumes vanishing shear modulus). In response to Van Horn, Schumaker & Thorne (1983) have developed a variant of the formalism valid for torsional modes; and McDermott, Van Horn, & Scholl (1983) have developed a variant (the "relativistic Cowling approximation") usable for g-modes.

The standard formalism faces two severe numerical difficulties in numerical studies of low-frequency g-modes. First, there are delicate numerical cancellations in the low-frequency limit that lead to

numerical error. Second, the outgoing-wave boundary condition at infinity becomes very difficult to implement numerically when the reduced wavelength $\lambda\!\!\!^{-}\equiv 2\pi c/\omega$ of the waves becomes large.

The relativistic Cowling approximation avoids some of the difficulties of the standard formalism by setting precisely to zero all Eulerian perturbations of the gravitational field (metric). The purpose of this paper is to develop an alternative variant for g-modes, a "slow-motion formalism," which has higher accuracy than the relativistic Cowling approximation. The slow-motion formalism achieves its higher accuracy by retaining all gravitational perturbations.

In the slow-motion formalism, the delicate numerical cancellations in the low-frequency limit are removed by several changes of perturbation variables; and the difficulties involved in applying the out-going wave boundary condition are circumvented by means of an "instantaneous gravity approximation," which gets rid of the dynamical degrees of freedom in the external gravitational field and permits a simple boundary condition to be imposed at the star's surface. The resulting slow-motion formalism makes fractional errors of order $(\mathcal{R}/\lambda\!\!\!^{-})^2$, where $\lambda\!\!\!^{-}$ is the reduced wavelength of the gravitational radiation, and $\mathcal{R}$ is the radius of the star.

Like the relativistic Cowling approximation, however, the slow-motion formalism presumes vanishing shear modulus and so cannot be used to study either torsional mode oscillations or the effects of a solid crust on compressional modes. In a future paper I hope to generalize the slow-motion formalism to include a non-zero shear modulus.

The remainder of §1 establishes the notations and conventions that will be used throughout this work. In §2 the standard formalism for studying relativistic stellar pulsations is reviewed and the difficulties that motivate the slow-motion formalism are discussed. The slow-motion formalism is presented in §3, and in §4 it is applied to find g-modes of zero-temperature relativistic polytropes. The conclusions are presented in §5. Appendix A describes the numerical techniques used to determine the quasinormal mode eigenfrequencies and eigenfunctions in the slow motion formalism, and Appendix B describes the derivation of the key equations of the slow motion formalism.

1.2. NOTATION

This paper relies heavily on the work of Thorne & Campolattaro (1967), cited henceforth as Paper I. Equations from Paper I are referred to by their equation number from Paper I and prefixed by I; *e.g.*, equation (7b) of Paper I is referenced as equation (I,7b). Except when explicitly noted otherwise, the notation and conventions of Paper I are used throughout this work. In particular, geometrised units are used ($G = c = 1$, *cf.* box 1.8 of Misner, Thorne, & Wheeler 1973) and the metric signature is $(+---)$. Primes are used to denote radial derivatives and commas to denote partial derivatives:

$$F' \equiv \frac{dF}{dr} \ , \ F_{,t} \equiv \frac{\partial F}{\partial t} \ .$$

2. The Thorne-Campolattaro Formalism

2.1. THE STATIC BACKGROUND

The goal of this analysis of stellar pulsations is the determination of the (complex) eigenfrequencies and eigenfunctions that characterize the free oscillations of a star. The analysis begins from an exact solution of the Einstein Field Equations (EFE) corresponding to a static, spherically symmetric, perfect fluid sphere. The line element of that solution is

$$ds^2 = e^{\nu(r)}dt^2 - e^{\lambda(r)}dr^2 - r^2(d\theta^2 + \sin^2\theta\, d\phi^2). \tag{1}$$

The exact solution is characterized by two functions, $\nu(r)$ and $\lambda(r)$. In terms of the pressure, p, and the energy density, ρ, these functions are given by

$$\frac{d\nu}{dr} = 2\frac{m+4\pi r^3 p}{r(r-2m)}, \tag{2a}$$

$$e^{-\lambda} = 1-2m/r, \tag{2b}$$

$$\frac{dm}{dr} = 4\pi r^2 \rho, \tag{2c}$$

$$\frac{dp}{dr} = -\frac{\rho+p}{2}\frac{d\nu}{dr}. \tag{2d}$$

The pressure and the energy density are related through the equation of state. The normalization of ν is chosen so that $\nu = -\lambda$ in the region outside the star. Regularity of the metric requires that $m(0)=0$. The

function $m(r)$ is interpreted as the gravitational mass inside a radius r.

2.2. THE EIGENVALUE PROBLEM

Paper I (Thorne & Campolattaro 1967) considers first-order perturbations, with spherical harmonic order $l \geq 2$, of the fluid and spacetime geometry about the exact solution (eqs. [1], [2]) for a perfect fluid star. The perturbation of the EFE is carried out in Regge-Wheeler gauge (Regge & Wheeler 1957). Only the even parity perturbations are considered: odd parity perturbations correspond to differential rotation of the perfect fluid and not to pulsations.

In a realistic neutron star, there is a crystalline crust with non-zero shear modulus. The shear modulus will contribute to the restoring force for the even parity, compressional pulsations. In addition, the non-zero shear modulus permits the star to support odd-parity torsional oscillations. Schumaker & Thorne (1983) have developed a formalism for studying these shear-modulus-supported torsional modes. In a later work, I will extend the analysis of compressional modes presented here to include the effects of a non-zero shear modulus.

In the standard formalism developed by Thorne & Campolattaro (1967), there are two fluid degrees of freedom, described by the perturbation variables W and V. Restricting attention to the single spherical harmonic order l and azimuthal order m, W and V are related to the displacement ξ of a fluid element from its equilibrium position:

$$W \equiv r^2 e^{\lambda/2} \xi^r / Y_{lm}(\theta,\phi) , \tag{3a}$$

$$V \equiv -r^2 \xi^\theta / \partial_\theta Y_{\ell m}(\theta,\phi)$$

$$= -r^2 \xi^\phi / \sin^2\theta \, \partial_\phi Y_{\ell m}(\theta,\phi) \, , \qquad (3b)$$

where $\partial_\theta \equiv \partial/\partial\theta$, $\partial_\phi \equiv \partial/\partial\phi$, and $Y_{\ell m}(\theta,\phi)$ is the scalar spherical harmonic. (Here and henceforth assume that the real part of all complex expressions is taken).

There are also two gravitational degrees of freedom. These are described by the perturbation variables K and H_0. When specialized to multipole order ℓm, the perturbed line element is

$$ds^2 = e^\nu (1 + H_0 Y_{\ell m}) dt^2 + 2 H_{1,t} Y_{\ell m} dt \, dr$$

$$- e^\lambda (1 - H_0 Y_{\ell m}) dr^2 - r^2 (1 - K Y_{\ell m})(d\theta^2 + \sin^2\theta \, d\phi^2). \qquad (4)$$

The H_1 defined in this paper differs from the H_1 of paper I by a time derivative (*cf.* [I,7b]; Detweiler & Ipser 1973 eq. [6]). It is algebraically related to the variables K, H_0, and W. The K, H_0, W, and V given here also differ slightly from their Paper I definitions: in Paper I the spherical harmonic dependence was specialized to $m = 0$ and Legendre polynomials were used to characterize the angular dependence of ξ^r and ξ^θ. This restriction is unnecessary; spherical harmonic angular dependence, with no specialization, is used here.

The perturbed EFE (eq. [I,8a-d], [I,9a-c]) may be combined to form a coupled set of four first-order ordinary differential equations for K, H_0, W, and V. To complete the specification of the eigenvalue problem for quasi-normal modes, boundary conditions are specified at three places:

at $r = 0$, regularity requires $K = H_0 = W = V = 0$; at $r=\mathcal{R}$ ($\mathcal{R}$ the coordinate radius of the unperturbed star) the Lagrangian pressure perturbation vanishes; and at infinity the gravitational radiation is strictly outgoing. The boundary condition at $r=0$ is required to keep the physical perturbations regular. The boundary condition at $r=\mathcal{R}$ corresponds physically to the definition of the stellar surface as the place where the pressure vanishes: vanishing of the Lagrangian pressure perturbation at $r=\mathcal{R}$ is equivalent to vanishing of the pressure at the surface of the *perturbed* star. Finally, the boundary condition at infinity is the insistence that the star's pulsations are not driven by gravitational waves, but instead are free. Subject to these boundary conditions, the perturbation equations have complex solutions only for discrete values of complex pulsation frequency ω, the "quasi-normal mode eigenfrequencies."

The numerical study of pulsational modes in the standard formalism was first undertaken by Thorne (1969). More recently, Lindblom & Detweiler (1983) have explored $l=2$ f-mode oscillations for a variety of model neutron stars using a modified version of Thorne's computational algorithm that produces a more accurate measure of the damping time of the pulsation (the imaginary part of the complex quasi-normal mode eigenfrequency). In either of these algorithms the quasi-normal mode eigenfrequencies, corresponding to strictly outgoing radiation at infinity and an undriven (free) oscillation of the star, are found by exploring the associated normal mode eigenfrequencies, corresponding to equal amounts of ingoing and

outgoing gravitational radiation at infinity (standing waves) and to resonantly driven oscillations of the star.

The connection between the normal and quasi-normal modes may be understood by analogy with a damped simple harmonic oscillator. Regard each quasi-normal mode of the star as a damped harmonic oscillator. The free (quasi-normal mode) pulsation of the star in a particular mode corresponds to the free oscillation of the corresponding damped oscillator. Associated with each quasi-normal mode is a normal mode, corresponding to the resonant frequency of the *driven* damped oscillator. For a damped harmonic oscillator, the frequency of the energy resonance is the real part of the quasi-normal mode frequency. The width of the energy resonance is related to the imaginary part of the quasi-normal mode eigenfrequency.

In Thorne (1969) the normal mode problem (standing waves at infinity) was solved numerically for various trial values of the real frequency ω. For each ω, the ratio of the star's pulsation energy to the energy in one wavelength of standing waves far from the star was computed. This energy ratio as a function of ω showed resonances: each resonant frequency was identified as a normal mode frequency, and also as the real part of a quasi-normal mode frequency. The imaginary part of the quasi-normal mode eigenfrequency was determined from the width of the resonance.

When integrating the perturbation equations, Lindblom & Detweiler (1983) also abandoned the outgoing-wave boundary condition in favor of a standing wave, resonant boundary condition. For each (real) trial

frequency the gravitational perturbations were integrated far into the wave zone. There the gravitational radiation was resolved into ingoing and outgoing waves (with equal amplitudes but different phases), and the (complex) amplitude of the ingoing wave was determined. When the real frequency approached a normal mode, the modulus of the amplitude of the ingoing radiation passed through a minimum and its phase changed rapidly. Lindblom & Detweiler (1983) found the complex quasi-normal mode eigenfrequencies by fitting the (complex) amplitude of the ingoing radiation at frequencies near a normal mode to a polynomial in frequency. The complex-frequency root of that polynomial fit was identified as the complex quasi-normal mode eigenfrequency.

In either case, the complex quasi-normal mode eigenfrequencies determined by Thorne (1969) or by Lindblom & Detweiler (1983) are the same as those that would be obtained by an integration with complex trial frequencies.

2.3. G-MODES IN THE STANDARD FORMALISM

The standard formalism is a complete treatment of linear perturbations of a perfect fluid star. As such, it is completely capable of treating p-, f-, and g-modes. In the regime of g-modes, however, there are difficulties with the numerical implementation of the analytic formalism. In this subsection, I will describe certain important features of the g-mode regime and will discuss how they complicate a *numerical* analysis of g-modes.

G-mode pulsations have long periods; the real part σ of the frequency of a g-mode is much smaller than the frequency of the fundamental mode:

$$\sigma^2 \ll \rho_c, \tag{5a}$$

ρ_c being the central density of the star. In particular, this implies

$$(\sigma\mathcal{R})^2 \ll \mathcal{M}/\mathcal{R} < 1, \tag{5b}$$

where $\mathcal{M}$ is the star's mass and $\mathcal{R}$ its radius. The imaginary part of a g-mode eigenfrequency is also small, much smaller than the real part of the eigenfrequency. One can estimate the amplitude damping time τ as the ratio of the energy in the star's pulsation to the power in the gravitational radiation; such an estimate gives

$$\frac{\sigma\tau}{2} \equiv (\text{Q of mode}) \sim (\mathcal{R}/\mathcal{M})(\sigma\mathcal{R})^{1-2l} \gg 1. \tag{6}$$

A fluid element in a g-mode pulsation remains very nearly in pressure equilibrium during the entire pulsation — the Eulerian pressure perturbation vanishes in the limit of a zero frequency g-mode. Consequently, a chemically homogeneous, isentropic star has only zero-frequency g-modes (in such a star, there is no distinction between pressure equilibrium and density equilibrium — a displaced fluid element is neutrally buoyant). McDermott, Van Horn, & Scholl (1983) have investigated, in the context of their "relativistic Cowling approximation," finite frequency g-modes of neutron star models that are presumed chemically homogeneous but not isentropic in the region

of significant g-mode amplitude. In a future paper, I will apply the slow-motion formalism to study finite frequency g-modes induced by chemical inhomogeneities.

Since g-mode frequencies are so small, one measure of the suitability of a numerical algorithm for studying them is its properties in the limit of low frequency $(\sigma\mathcal{R})^2 \ll \mathcal{M}/\mathcal{R}$. One way to investigate that limit is through the properties of g-modes in a star that has only zero-frequency g-modes.

For an isentropic, chemically homogeneous, perfect fluid star, Thorne (1969) has shown that all the g-modes lie at zero frequency and have a form dictated by the demand that the Eulerian pressure and density perturbations vanish:

$$\mathcal{W}(r) \equiv \begin{bmatrix}\text{arbitrary piecewise}\\ \text{differentiable function}\end{bmatrix}, \ \mathcal{W} \text{ vanishing at } r=0, \mathcal{R}, \tag{7a}$$

$$K = H_0 = 0 , \tag{7b}$$

$$W = \mathcal{W}(r)t , \tag{7c}$$

$$V = -\frac{e^{-\lambda/2}}{l(l+1)}\left(\frac{d\mathcal{W}}{dr}+\frac{dp/dr}{\gamma_0 p}\mathcal{W}\right)t . \tag{7d}$$

Note that V is determined by W and does not represent a truly independent degree of freedom of the fluid.

At non-zero frequencies, W represents one fluid degree of freedom, and the second fluid degree of freedom is the order $O[(\sigma\mathcal{R})^2 V]$ difference between V and its zero frequency limit (eq. [7d]). In a numerical

calculation, differences of this kind introduce large errors owing to the finite precision of the computation and are to be avoided.

The two gravitational variables, H_0 and K, are sources of numerical error in a limit different from $\omega \to 0$; in the limit $r \ll \mathcal{R}$, the two gravitational variables become degenerate:

$$\lim_{r \to 0} H_0 - K = O[(r/\mathcal{R})^2 K] \,. \tag{8}$$

Thus H_0 and K describe the same degree of freedom of the gravitational field in the core of the star. Any dependence of the structure of the perturbation on the second degree of freedom involves the small difference between the two nearly equal quantities H_0 and K. Again, a small difference; again, to be avoided in a numerical calculation.

Thorne & Campolattaro (1967) used a fifth-order system of differential equation for K, H_0, W, and V. Subsequently, Ipser & Thorne (1973) showed it could be replaced by an equivalent fourth-order system. More recently, Detweiler & Lindblom (1985) have pointed out that the fourth-order system of equations is singular for some r, $0 < r < \mathcal{R}$ whenever $\omega^2 \gtrsim l(l+1)\rho_c/2$. While not important for the study of g-modes, whose frequencies satisfy $\omega^2 \ll \rho_c$, this singularity can affect the study of f-modes, complicating the validation of a numerical computer code.

The resonant standing-wave boundary condition is also a source of difficulty in the low-frequency, g-mode regime. The standard formalism requires that the perturbation equations be integrated well into the wave-zone ($\sigma r \gg 1$) before this boundary condition may be applied.

Since the frequency tends to zero for g-modes, both the effort and the error involved in this integration become large. Since the imaginary part of the eigenfrequency is fractionally so small compared to the real part, a small fractional error in the real frequency can seriously affect the estimate of the damping time. More seriously, since the imaginary part of the eigenfrequency approaches zero much more rapidly than the real part (eq. [6]), the resonances used by Thorne (1969) to locate eigenfrequencies become exceedingly narrow, the widths become exceedingly difficult to resolve numerically, and the resonances my even be impossible to find in a numerical search. Similar problems plague the algorithm of Lindblom & Detweiler (1983).

To summarize, in the low-frequency (g-mode) regime a numerical implementation of the standard formalism suffers from a choice of variables that do not represent the independent degrees of freedom of the gravitational field and fluid motion, from the necessity of applying the boundary condition of outgoing waves far ($r \gg 1/\sigma$) from the star, and from the difficulty of resolving narrow resonances. In the first difficulty, the important physics of a small but finite Eulerian pressure perturbation is not recognized by the implementation; and in the second and third the method of application of the boundary condition obscures the physics it represents — resonant frequencies and gravitational radiation damping of the perturbed star.

3. The Slow-Motion Formalism

The slow-motion formalism introduced herein consists of three distinct parts: (*i*) a new choice of perturbation variables, (*ii*) an instantaneous-gravity approximation for simplifying the outgoing-wave boundary condition, and (*iii*) a prescription for determining the complex eigenfrequencies of the quasi-normal modes. The formalism is designed to eliminate the difficulties enumerated in the previous subsection. The first step in that direction is the new choice of perturbation variables.

3.1. CHOICE OF VARIABLES

Referring to equations (I,C3) and (I,C4), V may be expressed in terms of K, H_0, W, and the Eulerian pressure perturbation:

$$V = \frac{1}{l(l+1)}\left[-e^{-\lambda/2}W' - \frac{p'}{\gamma p}e^{-\lambda/2}W - \frac{r^2}{\gamma p}\beta + \frac{r^2}{2}(H_0+2K)\right], \tag{9a}$$

or, with equation (I,9c),

$$V = -\frac{1}{\omega^2 e^{-\nu}}\left[\frac{\beta}{\rho+p} + \frac{1}{2}H_0\right], \tag{9b}$$

where

$$\beta \equiv \delta p / Y_{lm}. \tag{9c}$$

Here and henceforth, the harmonic time dependence $e^{-i\omega t}$ is assumed for all the perturbation variables.

Comparing equation (9a) with equation (7d), it is apparent that β represents an independent degree of freedom of the fluid in the low frequency limit: it is part of the small difference between the finite frequency V and the zero frequency limit for V. In the slow-motion approximation, β replaces V as a perturbation variable: the small quantity β is calculated directly from its own differential equation, not indirectly as the small difference between V and its zero frequency limit (7d).

The singularity in the perturbation equations is also due to an unfortunate choice of perturbation variables. The algebraic constraint that links K, H_0, β, and H_1 is (*cf.* Detweiler & Lindblom 1985)

$$\left[\frac{(l+2)(l-1)}{2}+\frac{3m}{r}+4\pi r^2 p\right]H_0 =$$

$$\left[\frac{(l+2)(l-1)}{2}-(\omega r)^2 e^{-\nu}-e^{\lambda}\left(\frac{m}{r}+4\pi r^2 p\right)\left(\frac{3m}{r}+4\pi r^2 p-1\right)\right]K$$

$$+\frac{1}{r}\left[(\omega r)^2 e^{-(\lambda+\nu)}-\frac{l(l+1)}{2}\left[\frac{m}{r}+4\pi r^2 p\right]\right]H_1 \qquad (10)$$

$$-8\pi p' e^{-\lambda/2} W-8\pi r^2\beta.$$

The derivation of equation (10) is stated in Appendix B.

The coefficient of H_1 in the constraint equation (10) is not positive definite in the star when $\omega^2 \gtrsim l(l+1)\rho_c/2$; consequently, this constraint equation should not be used to eliminate H_1 from the perturbation equations. The coefficient of H_0 is positive definite, however, so H_0 may

be eliminated from the perturbation equations without introducing a singularity.

Eliminating H_0 introduces H_1 as a perturbation variable; however, for the same reason that V is not a wise choice of variable in the low-frequency limit, H_1 is not a suitable perturbation variable: in the limit of zero frequency, equation (10) becomes

$$H_1 = \frac{16\pi(\rho+p)e^{\lambda/2}}{l(l+1)}W \ . \tag{11}$$

Like V, at low frequencies H_1 is determined predominantly by W. The slow-motion approximation introduces the new variable

$$J \equiv H_1 - \frac{16\pi(\rho+p)e^{\lambda/2}}{l(l+1)}W \ , \tag{12}$$

which vanishes in the zero frequency limit. Now, however, in the core of the star $K \approx J'/2$; thus, in the small r limit K and J do not represent truly independent degrees of freedom of the gravitational field. To remedy this final deficiency, the slow motion approximation introduces the new variable F in place of K:

$$F \equiv H_0 - K \ . \tag{13}$$

In terms of the new perturbation variables F, J, W, and β, the perturbation equations are

$$F' = -\omega^2 e^{-\nu} J - \frac{16\pi(\rho+p)\omega^2 e^{-\nu} e^{\lambda/2}}{l(l+1)}W - \nu'(F+K) \ , \tag{14a}$$

$$J' = -\frac{1}{2}(\nu'-\lambda')J + 2e^{\lambda}\left[1 - \frac{12\pi r^2(\rho+p)}{l(l+1)}\right]K \tag{14b}$$

$$+e^{\lambda}\left[1-\frac{8\pi r^2(\rho+p)}{l(l+1)}\right]F+\frac{16\pi r^2 e^{\lambda}}{l(l+1)}\mu\,,$$

$$\beta' = -\frac{\nu'}{2}(\mu+\beta)-\left[p'+\frac{\rho+p}{2r}\right]F-\frac{p'}{2}K \tag{14c}$$

$$-\frac{\omega^2 e^{-\nu}(\rho+p)}{2}\left[1+\frac{l(l+1)}{2(\omega r)^2 e^{-\nu}}\right]J$$

$$+\frac{e^{\lambda/2}(\rho+p)\omega^2 e^{-\nu}}{r^2}\left[1-\frac{8\pi r^2(\rho+p)}{l(l+1)}\right]W\,,$$

$$W' = -\frac{p'}{\gamma p}W-\frac{r^2}{\gamma p}\left[1-\frac{l(l+1)}{(\omega r)^2 e^{-\nu}}\frac{\gamma p}{\rho+p}\right]\beta \tag{14d}$$

$$+\frac{r^2 e^{\lambda/2}}{2}\left[1+\frac{l(l+1)}{(\omega r)^2 e^{-\nu}}\right]F+\frac{r^2 e^{\lambda/2}}{2}\left[3+\frac{l(l+1)}{(\omega r)^2 e^{-\nu}}\right]K\,.$$

In these equations the Eulerian density perturbation is represented by μ:

$$\mu \equiv \frac{\delta\rho}{Y_{lm}} = \frac{\rho+p}{\gamma p}\beta-\frac{\rho'}{r^2}\frac{\gamma-\gamma_0}{\gamma}e^{-\lambda/2}W\,, \tag{15a}$$

while γ and γ_0 represent the effective adiabatic index of the pulsating fluid and the adiabatic index reflected in the radial profile of pressure and density in the unperturbed star:

$$\gamma \equiv \frac{\Delta p}{\Delta\rho}\frac{\rho+p}{p}, \tag{15b}$$

$$\gamma_0 \equiv \frac{dp/dr}{d\rho/dr}\frac{\rho+p}{p}\,.$$

The metric perturbation K, which appears in the perturbation equations above and which I shall use below, can be computed from equation (10) in terms of the new fundamental variables F, J, W, β with equations (12) and (13):

$$\left[(\omega r)^2 e^{-\nu}+\frac{2m}{r}+e^{\lambda}\left[\frac{m}{r}+4\pi r^2 p\right]^2\right]K \tag{15c}$$

$$=\frac{16\pi(\rho+p)e^{-\lambda/2}(\omega r)^2 e^{-\nu}}{l(l+1)}\frac{W}{r}$$

$$+\left[(\omega r)^2 e^{-(\nu+\lambda)}-\frac{l(l+1)}{2}\left[\frac{m}{r}+4\pi r^2 p\right]\right]\frac{J}{r}$$

$$-\left[\frac{(l+2)(l-1)}{2}+\frac{3m}{r}+4\pi r^2 p\right]F-8\pi r^2\beta.$$

Detailed instructions for deriving these perturbation equations are given in Appendix B.

The introduction of these new perturbation variables solves the problems of the singularity in the differential equations, and the small differences between nearly equal quantities in a numerical study of g-mode pulsations. The second feature of the slow-motion formalism is an instantaneous-gravity approximation to simplify the boundary condition at infinity.

3.2. INSTANTANEOUS-GRAVITY APPROXIMATION

G-mode pulsations satisfy $\sigma\mathcal{R}\ll 1$; consequently, the pulsating star is deep in its own near-zone gravitational field. In the near zone, retardation across the body of the star is negligible: the dynamical aspect of the gravitational field may be viewed as a small correction to an otherwise instantaneous field (the correction to the instantaneous field at the surface of the star is of fractional order $O[(\sigma\mathcal{R})^2]$, Finn 1985; radiation reaction forces a correction of fractional order $O[(\sigma\mathcal{R})^{2l+1}]$, Ipser 1971). This observation is formalized in the "instantaneous gravity boundary condition" (§ XII.A of Thorne 1980), an approximation to the boundary condition of strictly outgoing gravitational waves at infinity: the gravitational field exterior to the star is taken to be the $\omega=0$ limit of strictly outgoing gravitational waves.

The zero frequency limit of the vacuum gravitational perturbation has been studied in detail by Fackerell (1971). The perturbation equations simplify considerably in this case: the differential equation for K may be solved exactly (Ipser 1971; Fackerell 1971); the remaining gravitational perturbation J (note that outside the star $H_1=J$) is described by a simple first-order ordinary differential equation with K as a source.

There are two linearly independent solutions for K (and thus two solutions for J) in the zero frequency limit; only one corresponds to the zero frequency limit of outgoing waves at infinity (Ipser 1971; Fackerell 1971):

$$K(r)=-\frac{2D(2l+1)!!}{(l+2)!\mathcal{M}^{l+1}}\left\{Q_l^2(2x-1)+[x(x-1)]^{-1/2}Q_l^1(2x-1)\right\} \tag{16a}$$

$$\sim -\frac{2D}{r^{(l+1)}} \text{ for } r/\mathcal{M}\gg 1,$$

$$J(r)=h(r)v(r)+k(r)\left[1-\frac{2\mathcal{M}}{r}\right]\frac{dv}{dr} \tag{16b}$$

$$\sim \frac{-4D}{l}\frac{1}{r^l} \text{ for } r/\mathcal{M}\gg 1,$$

where

$$Q_l^m(z) \equiv \left[\begin{array}{l}\text{associated Legendre function}\\ \text{of the second kind}\end{array}\right], \tag{16c}$$

$$x\equiv r/2\mathcal{M}\,, \tag{16d}$$

$$h(r)=\frac{(l+2)(l-1)(r^2-3\mathcal{M}r)-6\mathcal{M}^2}{[(l+2)(l-1)r+6\mathcal{M}](r-2\mathcal{M})}\,, \tag{16e}$$

$$k(r)=\frac{r^2}{r-2\mathcal{M}}\,, \tag{16f}$$

$$\frac{dv}{dx}+\left[-\frac{1}{x}+\frac{l(l+1)}{2(x-1)}+\frac{4}{4x+3l(l+1)}\right]v=\frac{2\mathcal{M}x}{x-1}K(r)\,, \tag{16g}$$

$$v(x)\sim -\frac{4D}{l(l-1)}\frac{1}{r^l} \text{ for } r\gg 2\mathcal{M},$$

and D is the amplitude of the gravitational perturbation.

This solution tends to zero as $r\to\infty$; the second (discarded) solution diverges as $r\to\infty$. The choice of solutions may be understood in terms of

the resonant boundary condition. Recalling that in the near zone $r \lesssim 1/\sigma$, the radiation field of finite but small frequency σ and the zero frequency limit of that field are similar, consider the behavior of the gravitational field near the surface of the star for real frequencies both on and off resonance. On resonance, the gravitational field immediately outside the star decreases rapidly in magnitude with increasing distance from the star, thereby causing the energy in the pulsation to be large compared to the energy in one wavelength (or several) of the gravitational field; off resonance, the situation is reversed: the field increases rapidly with distance from the star causing the energy in one wavelength (or several) of the field to be far larger than the star's pulsation energy. In the zero frequency limit, it is this local behavior of the field near the surface of the star that is preserved; consequently, the solution that dies out at infinity, equation (16), corresponds to the boundary condition of resonance.

G-mode frequencies satisfy $(\omega\mathcal{R})^2 \ll \mathcal{M}/\mathcal{R}$. For sufficiently low frequency, there always exists a regime where simultaneously $(\omega r)^2 \ll 1$ and $\mathcal{M} \ll r$. At such frequencies, the results of Finn (1985) for the weak field, near-zone limit of gravitational radiation may be applied to quantify more precisely the fractional error made in the instantaneous gravity approximation. After a gauge change to remove the unphysical $\sim r$ divergence of H_0 and H_1 and the asymptotically constant value of K in the limit $r \to \infty$ (Price & Thorne 1969), K must behave as $\sim h^{l-2}(\omega r)$, where $h^l(\omega r)$ is the spherical Hankel function with asymptotic form $\sim \exp(i\omega r)/\omega r$. The error made in going to the limit $\omega \to 0$, $\omega r \to$ constant is

of fractional order $(\omega r)^2/2(2l-5)$. Consequently, the error in K at $r=\mathcal{R}$ in the instantaneous gravity approximation is expected to be of fractional order

$$\left[\begin{array}{l}\text{fractional error committed by} \\ \text{instantaneous gravity approximation}\end{array}\right] \approx \frac{(\omega\mathcal{R})^2}{2(2l-5)}. \qquad (17)$$

For a 10 km radius, $1\,\mathcal{M}_\odot$ neutron star, equation (17) applies for all modes with period $\gtrsim 1$ ms; thus, equation (17) applies for all g-modes.

The instantaneous gravity approximation reformulates the outgoing wave boundary condition at infinity as a boundary condition at the surface of the star: namely, that the ratio F/J at the surface of the star, determined by integrating the perturbation equations within the star subject to the boundary condition of regularity at $r=0$ and vanishing Lagrangian pressure perturbation at $r=\mathcal{R}$, takes on the value appropriate to the zero frequency limit of the outgoing-wave boundary condition (equivalent to the zero frequency limit of the resonant boundary condition). The zero frequency limit of F/J for a particular l depends only on $\mathcal{R}/\mathcal{M}$ and so may be tabulated once and applied to any star. This reformulation of the boundary condition at infinity avoids the difficulty of integrating the gravitational perturbation far from the star's surface out to the wave zone, and indeed becomes more accurate with lower frequency. The other two boundary conditions, that the perturbations vanish at $r=0$ and that the Lagrangian pressure perturbation vanish at $r=\mathcal{R}$, remain unchanged in the slow motion formalism.

At this stage, both the differential equations (eq. [14]) and boundary conditions have been specified: a complete eigenvalue problem exists. The eigenfrequencies may be found by any standard technique; the technique I have used is described in Appendix A.

3.3. DETERMINING THE QUASI-NORMAL MODE EIGENFREQUENCIES

The eigenfrequencies found by solving the perturbation equations (14) with the instantaneous gravity boundary condition are real, because in the zero frequency limit there is no energy carried off by gravitational waves and thus no damping of the pulsations. The third distinct part of the slow motion formalism is a prescription for determining the (complex) quasi-normal mode eigenfrequencies from the real solutions of the eigenvalue problem stated above.

In the slow-motion formalism the real frequency solutions to the stated eigenvalue problem are taken to be the real part of the associated quasi-normal mode eigenfrequencies. The damping time of the pulsation (the reciprocal of the imaginary part of the quasi-normal mode eigenfrequency) is given by twice the ratio of the energy in the pulsation to the energy flux in gravitational waves (*cf*. Detweiler 1975). This requires an expression for the energy in the pulsations and an expression for the power in outgoing gravitational radiation.

The difference between the eigenfunctions in the star determined using the instantaneous gravity boundary condition and the true eigenfunctions of a quasi-normal mode is of fractional order $O[(\sigma\mathcal{R})^2]$ (eq. [17]). Thus, even though the instantaneous gravity boundary

condition explicitly assumes that there is no gravitational radiation present, the eigenfunctions calculated may be used to determine the power in gravitational waves by asymptotically matching the near zone field, determined by the values of the gravitational variables F and J at $r=\mathcal{R}$, to the wave zone field and determining the amplitude of outgoing gravitational radiation. The time-averaged power radiated as determined by this procedure is (Ipser 1971, eq. [25a])

$$\frac{d\mathcal{E}}{dt}=-\frac{1}{4\pi}\frac{(l+2)(l+1)}{l(l-1)}\left[\frac{\omega^{l+1}D}{(2l-1)!!}\right]^2 , \tag{18}$$

where D is defined by equation (16a) in terms of the amplitude of the gravitational perturbation K at the surface of the star. The error in the power calculated by this procedure is of fractional order $O[(\omega\mathcal{R})^2]$ in the true power.

Detweiler & Ipser (1973) derived a variational principle for non-radial pulsational modes; associated with that variational principle is a conservation law for the pulsational energy in the star. The time rate of change of that pulsational energy, as given by the variational principle, is equal to minus the power carried off by gravitational waves. Equation (25) of Detweiler & Ipser gives the energy in the pulsations (note a factor of ½ is missing from the final surface integral of Detweiler & Ipser 1973,eq. [25]):

$$\mathcal{E}(\omega,\mathcal{R}_\infty,t)\equiv\int_0^{\mathcal{R}_\infty}|\omega r|^2 dr\; e^{(\lambda-\nu)/2}\left\{\frac{(\rho+p)}{2}\left[\left|\frac{W}{r^2}\right|^2+l(l+1)\left|\frac{V}{r}\right|^2\right]\right. \tag{19}$$

$$-\frac{l(l+1)e^{-\lambda}}{32\pi r^2}|H_1|^2-\frac{1}{32\pi}(2H_0K+|K|^2)\Bigg\}$$

$$+\frac{1}{2}\int_0^{\mathcal{R}_\infty} r^2 dr e^{(\nu+\lambda)/2}\Bigg[p\gamma_0\left|\frac{\mu}{(\rho+p)}\right|^2+\frac{e^{-\lambda}}{8\pi}K'(H_0'+\nu'H_0)$$

$$+H_0\mu-\frac{S}{(\rho+p)p'}|\mu+\frac{e^{-\lambda/2}}{r^2}\rho' W|^2$$

$$+\left[\frac{l(l+1)}{16\pi r^2}-\frac{3}{4}(\rho+p)\right]|H_0|^2-\frac{e^{-\lambda}}{16\pi}|K'|^2\Bigg]$$

$$+\frac{r^2}{2}\left[\rho\frac{e^{-\lambda/2}}{r^2}WH_0-p'\frac{e^{-\lambda}}{r^4}|W|^2\right]_{r=\mathcal{R}},$$

where S is the relativistic Schwarzschild discriminant,

$$S \equiv p'-\gamma p\rho'/(\rho+p)\ .$$

In light of the many errors elsewhere in the literature on stellar pulsation energy, I have carefully rederived this Detweiler & Ipser (1973) expression and found it to be correct aside from the factor of ½ in the surface integral. As given above, it differs from Detweiler & Ipser (1973), equation (25) only by modest changes of notation and the correction and evaluation of the final surface integral.

The integrals above are carried out to a radius $\mathcal{R}_\infty \gg 1/\omega$ from the star. Outside the star, the gravitational perturbation variables are calculated from equations (16).

In terms of the pulsation energy (19) and power radiated (18), the amplitude damping time of the quasi-normal-mode pulsations is

$$\mathrm{Im}(\omega)=\frac{1}{\tau}=-\frac{1}{2}\frac{d\mathcal{E}}{dt}\frac{1}{\mathcal{E}} . \qquad (20)$$

In the slow-motion formalism $\mathrm{Im}(\omega)$ is evaluated numerically using equations (18)-(20).

To summarize, in the slow-motion formalism variables that are independent in the low frequency limit are chosen; the dominant, non-dynamical character of the gravitational field is exploited to convert the boundary condition of outgoing radiation at infinity into a boundary condition that may be imposed on the surface of the star without reference to a distant infinity; and the damping time of a pulsation mode is found by using an energy principle.

4. Demonstration -- G-Modes in Polytropes

This section discusses the performance of the slow-motion formalism on stellar models with a simple equation of state. Model stars with g-modes of non-zero frequency are created by artificial means. The discussion is intended to demonstrate the performance of the formalism; in a future paper the formalism will be applied to study more realistic equations of state, and the physical sources of finite-frequency g-modes will be considered in detail.

The slow-motion formalism is designed to study long period g-mode pulsations; it is not expected to yield accurate results (especially

damping times) for f-modes, and is certainly not applicable to p-mode pulsations, where the dynamics of the gravitational field play a major role. Validation of an implementation of the slow-motion formalism is complicated by the lack of overlap with any previous numerical calculations in the g-mode domain that are expected to be more accurate.

To demonstrate the slow-motion formalism, neutron star models with polytropic equations of state

$$p = k\rho^{1+1/n} \tag{21}$$

were constructed. This equation of state is chosen for two reasons: (i) to eliminate equation-of-state side-effects that could obscure the validation of the code; and (ii) Balbinski *et al.* (1985) have studied f-modes in model neutron stars constructed from this equation of state with $n=1$ and $k=100$ (ρ and p measured in units of km^{-2}) using the algorithm of Lindblom & Detweiler (1983); this permits a comparison with the slow-motion formalism in a regime where the formalism is marginally accurate.

Table 1 gives the vital statistics (central density, radius, and mass) of the static models constructed from the equation of state (21) (with $n=1$, $k=100$; ρ and p in units of km^{-2} as in Balbinski *et al.* 1985) at three different densities. Table 1 also shows the periods and damping times of the quadrupole f-modes as I have calculated them using the slow-motion formalism (denoted SM in the Table) and as calculated by Lindblom & Detweiler in Balbinski *et al.* (1985) (denoted BSDL in the

Table). To judge the magnitude of the expected errors, the quantity $(\omega\mathcal{R})^2$ is tabulated in the final column for each model.

Both the periods and the damping times as generated by the slow-motion formalism show good agreement with the non-slow-motion ones. This gives confidence that the slow-motion formalism as described above has been correctly posed and implemented.

To study the performance of the slow-motion formalism in determining characteristics of g-modes, it is necessary to provide a mechanism for generating g-modes at non-zero frequency. This is done by enforcing a non-zero $\tilde{\gamma} \equiv \gamma - \gamma_0$ (*cf.* eq. [15a]). In a real physical situation, this difference is generated by deviations from isentropy or by chemical inhomogeneities.

In a realistic neutron star model, $\tilde{\gamma}$ is expected to be significant only at densities $\rho \lesssim 2\times10^{11}$ g cm^{-3} (*cf.* Meltzer & Thorne 1966; McDermott, Van Horn, & Scholl 1983). In order to demonstrate the slow-motion formalism under somewhat realistic conditions, $\tilde{\gamma}/\gamma_0 - 1$ was set to a constant, non-zero value in a 1 km "surface layer" of the models studied. No physical effects were used to determine the choice of $\tilde{\gamma}$ in this region; $\tilde{\gamma}$ was adjusted to probe the ability of the slow motion formalism to find g-mode periods in what is expected to be the physically relevant regime $T_g \gtrsim 100$ ms (*cf.* McDermott, Van Horn, & Scholl 1983).

To estimate the frequency of the first g-mode, the Brunt-Väisälä frequency (*cf.* Cox 1980) may be reexpressed to show that, to order of magnitude, the first g-mode frequency is expected to satisfy

$$(\omega_g \mathcal{R})^2 \approx \frac{\tilde{\gamma}}{\gamma_0^2}\left[\frac{\mathcal{M}}{\mathcal{R}}\right]^2 \frac{\rho}{p} \tag{22}$$

averaged over the star. For the model studied (Table 1), this formula gives $T_g \equiv 2\pi/\omega_g \gtrsim 100\text{ms}$ if we choose $\tilde{\gamma}/\gamma_0 = 10^{-3}$ within 1 km of the surface.

Table 2 shows the first six $l=2$ g-mode periods and damping times for the Table 1 model with central density 10^{15} g cm^{-3}, and with $\tilde{\gamma}/\gamma_0 - 1 = 10^{-3}$ within 1 km of the surface. The period of the first g-mode is consistent with the crude estimate provided by equation (22); subsequent modes are nearly equally spaced in period.

Also tabulated is the pulsational energy determined by equation (19). In evaluating equation (19), the perturbation is normalized to $\xi^r/\mathcal{R} = 1$ at the surface, and the energy scales as the square of this quantity.

Damping time is expected to scale with ω, $\mathcal{R}$, $\mathcal{M}$, and the number of radial nodes n in the eigenfunction W is expected to scale roughly as (*cf.* Misner, Thorne, & Wheeler 1973, exercise 37.13)

$$\tau \sim \left(\frac{\mathcal{R}}{\mathcal{M}}\right)\left[\frac{2n-1}{(\sigma\mathcal{R})}\right]^{2l}\mathcal{R}\,. \tag{24}$$

The final column of Table 2 expresses τ in terms of this expected scaling. The damping times are found to scale roughly in the expected fashion, although the higher modes damp a bit more slowly.

Figure 1 shows F and K for the g_6 mode of Table 2. Note the difference in magnitude between F and K. In the non-slow-motion

formalism F is computed as the difference between H_0 and K (eq. [13]); in the slow-motion formalism F is a fundamental variable and is calculated directly from its own differential equation (eq. [14a]). The non-slow-motion formalism must work much harder than the slow-motion formalism to achieve the same fractional accuracy in F. The abrupt turn-on of $\tilde{\gamma}$ is responsible for the abrupt change of K near $1-r/\mathcal{R}\approx 10^{-1}$.

5. Conclusions

The slow-motion formalism provides a new framework for studying non-radial pulsations of relativistic stars in the limit of low-frequency — a framework particularly well suited for numerical work. The key features of the slow-motion formalism are (*i*) a choice of perturbation functions that exploit the low-frequency limit to isolate the independent degrees of freedom of the gravitational field and fluid motion; (*ii*) an instantaneous gravity approximation that recognizes the unimportance of the dynamics of the gravitational field to the structure of the perturbation and permits the outgoing-waves boundary condition, which must be applied far from the star, to be reformulated as a boundary condition at the surface of the star; and (*iii*) an expression for the damping time of a quasi-normal mode in terms of the surface value of the gravitational perturbations and an integral over real eigenfunctions.

An implementation of the slow-motion formalism shows it to be capable of locating and studying g-mode eigenfrequencies in polytropic

stars. Eigenfrequencies can be estimated crudely and are found to agree with the numerical calculations; damping times scale with frequency and mode number as expected. Though the slow-motion formalism is not expected to be very accurate in the regime of f-modes, and not at all applicable to the regime of p-modes, f-mode eigenfrequencies and damping times computed with the formalism show good agreement with the f-mode calculations of Balbinski *et al.* (1985).

Future work will apply the slow-motion formalism to study more realistic equations of state and realistic sources of non-zero g-mode frequency, and will extend the formalism to include the effects of an isotropic shear stress.

Acknowledgements

The slow-motion formalism was conceived in principle but not in detail by Kip S. Thorne, and he laid some of the groundwork for what appears here. I gratefully acknowledge many helpful discussions with him. This work was supported in part by the National Science Foundation (AST 84-14126 and NSF 84-51725).

References

Balbinski, E., Detweiler, S., Lindblom, L., & Schutz, B. F. 1985. *Mon. Not. R. astr. Soc.*, **213,** 553.

Cox, J. P. 1980. *Theory of Stellar Pulsation*, Princeton University Press, Princeton (New Jersey).

Detweiler, S. L. 1975. *Astrophys. J.*, **197,** 203.

Detweiler, S. L., & Ipser, J. R. 1973. *Astrophys. J.*, **185,** 685.

Detweiler, S. L., & Lindblom, L. 1985. *Astrophys. J.*, **292,** 12.

Fackerell, E. D. 1971. *Astrophys. J.*, **166** 197.

Finn, L. S. 1985. *Class. Quantum Grav.*, **2,** 381.

Gear, C. W. 1971. **Numerical Initial Value Problems in Ordinary Differential Equations,** Prentice-Hall, Englewood Cliffs (New Jersey).

Ipser, J. R. 1971. *Astrophys. J.*, **166,** 175.

Ipser, J. R., & Thorne, K. S. 1973. *Astrophys. J.*, **181,** 181.

Lindblom, L., & Detweiler, S. L. 1983. *Astrophys.*J. **53,** 73.

McDermott, P. N., Van Horn, H. M., & Scholl, J. F. 1983. *Astrophys.*J., **268,** 837.

Meltzer, D. W., & Thorne, K. S. 1966. *Astrophys. J.*, **145,** 514.

Misner, C. W., Thorne, K. S., & Wheeler, J. A. 1973. *Gravitation*, Freeman, San Francisco.

Price, R., & Thorne, K. S. 1969. *Astrophys. J.*, **155,** 163

Regge, T., & Wheeler, J. A. 1957. *Phys. Rev.*, **108,** 1063.

Schumaker, B. L., & Thorne, K. S. 1983. *Mon. Not. R. astr. Soc.*, **203,** 457.

Thorne, K. S., & Campolattaro, A. 1967. *Astrophys. J.*, **149,** 591. (Cited in

text as paper I).

Thorne, K. S. 1969. *Astrophys. J.*, **158**, 1.

Thorne, K. S. 1980. *Rev. Mod. Phys.*, **52**, 299.

Van Horn, H. M. 1980. *Astrophys. J.*, **236**, 899.

Appendix A: Computing quasi-normal modes in the slow-motion formalism

This appendix is devoted to a detailed description of the author's numerical implementation of the slow-motion formalism.

1. THE STATIC BACKGROUND

The static background is described by the line element of equation (1). A fourth-order Runge-Kutta integrator is used to integrate equations (2) from the center of the star to the surface. An adaptive step-size algorithm (*cf.* Gear 1971) is used to insure that the increment at each step involves a fractional error below a given level (10^{-4} for the calculations reported here). Pressure p, density ρ, mass m, potential ν, and adiabatic index γ_0 are recorded initially on a "data grid" of typical resolution 30 meters, independent of the step size chosen by the integrator; near the surface, data are recorded more frequently, with a minimum data-grid size of 5 cm. The resolution of the data grid is increased whenever the integrator finds that more than 1000 steps are required to move between data grid points. (Over the bulk of the star, the step size required for a fractional accuracy of a part in 10^{-4} is larger than 30 m — thus, the expected accuracy of the integration is better than a part in 10^{-4}.) Integration is terminated when the data grid resolution increases beyond 5 cm (*i.e.*, when data are recorded more often than every 5 cm), or when the density falls below that of ^{56}Fe. All the variables are then extended analytically to a surface at zero pressure by matching onto a polytropic "atmosphere" (*cf.* Lindblom &

Detweiler 1983):

$$p = p_0[(\mathcal{R}-r)/\mathcal{R}]^{n+1}, \qquad \text{(A1)}$$

$$\rho = \rho_0[(\mathcal{R}-r)/\mathcal{R}]^{n}.$$

(The atmosphere is taken to be polytropic even if the interior is not.) The parameters p_0, ρ_0, n, and $\mathcal{R}$ are determined by insisting that dp/dr, p, ρ, and $\gamma_0 = 1+1/n$ be continuous.

2. SOLVING THE EIGENPROBLEM

In this section, I first describe the general procedure for finding the quasi-normal modes of a model star, and then return to focus on each part of the procedure in more detail.

2.1. THE GENERAL PROCEDURE

For a given trial frequency, the boundary condition of regularity at $r=0$ chooses a two-parameter family of solutions to the differential equations (14). Each of these two solutions is integrated separately from the core of the star to the star's midpoint. At the surface of the star, the instantaneous gravity boundary condition and the boundary condition of vanishing Lagrangian pressure perturbation also determine a two-parameter family of solutions. Each of these solutions is integrated from the surface of the star to the midpoint.

If the trial frequency is an eigenfrequency, then the eigenfunctions F, J, W, and β are continuous at the midpoint. In the region between

$r=0$ and the midpoint, the eigenfunctions are given by a linear superposition of the two core solutions; in the region between the midpoint and $r=\mathcal{R}$, the eigenfunctions are given by a linear superposition of the two surface solutions. To determine if the trial frequency is an eigenfrequency, a linear superposition of the two surface solutions and of the two core solutions is sought for which the four eigenfunctions are continuous. Only for an eigenfrequency does such a solution exist.

Having found an eigenfrequency, the integral expression equation (14) is evaluated with the tabulated eigenfunctions to find the energy in the pulsations. The power radiated in gravitational radiation is evaluated with equations (18), (16), and the value of K at the surface of the star; and the damping time is determined from equation (20).

2.2. THE CORE SOLUTIONS

The differential equations (14) are singular at the core of the star; it is possible to expand the perturbations as well as certain quantities that describe the unperturbed star in a power series about $r=0$ to obtain

$$F=\left[F_0+\frac{r^2}{2}F_2+O(r^4)\right]r^{l+2}, \tag{A2a}$$

$$J=\left[J_0+\frac{r^2}{2}J_2+O(r^4)\right]r^{l+1}, \tag{A2b}$$

$$W=\left[W_0+\frac{r^2}{2}W_2+O(r^4)\right]r^{l+1}, \tag{A2c}$$

$$\beta=\left[\beta_0+\frac{r^2}{2}\beta_2+O(r^4)\right]r^l, \tag{A2d}$$

$$K=\left[K_0+\frac{r^2}{2}K_2+O(r^4)\right]r^l, \tag{A2e}$$

$$\nu=\nu_0+\frac{r^2}{2}\nu_2+\frac{r^4}{4!}\nu_4+O(r^6), \tag{A2f}$$

$$p=p_0+\frac{r^2}{2}p_2+O(r^4), \tag{A2g}$$

and

$$\rho=\rho_0+\frac{r^2}{2}\rho_2+O(r^4). \tag{A2h}$$

The quantities ρ_0, p_0, and ν_0 are the values of ρ, p, and ν at $r=0$. The remaining quantities that describe the unperturbed star are

$$\nu_2=8\pi(\rho_0+3p_0)/3, \tag{A2i}$$

$$\nu_4=16\pi\left[\frac{8\pi}{3}\rho_0(3p_0+\rho_0)+\frac{\rho_2+3p_2}{2}\right] \tag{A2j}$$

$$p_2=-4\pi(\rho_0+p_0)(\rho_0+3p_0)/3, \tag{A2k}$$

and

$$\rho_2=\frac{\rho_0+p_0}{\gamma_0 p_0}p_2. \tag{A2l}$$

The perturbation equations (14) may be evaluated to yield a linear system of equations that is solved numerically to determine the

coefficients in equations (A2a-e). The expansions (A2a-e) select a two-parameter family of solutions to the differential equations (14); the two parameters that specify a solution are taken to be W_0 and J_0. In order to obtain starting values for the integration, the system is solved twice, once with $W_0=\mathcal{R}^{2-l}$ and $J_0=0$, and once with $W_0=0$ and $J_0=\mathcal{R}^{-l}$. The linear system of equations is

$$(l+2)F_0=-\frac{16\pi\omega^2 e^{-\nu_0}(\rho_0+p_0)}{l(l+1)}W_0-\nu_2K_0-\omega^2e^{-\nu_0}J_0, \tag{A3a}$$

$$l\beta_0=\omega^2e^{-\nu_0}(\rho_0+p_0)W_0-\frac{l(l+1)(\rho_0+p_0)}{4}J_0, \tag{A3b}$$

$$K_0=\frac{l+1}{2}J_0, \tag{A3c}$$

$$\begin{aligned}\frac{(l+4)}{2}F_2=&-\nu_2F_0-\nu_4K_0+\frac{\nu_2\omega^2e^{-\nu_0}}{2}J_0\\&-\frac{8\pi\omega^2e^{-\nu_0}(\rho_2+p_2+(\rho_0+p_0)(8\pi\rho_0-3\nu_2)/3)}{l(l+1)}W_0\\&-\frac{\nu_2}{2}K_2-\frac{\omega^2e^{-\nu_0}}{2}J_2-\frac{8\pi\omega^2e^{-\nu_0}(\rho_0+p_0)}{l(l+1)}W_2,\end{aligned} \tag{A3d}$$

$$\begin{aligned}\frac{(l+3)}{2}J_2=&F_0+\left[\frac{16\pi\rho_0}{3}-\frac{24\pi(\rho_0+p_0)}{l(l+1)}\right]K_0-\frac{4\pi(3p_0-\rho_0)}{3}J_0\\&-\frac{16\pi\tilde{\gamma}\rho_2}{\gamma l(l+1)}W_0+\frac{16\pi(\rho_0+p_0)}{\gamma p_0 l(l+1)}\beta_0+K_2,\end{aligned} \tag{A3e}$$

$$\frac{K_2}{2}=\left[-\frac{4\pi(\rho_0+p_0)}{8\pi\rho_0/3+\omega^2e^{-\nu_0}}\right.$$

$$+\frac{9(l+2)(l-1)(2\pi(9\rho_2+20\pi(3p_0+\rho_0)^2)/45-\omega^2e^{-\nu_0}\nu_2/4)}{(3\omega^2e^{-\nu_0}+8\pi\rho_0^2)}\Bigg]F_0$$

$$+\Bigg[\frac{(3\omega^2e^{-\nu_0}+2\pi l(l+1)(3p_0+\rho_0))}{30(3\omega^2e^{-\nu_0}+8\pi\rho_0)^2}$$

$$\times(45\nu_2\omega^2e^{-\nu_0}-72\pi\rho_2-160\pi^2(3p_0+\rho_0)^2)$$

$$+\frac{-\omega^2e^{-\nu_0}(\nu_2/2+8\pi\rho_0/3)+l(l+1)(p_2+\rho_2/5)}{8\pi\rho_0/3+\omega^2e^{-\nu_0}}\Bigg]J_0$$

$$+\frac{8\pi\omega^2e^{-\nu_0}}{l(l+1)(8\pi\rho_0+3\omega^2e^{-\nu_0})}\Big[3(\rho_2+p_2)-(\rho_0+p_0)(3\nu_2+8\pi\rho_0)$$

$$-\frac{(\rho_0+p_0)(-45\nu_2\omega^2e^{-\nu_0}+72\rho_2\pi+160\pi^2(3p_0+\rho_0)^2)}{5(3\omega^2e^{-\nu_0}+8\pi\rho_0)}\Bigg]W_0$$

$$+9\frac{32\rho_2\pi^2/5+128\pi^3(3p_0+\rho_0)^2/9-4\pi\nu_2\omega^2e^{-\nu_0}}{(3\omega^2e^{-\nu_0}+8\pi\rho_0)^2}\beta_0$$

$$\frac{\omega^2e^{-\nu_0}/2+l(l+1)(3p_0+\rho_0)\pi/3}{8\pi\rho_0/3+\omega^2e^{-\nu_0}}J_2+\frac{8\pi\omega^2e^{-\nu_0}(\rho_0+p_0)}{l(l+1)(8\pi\rho_0/3+\omega^2e^{-\nu_0})}W_2$$

$$-\frac{4\pi}{8\pi\rho_0/3+\omega^2e^{-\nu_0}}\beta_2-\frac{(l+2)(l-1)}{4(8\pi\rho_0/3+\omega^2e^{-\nu_0})}F_2, \qquad \text{(A3f)}$$

$$\frac{(l+3)}{2}W_2=\frac{l(l+1)}{2\omega^2e^{-\nu_0}}\Bigg[\frac{\beta_2}{\rho_0+p_0}+F_0+\frac{K_2}{2}+\frac{-\rho_2-p_2+(8\pi\rho_0/3+\nu_2)(\rho_0+p_0)}{(\rho_0+p_0)^2}\beta_0$$

$$+\frac{3\nu_2+8\pi\rho_0}{6}K_0\Bigg]+\frac{3}{2}K_0-\frac{\beta_0+p_2W_0}{\gamma p_0}, \qquad \text{(A3g)}$$

$$\frac{(l+2)}{2}\beta_2=-\frac{\rho_0+p_0}{2}F_0-\frac{p_2}{2}K_0-\left[\frac{l(l+1)(p_2+\rho_2)}{8}+\frac{\omega^2e^{-\nu_0}(p_0+\rho_0)}{2}\right]J_0$$

$$+\left\{\frac{\tilde{\gamma}\rho_2\nu_2}{2\gamma}+\omega^2e^{-\nu_0}\left[\frac{p_2+\rho_2}{2}\right.\right.$$

$$\left.\left.+(\rho_0+p_0)\left(\frac{4\pi\rho_0}{3}-\frac{\nu_2}{2}-\frac{8\pi(\rho_0+p_0)}{l(l+1)}\right)\right]\right\}W_0$$

$$-\frac{\nu_2}{2}\left(1+\frac{\rho_0+p_0}{\gamma p_0}\right)\beta_0-\frac{l(l+1)(\rho_0+p_0)}{8}J_2+\frac{\omega^2e^{-\nu_0}(\rho_0+p_0)}{2}W_2. \qquad \text{(A3h)}$$

With this power-series solution, starting values for a fourth-order Runge-Kutta integration are found at a non-zero starting radius r_s. The Runge-Kutta integration is performed with an adaptive step-size algorithm (Gear 1971) that keeps fractional errors below a given level (a part in 10^{-4} for the calculations reported here). To insure stable numerical performance, the integrator never crosses a data-grid point with a step; however, it may take multiple steps within a data grid zone. Within a grid zone, p and ρ are logarithmically interpolated on the distance from the surface. The choice of r_s is made to be consistent with the fractional accuracy of the integrator. Values of the two integrated solutions are recorded at every point of the data grid.

2.3. THE SURFACE SOLUTIONS

Two boundary conditions are applied at the surface of the star to determine the two-parameter family of solutions that are integrated to the midpoint. The instantaneous gravity boundary condition fixes the ratio F/J at $\mathcal{R}$, but it does not determine the relative values of F and J with respect to either β or W. The boundary condition of vanishing Lagrangian pressure perturbation is

$$\lim_{r\to\mathcal{R}} \beta+p'\frac{e^{-\lambda/2}}{r^2}W=0\ , \tag{A4}$$

and thus determines the ratio of β to ρW at $\mathcal{R}$. The remaining freedom is represented in the relative values of $\beta/\rho W$ and F/J. As $W/\mathcal{R}^3 \gg J/\mathcal{R}, F$ for g-mode pulsations, the two independent solutions that are integrated are chosen to have initial values at $\mathcal{R}$ of $\{W=0, J=\mathcal{R}\}$ and $\{W=\mathcal{R}^3, F=J=0\}$ (in the first solution, F is chosen to satisfy the instantaneous gravity boundary condition on F/J). The second of these solutions is the predominant part of the actual eigenfunction; the first solution is a small correction.

To determine the value of F/J, equation (16g) is numerically integrated for a given ℓ and the table of values of $v/\mathcal{M}$ is kept. Once a static model (*i.e.*, $\mathcal{R}/2\mathcal{M}$) has been specified, the value of F/J is determined via equations (16) and (15c). I wish to emphasize that the integration of equation (16g) does not require anything other than a choice of ℓ, and that once $v/\mathcal{M}$ has been tabulated it can be used to determine F/J as a function of $\mathcal{R}/2\mathcal{M}$.

Application of the boundary condition of vanishing Lagrangian pressure perturbation is complicated by a singularity of the differential equations (14) at $\mathcal{R}$: *i.e.*, in equation (14d) p vanishes at $r=\mathcal{R}$ while W does not, and also β/p is divergent as $r\to\mathcal{R}$. The boundary condition (A4) is applied by reexpressing equations (14c), (14d), and (15a) in terms not of the Eulerian pressure perturbation β but the Lagrangian pressure perturbation X:

$$X=\beta+p'\frac{e^{-\lambda/2}}{r^2}W, \tag{A5a}$$

$$\frac{dX}{dr}=-\frac{\nu'}{2}\left[1+\frac{\ell(\ell+1)}{(\omega r)^2e^{-\nu}}\right]X-\left[\frac{p'}{2}\left[1-\frac{\ell(\ell+1)}{(\omega r)^2e^{-\nu}}\right]+\frac{\rho+p}{2r}\right]F \tag{A5b}$$

$$+p'\left[1+\frac{\ell(\ell+1)}{2(\omega r)^2e^{-\nu}}\right]K-\frac{\omega^2e^{-\nu}(\rho+p)}{2}\left[1+\frac{\ell(\ell+1)}{2(\omega r)^2e^{-\nu}}\right]J$$

$$-\frac{\rho+p}{r^2}\left\{e^{\lambda/2}\left[4\pi(\rho+3p)-\omega^2e^{-\nu}\left[1-\frac{8\pi r^2(\rho+p)}{\ell(\ell+1)}\right]\right]\right.$$

$$\left.-e^{-\lambda/2}\frac{\nu'}{r}\left[2+\frac{r\nu'}{4}\left[1-\frac{\ell(\ell+1)}{(\omega r)^2e^{-\nu}}\right]\right]\right\}W,$$

$$\frac{dW}{dr}=-r^2e^{\lambda/2}\left[1-\frac{\ell(\ell+1)\gamma p}{(\omega r)^2e^{-\nu}(\rho+p)}\right]\frac{X}{\gamma p}+\frac{\ell(\ell+1)\nu'}{2(\omega r)^2e^{-\nu}}W \tag{A5c}$$

$$+\frac{r^2e^{\lambda/2}}{2}\left[2K+\left[1+\frac{\ell(\ell+1)}{(\omega r)^2e^{-\nu}}\right](F+K)\right],$$

$$\mu=(\rho+p)\frac{X}{\gamma p}-\rho'\frac{e^{-\lambda/2}}{r^2}W. \tag{A5d}$$

Vanishing of the Lagrangian pressure perturbation and regularity of the perturbation requires that X/p remain finite as the surface of the star is approached and $p\to 0$. The ratio X/p at $\mathcal{R}$ is then X'/p' and is evaluated with equations (A5b) and (2d):

$$\frac{X}{p}=\frac{X'}{p'} \tag{A5e}$$

$$=-\left[\frac{1}{2}\left[1-\frac{l(l+1)}{(\omega r)^2e^{-\nu}}\right]-\frac{1}{r\nu'}\right]F+\left[1+\frac{l(l+1)}{2(\omega r)^2e^{-\nu}}\right]K$$

$$-\frac{2}{r^2\nu'}\left\{\omega^2e^{\lambda/2-\nu}+e^{-\lambda/2}\frac{\nu'}{r}\left[2+\frac{r\nu'}{4}\left[1-\frac{l(l+1)}{(\omega r)^2e^{-\nu}}\right]\right]\right\}W$$

$$+\frac{\omega^2e^{-\nu}}{\nu'}\left[1+\frac{l(l+1)}{2(\omega r)^2e^{-\nu}}\right]J\ .$$

With this expression for X and expression (A5e) for X/p, all references to X/p may be eliminated from the perturbation equations near the surface, leaving a non-singular set of equations.

The perturbation equations for F, J, and W are numerically integrated directly from the surface with the approximation X/p, β/ρ constant for a small distance. That distance is a fraction of the scale height of β/ρ at the surface, a fraction chosen to be consistent with the fractional accuracy (a part in 10^{-4}) of the Runge-Kutta integration. For

the solution with initial value $W=0$ at $\mathcal{R}$, β/ρ vanishes at $r=\mathcal{R}$, and grows linearly with $\mathcal{R}-r$. Since for g-modes this solution is a small correction to the $F=J=0$ solution, the scale height in this case is determined from the $\{W=\mathcal{R}^3, F=J=0\}$ solution. The reciprocal of the scale height of β/ρ at $\mathcal{R}$ in the case $\{W=\mathcal{R}^3, F=J=0\}$ is

$$\frac{1}{\text{scale height}} = \frac{(\beta/\rho)'}{\beta/\rho} = -\frac{\nu'}{2} + \frac{2\omega^2 e^{\lambda-\nu}}{\nu'} + \frac{\tilde{\gamma}}{\gamma\gamma_0} r^2 e^{\lambda/2} \frac{X}{p} \frac{1}{W} \tag{A6}$$

evaluated at $r=\mathcal{R}$.

After the two surface solutions are started in this fashion, the integration continues in F, J, W, and X until $X \cong \beta$ for one of the surface solutions. From that point onward, the variables used in the integration are F, J, W, and β. For g-modes, this change of variables typically occurs as soon as the X/p, β/ρ constant assumption is dropped.

Once the X/p, β/ρ constant assumption is dropped, the solutions are tabulated at every data grid point and at intermediate points, to insure that there are a minimum (typically 10 to 20) number of data points per e-folding distance from the surface. This is necessary because the eigenfunctions vary rapidly near the surface. Figure 2 shows the rapid variation in W and β/ρ with $\log((\mathcal{R}-r)/\mathcal{R})$ for the g_6 mode of Table 2. The point closest to the surface is the first point where β is allowed to vary independently of ρ. The abrupt "turn-on" of a non-zero $\tilde{\gamma}$ is responsible for the abrupt change in W and β/ρ at $(\mathcal{R}-r)/\mathcal{R} = 10^{-1}$.

Near the surface of the star, linear interpolation is not adequate to represent p and ρ, particularly as β/ρ and X/p are constant sources to the perturbation equations in this region. Logarithmic interpolation on the distance from the surface is used to determine ρ and p between points of the data grid. This procedure is more faithful to the true behavior of p and ρ near the surface than is linear interpolation.

2.4. CRITERION FOR AN EIGENFREQUENCY

At the midpoint of the star, four solutions of the perturbation equations are brought together and the demand is made that some linear combination of the core solutions match smoothly onto some linear combination of the surface solutions. As the perturbation equations are homogeneous, however, this problem is overdetermined and will have a solution only for special values of the frequency ω — the eigenfrequencies.

To have some measure of how close the trial frequency is to an eigenfrequency, the demand for continuity of F, J, W, and β at the midpoint is weakened: the unique core and surface solution (up to an overall scale) that matches F, J, and β smoothly at the midpoint is determined, and a measure of the discontinuity in W, the quantity

$$\varepsilon \equiv \frac{W_{\text{core}} - W_{\text{surface}}}{W_{\text{core}} + W_{\text{surface}}}, \tag{A7}$$

is determined (W_{core} and W_{surface} are the values of W, determined by the core and surface solutions, at the midpoint). Only at an eigenfrequency

will ε vanish. In practice, ε hovers about 1 when far from an eigenfrequency, passing through ∞, changing sign, and then passing through 0 near an eigenfrequency. The accuracy to which ε should vanish for an eigenfrequency is taken to be the fractional accuracy of the integrator (a part in 10^{-4} for the calculations reported here).

2.5. DETERMINING THE ENERGY IN THE PULSATIONS

Before determining the damping time, the energy in the pulsations must be determined. Equation (19) for the energy requires an upper bound $\mathcal{R}_\infty$ for the integration. The upper bound should be taken far out in the wave zone ($r \gg 1/\sigma$, σ the trial frequency) to insure that the power radiated as computed from the variational principle is the true power in gravitational radiation. In the slow-motion formalism, $\mathcal{R}_\infty$ is take to be $1/\sigma$, as this is where the instantaneous gravity approximation breaks down. For small $(\omega r)^2$ the choice of $\mathcal{R}_\infty$ is not very critical since the contribution to the pulsation energy from the near-zone gravitational field is a small fraction of the total pulsational energy: for small $(\omega r)^2$ equations (14d) and (15c) establish

$$\omega^2 W/\mathcal{R} \sim K. \tag{A8}$$

An order of magnitude calculation of the contribution of the vacuum integrals in equation (20) to the energy in the pulsation gives (recall the normalization of the perturbation $\xi^r/\mathcal{R}=1$ at $r=\mathcal{R}$):

$$\left[\begin{array}{l}\text{contribution of vacuum} \\ \text{integral pulsational energy}\end{array}\right] \approx \frac{l(l+1)}{4\pi}\frac{D^2}{\mathcal{R}^{2l+1}} \approx \frac{l(l+1)}{16\pi}(\omega\mathcal{R})^4\mathcal{R}\,. \tag{A9}$$

This is to be compared with the energy in the pulsation, which scales as $\mathcal{M}(\omega\mathcal{R})^2$. Thus, the errors committed by the instantaneous gravity approximation in the evaluation of the energy integral are at worst of order

$$\left[\begin{array}{l}\text{fractional errors committed} \\ \text{in the evaluation of energy}\end{array}\right] \sim O\left[(\omega\mathcal{R})^2\right] . \tag{A10}$$

Evaluation of the integrals in equation (20) is performed via the trapezoid rule; there are a sufficient number of data grid points available to make the gain in accuracy of a more sophisticated integration technique superfluous.

2.6. COMMENTS ON ACCURACY

The adaptive step-size algorithm used maintains the fractional error of the increment between steps below a fixed level of 10^{-4} in these calculations. Over most of the star the resolution demanded of the data grid (data points at least every 30 meters, see subsections 2, 3, 4) enforces a step size much smaller than necessary for that accuracy. As a crude check on the accuracy of the eigenfrequencies, the number of points per e-folding near the surface was halved and the maximum fractional error of the integrator was reduced to 10^{-3} and several high order g-modes reevaluated. Fractional changes in the periods were well below 10^{-4}; fractional changes in the damping times were at the 10^{-4} level.

APPENDIX B -- DERIVATIONS OF KEY EQUATIONS

This appendix describes the construction of the constraint equation (10) and the perturbation equations (14). The descriptions are based on the equations of Paper I; Paper I is necessary to follow the derivations.

The algebraic constraint that describes the relationship between K, H_0, H_1, β, and W (eq. [10]) is found in the following fashion:

i) eliminate V from the perturbation equations (I,8) and (I,9) with equation (9b), and use the resulting (I,8) and (I,9) in what follows,

ii) eliminate K'' from equation (I,8a) with equation (I,9a),

iii) eliminate W' from the result with equation (I,9c),

iv) eliminate H_0' from the result with equation (I,8c), and

v) eliminate K' from the result with equation (I,8b).

The perturbation equation for F' (eq. [14a]) is just equation (I,8c) with equations (13) and (12) (the definitions of F and J).

To derive equation (14b) for J'

i) combine $\frac{d}{dr}$(I,8b) with (I,8a) to eliminate K'', H_0', and W',

ii) eliminate K' from the result with (I,8b),

iii) reexpress H_1 with equation (12),

iv) eliminate W' with equation (I,9c), and

v) reexpress V and H_0 with equations (9b) and (13).

To find equation (14c)

i) eliminate V from (I,9b) with equation (9b),

ii) eliminate H_0' with (I,8c),

iii) eliminate K' with (I,8b),

iv) eliminate W' with (I,9c), and

v) reexpress H_0 and H_1 with equations (13) and (12).

Finally, equation (14d) for W' is just equation (I,9c) with V and H_0 reexpressed with equations (9b) and (13).

Table 1. Quadrupole f-mode periods and damping times for selected $n=1$ polytropes with $p\,(\mathrm{km}^{-2})=100[\rho(\mathrm{km}^{-2})]^2$.

Central Density (10^{15}g cm^{-3})	Radius (km)	Mass[a] (km)	Period (ms)		Damping Time (sec)		$(\omega\mathcal{R})^2$
			SM[b]	BDLS[c]	SM	BDLS	
3.0	8.86	1.87	.404	.348	.0849	.108	.21
2.0	9.67	1.66	.438	.412	.149	.155	.21
1.0	10.8	1.18	.577	.564	.474	.435	.15

[a] Recall that in geometrised units the Sun's mass is 1.477 km.

[b] Computed by the author with the slow-motion formalism.

[c] Computed by Balbinski et al. (1985) with no slow-motion approximation.

Table 2. Quadrupole g-modes for the model in Table 1 with $\rho_c = 10^{15}$g cm^{-3}.

Mode	Period	Damping time τ	Pulsation Energy[a]	$\tau\left[\frac{\omega\mathcal{R}}{2n-1}\right]^4$
	(ms)	(sec)	(10^{53} ergs)	(10^{13} sec)
1	50.38	1.734(+17)	23.2	2.13
2	93.84	2.038(+20)	14.0	2.61
3	136.7	9.286(+21)	9.84	3.36
4	179.3	1.444(+23)	7.59	4.58
5	221.8	1.220(+24)	6.16	6.07
6	264.3	7.151(+24)	5.19	7.92

[a] Normalised to $\xi^r/\mathcal{R}=1$ at surface of star.

Figure Captions

Figure 1.

Gravitational perturbations F and K (*cf.* eq. [13], [4]) vs. logarithmic fractional distance from the surface of a neutron star model (*cf.* §4, Tables 1, 2) with polytropic equation of state (eq. [21]) and central density $\rho_c = 1.0 \times 10^{-15}$ g cm^{-3}. This is the g_6 mode of Table 2. Note the magnitude of F relative to the magnitude of K — in the standard formalism F is calculated as the small difference between H_0 and K, leading to large numerical errors. The slow-motion formalism calculates F directly, avoiding the numerical errors of the standard formalism. The abrupt change in K near $1 - r/\mathcal{R} \approx 10^{-1}$ is due to the abrupt "turn-on" of $\tilde{\gamma}$ (*cf.* §4). For more details on the choice of perturbation variables, see the discussion in §3.1.

Figure 2.

Fluid perturbation $W/\mathcal{R}^3$ (*cf.* eq. [3a]) and β/ρ (*cf.* eq. [9]) versus logarithmic fractional distance from the surface of a neutron star model (*cf.* §4, Tables 1, 2) with polytropic equation of state (eq. [21]) and central density $\rho_c = 1.0 \times 10^{-15}$ g cm^{-3}. This is for the g_6 mode of Table 2. Note the rapid, large amplitude variations of W and β/ρ near the surface of the star. Note also how β/ρ asymptotes to a constant as $r \to \mathcal{R}$. G-modes are very sensitive to conditions at the surface of the star and care must be taken in treating the surface numerically. The abrupt

change in β/ρ near $1-r/\mathcal{R}\approx 10^{-1}$ is due to the abrupt "turn-on" of $\tilde{\gamma}$ (*cf.* §4). For more details on the numerical treatment of the surface, see Appendix A, §2.3.

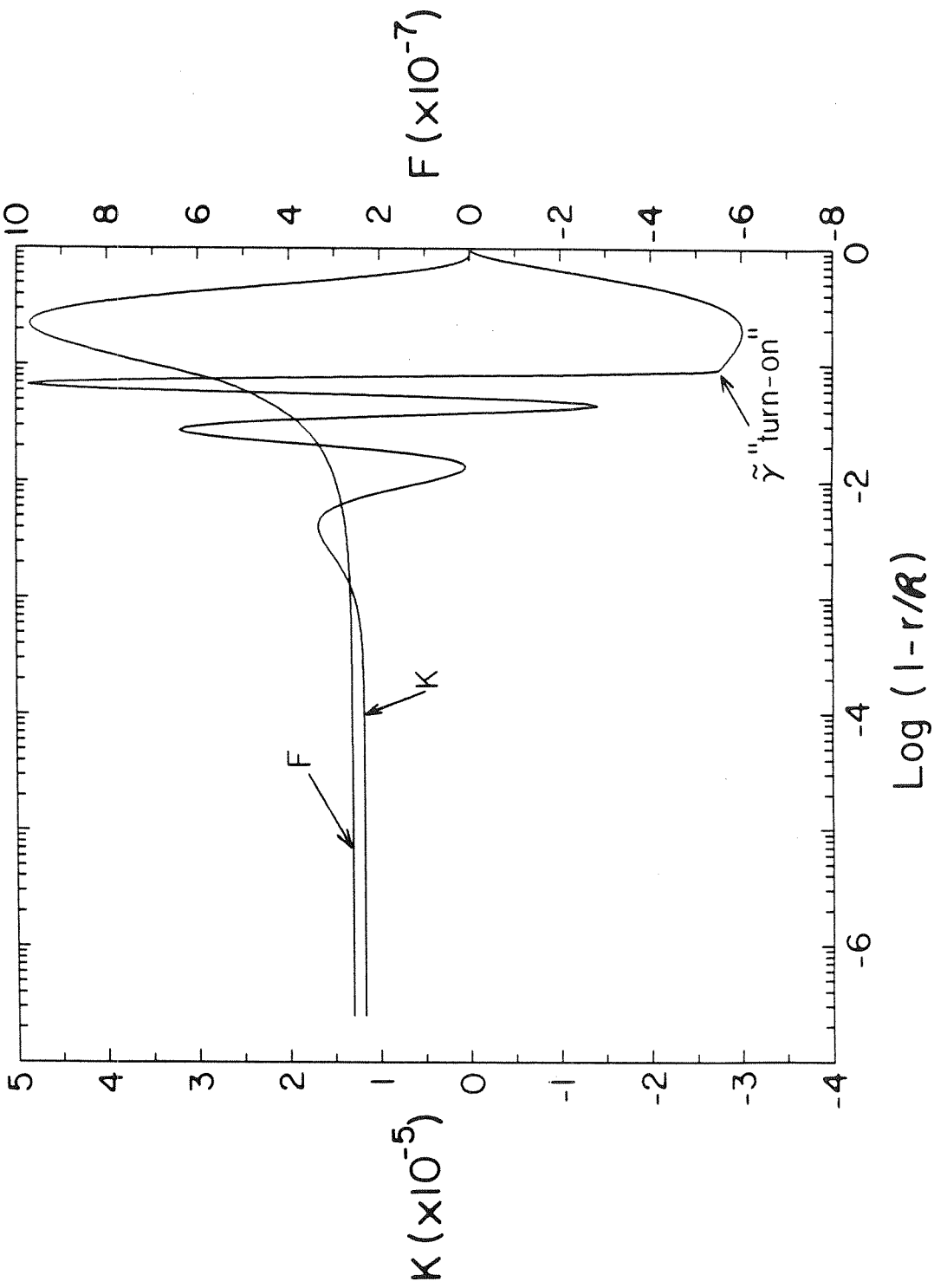

Figure 1

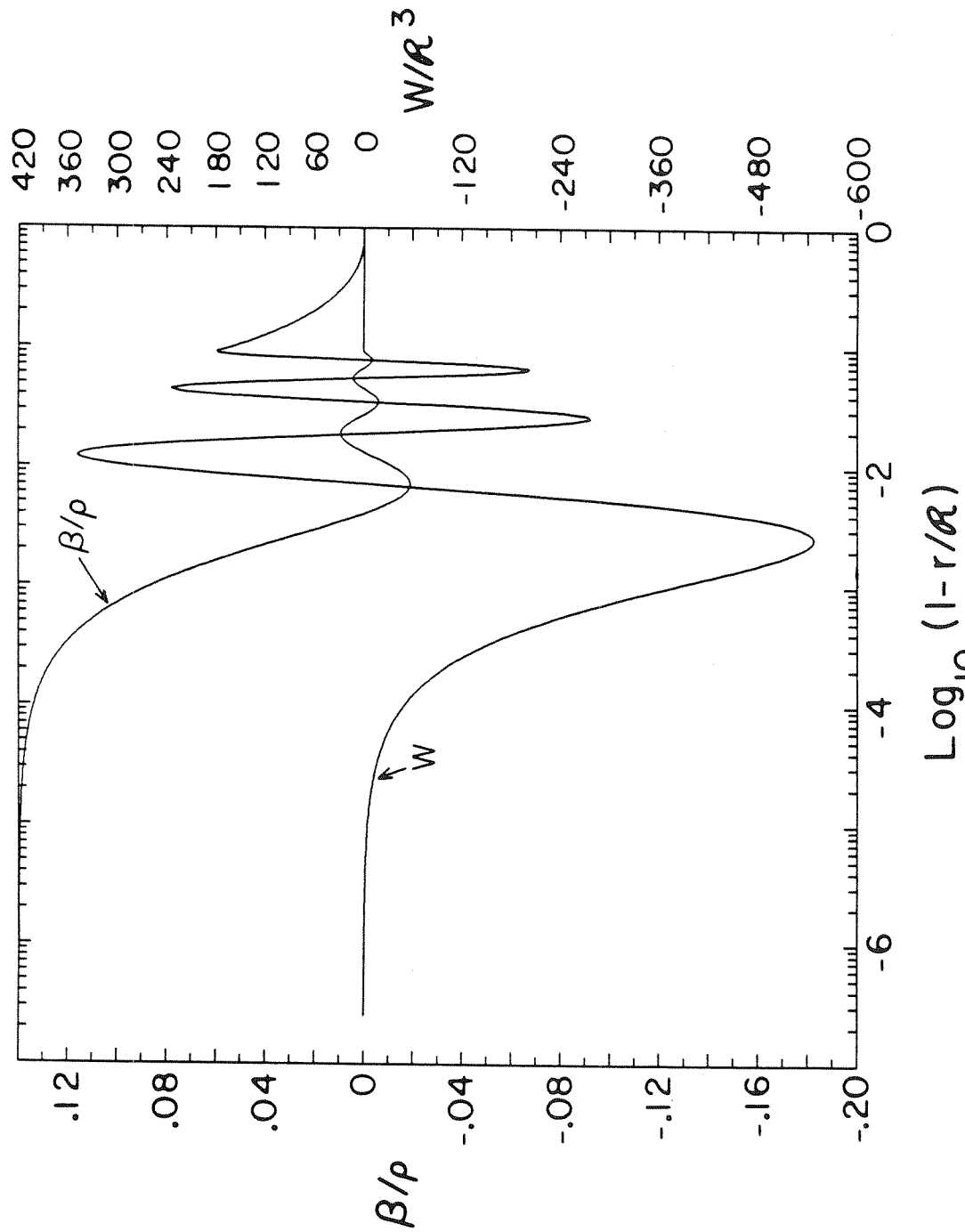
W/R^3
420
360
300
240
180
120
60
0
-120
-240
-360
-480
-600
β/ρ
W
.12
.08
.04
0
-.04
-.08
-.12
-.16
-.20
β/ρ
0
-2
-4
-6
Log10 (1- r/R)

Figure 2

Chapter 3

G-Modes In Zero Temperature Neutron Stars

Accepted for publication by *Monthly Notices of the Royal Astronomical Society.*

Abstract

It is well known that in an isentropic, perfect-fluid star, chemical inhomogeneities perturb some g-modes away from zero frequency. Here this phenomenon is studied for the idealized case of zero-temperature, perfect-fluid neutron stars. In realistic neutron stars, the chemical composition changes discontinuously several times at densities below neutron drip. Associated with each of these discontinuities are non-zero-frequency g-modes, referred to as discontinuity modes. There are only a finite number of discontinuity modes at fixed spherical harmonic order ℓ. In contrast, deviations from isentropy due to finite temperature in a neutron star also perturb some g-modes away from zero frequency. At fixed spherical harmonic order ℓ, there are a countable infinity of these finite-temperature modes.

The essential physics of discontinuity modes is captured by a simple physical analogy with gravity waves at the interface between two incompressible fluids. This analogy is exploited to provide estimates of the pulsation frequencies, energies, and damping times. The estimates are compared with detailed numerical calculations for simple model stars based on a polytropic equation of state, and for more complex model stars based on the equation of state of cold and fully catalyzed nuclear matter. The numerical calculations are done using the slow-motion approximation to the full theory of non-radial pulsations of relativistic stars. The highest frequency discontinuity modes in model stars based on the equation of state of cold and fully catalyzed nuclear matter have frequencies greater than the highest frequency finite-

temperature modes found by McDermott, Van Horn, & Scholl (1983); thus, chemical inhomogeneities in real neutron stars may be more important than finite temperature effects in determining the high-frequency end of the g-mode pulsation spectrum.

1. Introduction

1.1. MOTIVATION

Van Horn (1980) noted that certain observed neutron star phenomena take place with timescales that suggest g-mode pulsations of neutron stars. This led to the study of neutron star g-mode pulsations, a study that in recent years has revealed a rich spectrum of phenomena, which has been compared to the spectrum of terrestrial seismic modes (McDermott *et. al.* 1985).

In chemically homogeneous, zero-temperature (and hence isentropic) stars, all the g-modes are at zero frequency. Realistic stars, however, are neither chemically homogeneous nor isentropic. Deviations from isentropy due to finite temperature perturb some modes away from zero frequency. Such modes are referred to as "finite-temperature modes". Similarly, deviations from chemical homogeneity perturb some of the modes to non-zero frequency. These modes are referred to as "discontinuity modes."

In normal stars, discontinuity modes are unimportant and it is finite-temperature modes (modes due to a non-isentropic temperature gradient) that determine the g-mode spectrum. McDermott, Van Horn, & Scholl (1983) initiated work on g-mode pulsations of relativistic stars with a study of finite-temperature modes in neutron stars.

This paper examines discontinuity modes in neutron stars. Deviations from chemical homogeneity are particularly significant in

the surface regions of a neutron star. In the density regime 10^7 g cm$^{-3} \lesssim \rho \lesssim 10^{11}$ g cm^{-3}, the composition of a neutron star is thought to undergo a series of discontinuous transitions. Associated with each of these transitions are discontinuity modes. Discontinuity-mode frequencies are characteristically higher than the finite-temperature-mode frequencies found by McDermott, Van Horn, & Scholl; thus, chemical inhomogeneities in neutron stars may be more important in determining the high-frequency end of the g-mode spectrum than the effects of finite temperature.

The remainder of §1 describes the conventions and notation used throughout the remainder of this paper. The physical origins of g-modes are discussed in §2. Section 3 specializes to discontinuity modes, developing analytic results and intuitions necessary and useful for studying discontinuity modes. Results of numerical calculations, using the author's slow-motion approximation to the theory of non-radial pulsations of relativistic stars, are presented and discussed in §4. Conclusions are presented in §5. Appendix A is dedicated to a discussion of special problems arising in the numerical study of discontinuity modes.

1.2. CONVENTIONS AND NOTATION

All the numerical work described in this paper was carried out using the author's "slow-motion formalism." The slow-motion formalism was developed explicitly for studying g-modes in relativistic stars, and is described in Finn 1986. The reader is referred there for a

discussion of the conventions related to the formalism. Several particular conventions are noted here, however.

The metric signature used in this work is $(+---)$, and geometrised units ($G=c=1$, *cf.* box 1.8 of Misner, Thorne, & Wheeler 1973) are used throughout. Primes are used to denote a derivative with respect to the Schwarzschild-like radial coordinate r:

$$f' \equiv \frac{df}{dr} \ , \tag{1.1}$$

and square brackets about a quantity mean the discontinuity in that quantity:

$$[\rho]_r \equiv \lim_{\varepsilon \to 0} \{\rho(r+\varepsilon) - \rho(r-\varepsilon)\} \ . \tag{1.2}$$

The coordinate ("Eulerian") displacement of a fluid element undergoing pulsational motion is denoted $\vec{\xi}$. The stellar pulsations studied in this paper are all first-order perturbations about a static and spherically symmetric solution to the Einstein Field Equations; the line element representing that equilibrium solution is

$$ds^2 = e^{\nu(r)} dt^2 - e^{\lambda(r)} dr^2 - r^2 (d\theta^2 + \sin^2\theta d\phi^2) \ . \tag{1.3}$$

The perturbations are resolved into spherical harmonic angular dependence $Y_{\ell m}$ and exponential time dependence $\exp(-i\omega t)$ with complex frequency $\omega \equiv \sigma - i/\tau$ (σ and τ real). Since the equilibrium configuration is spherically symmetric, the perturbations at given angular order ℓ are $2\ell+1$ degenerate. When discussing the number of

pulsation modes in a star, fixed angular order ℓ is always assumed and the degeneracy in m ignored.

2. G-Mode Pulsations

In the discussion that follows, it is useful to identify a characteristic angular frequency related to the passage of sound waves around the circumference of a star:

$$\omega_0^2 \equiv \frac{p_c}{\rho_c}\frac{\ell(\ell+1)}{\mathcal{R}^2}$$

$$= (1.7\times10^4\ \mathrm{s}^{-1})^2 \left[\frac{\ell(\ell+1)}{6}\right]\left[\frac{10\ \mathrm{km}}{\mathcal{R}}\right]^2$$

$$\left[\frac{p_c}{5\times10^{35}\ \mathrm{dyne\ cm}^{-2}}\right]\left[\frac{10^{15}\ \mathrm{g\ cm}^{-3}}{\rho_c}\right] . \qquad (2.1)$$

In equation (2.1), ρ_c, p_c, and $\mathcal{R}$ represent the central energy density, central pressure, and radius of the star. The characteristic frequency ω_0 increases with ℓ as $L \equiv \{\ell(\ell+1)\}^{1/2}$ because of the increasing number of transverse nodes in the stationary sound wave.

In 1941, Cowling recognized that the Eulerian perturbation of the gravitational potential could be safely neglected in the study of Newtonian stellar pulsations (the "Cowling approximation"). The Cowling approximation permits the spectrum of Newtonian non-radial stellar pulsations to be separated analytically into three distinct regimes: the p-mode regime, the f-mode regime, and the g-mode regime. At fixed spherical harmonic order ℓ, the p-mode (pressure mode) regime is one

of high frequency ($\omega_p \gtrsim \omega_0$), with the fluid displacement predominantly radial, characterized by large Eulerian pressure perturbations, and reminiscent of longitudinal pressure waves. At each l, a star has a single f-mode (fundamental mode), characterized by Cowling as having a radially unchanging sign of the radial fluid displacement and the Eulerian density perturbation. The f-mode frequency is $\omega_f \approx \omega_0/l$ and lies below the lowest p-mode frequency. The g-mode (gravity mode) spectrum forms a low-frequency regime ($|\omega_g|^2 \lesssim \omega_0^2$), characterized by large transverse fluid displacement and small Eulerian pressure perturbations. At fixed l, the single f-mode separates the g-mode and the p-mode spectra.

Aside from the small imaginary part of a complex eigenfrequency associated with radiative boundary conditions (*e.g.*, damping owing to gravitational radiation) and other damping or driving mechanisms (viscosity, phase lags in opacity, etc.), a stellar model always has a real frequency f-mode and p-mode spectrum. The same is not true of g-modes: when damping mechanisms are ignored, a given stellar model may have any combination of real frequency g-modes, imaginary-frequency g-modes, or zero frequency g-modes. The squared frequency of a star's g-modes are closely related to its stability against convection: real, imaginary, and zero frequency modes correspond to convective stability, instability, and marginal stability. The g-modes present in a star depend on the radial variations in the specific entropy and chemical composition.

The importance of the specific entropy in a g-mode pulsation may be seen by following a fluid element undergoing a small, slow (compared to the local sound speed), radial displacement outward. As it rises, the element expands, remaining nearly in pressure equilibrium. Two fluid elements in pressure equilibrium but with different specific entropies have different densities. When the specific entropy of the surrounding unperturbed fluid is greater than that of the displaced element, the displaced element's density is greater than that of the unperturbed fluid; thus, the star's gravity provides a force to restore the displaced element to its original location (stability to convection). When the radial entropy gradient is equal to or less than zero, the displaced fluid element is of equal or lower density than the unperturbed fluid and gravity provides either no force (marginal stability) or a force to increase the displacement (instability to convection).

To first order in small quantities, the buoyancy force-per-unit-volume f_N acting on a fluid element displaced for a small radial distance δr in a Newtonian star is

$$f_N = g_N \rho \frac{dp}{dr}\left[\frac{1}{\Gamma_0 p} - \frac{1}{\rho}\frac{\Delta\rho}{\Delta p}\right]\delta r \quad , \tag{2.2}$$

where

$$\rho \equiv \begin{bmatrix}\text{energy}\\ \text{density}\end{bmatrix} \quad , \qquad p \equiv (\text{pressure}) \quad ,$$

$$g_N \equiv \begin{bmatrix}\text{(positive)}\\ \text{Newtonian}\\ \text{gravitational}\\ \text{acceleration}\end{bmatrix} = \frac{m(r)}{r} \quad , \quad \Gamma_0 \equiv \frac{dp/dr}{d\rho/dr}\frac{\rho}{p} \quad ,$$

$$\Delta p \equiv \begin{bmatrix}\text{Lagrangian}\\ \text{pressure}\\ \text{perturbation}\end{bmatrix} = \frac{dp}{dr}\delta r \quad , \quad \Delta\rho \equiv \begin{bmatrix}\text{Lagrangian}\\ \text{density}\\ \text{perturbation}\end{bmatrix} . \tag{2.3}$$

The derivatives dp/dr and $d\rho/dr$ are evaluated in the unperturbed star and the fluid element is presumed to maintain pressure equilibrium with its surroundings so that $\Delta p = (dp/dr)\delta r$. The Lagrangian density perturbation $\Delta\rho$ typically reflects an adiabatic displacement with chemical composition held constant — though in the rare case that heat can flow in and out of a fluid element or reactions can occur in it on the timescale of a pulsation period, $\Delta\rho$ is influenced accordingly.

The quantity

$$A_N \equiv \frac{dp}{dr}\left(\frac{1}{\Gamma_0 p} - \frac{1}{\rho}\frac{\Delta\rho}{\Delta p}\right) \tag{2.4}$$

(with the subscript N for Newtonian theory) is related to the Schwarzschild convection criterion. The relativistic generalizations of f_N and A_N are

$$f \equiv g(\rho + p)Ae^{\lambda/2}\delta r \quad , \tag{2.5}$$

$$A \equiv e^{-\lambda/2}\frac{dp}{dr}\left(\frac{1}{\gamma_0 p} - \frac{1}{\rho + p}\frac{\Delta\rho}{\Delta p}\right) , \tag{2.6}$$

where

$$\gamma_0 \equiv \frac{\rho + p}{p}\frac{dp/dr}{d\rho/dr} . \tag{2.7}$$

Where $A < 0$, the local buoyancy force is restoring and the star is stable

against convection; where $A \geq 0$, the star is neutrally stable or unstable against convection. The quantity A is referred to as the relativistic convective stability discriminant.

The relativistic buoyancy force density f (eq. 2.5) determines a frequency characteristic of local fluid oscillations. The relativistic Brunt-Väisälä frequency N,

$$N^2 \equiv -Ag = \frac{f}{(\rho+p)e^{\lambda/2}\delta r} \quad , \tag{2.8}$$

is the locally measured frequency with which a fluid element "bobs" about its equilibrium location.

The perturbation enters into the local pulsational frequency through the term $\Delta\rho/\Delta p$ in A. The first law of thermodynamics expressed in terms of $\Delta\rho$ is

$$\Delta\rho = T\Delta s + \sum_i \mu_i \Delta n_i \quad , \tag{2.9}$$

where the temperature T, the entropy density s, the chemical potential μ_i (including the rest mass) and the baryon density n_i for chemical species i, are measured by local observers. When the temperature vanishes, ρ is a function only of the n_i and is independent of s; consequently, only when the chemical composition of a perturbed fluid element differs from that of its surroundings (n_i/n_j not constant throughout the star) are A and N non-zero. Thus, only when the zero-temperature star's chemical composition is not homogeneous does a perturbed fluid element, which typically maintains its own composition

because nuclear reactions proceed so slowly, experience a buoyancy force that perturbs g-modes to finite frequency. The remainder of this paper is concerned with the pulsations caused by chemical inhomogeneities in zero-temperature stars.

3. Analytic Results

3.1. G-MODES FROM RADIALLY VARYING COMPOSITION – INTRODUCTION

In a g-mode pulsation, a displaced fluid element remains (roughly) in pressure equilibrium with its surroundings at all times; therefore, for a restoring force to act on the displaced element, pressure equilibrium must not correspond to density equality. As discussed in §2, in an isentropic zero-temperature star, variations in the chemical potentials μ_i control the relationship between density equality and pressure equilibrium for a perturbed fluid element; in order that they not correspond, the star's composition must vary with radius and a radially displaced fluid element must not alter its composition to match its surroundings. Gravity then provides a buoyancy force acting on the displaced fluid element.

The composition of a real neutron star does vary radially from surface to core. During the star's past history, shell burning, accretion, and flash nuclear burning built up layers of varying composition on the surface of the star, leaving a characteristic radial composition profile related to the star's progenitor and thermal history; even zero-temperature neutron stars made of fully catalyzed nuclear matter have

a distinctive radial composition profile.

Thus, the radial composition in a neutron star is layered: layers of homogeneous chemical composition lie one on top of another and at the interface between the layers, the composition changes abruptly. In a zero-temperature star, only a fluid element displaced across one of these boundaries feels a restoring force owing to gravity.

For there to be finite-frequency discontinuity-mode pulsations, it is also necessary that a displaced fluid element not adjust its composition to its surroundings during a pulsation. This is the case when the timescale for nuclear-reaction-induced composition change is much greater than the period of the pulsations.

Except in regions where shell burning or flash nuclear burning is occurring, at densities below neutron drip ($\rho_{drip} \equiv 4.3\times10^{11}$ g cm^{-3}), pyconuclear reactions govern the evolution of a neutron star's composition, and the corresponding reaction rates are all on the order of the age of the universe (Meltzer & Thorne 1966). This is apparent when one considers the thermal history of a neutron star.

An isolated neutron star cools rapidly after formation; within 10^5 years, the internal temperature is less than 10^7°K (Tsuruta 1979). At these temperatures, and at densities below ρ_{drip}, the zero-temperature pyconuclear reaction rates apply (Salpeter & Van Horn 1969).

A steadily accreting neutron star reaches an equilibrium state within $\sim10^5$ years after the onset of accretion. In this equilibrium state, energy generation by nuclear burning balances energy loss by photons

and neutrinos. For a mass accretion rate $\sim 3\times10^{-10} M_{\odot}\,\mathrm{yr}^{-1}$, the base of the hydrogen burning shell is at a density $\rho_{H}\sim 10^{6}\,\mathrm{g\,cm}^{-3}$ and temperatures everywhere are less than $T\lesssim 3\times10^{8}$°K (Fujimoto *et al.* 1984). At densities above ρ_{H}, the nuclear reaction rates are well approximated by the zero-temperature pyconuclear reaction rates (Salpeter & Van Horn).

Accretion is rarely steady (in X-ray bursters it varies on timescales of days), and so this equilibrium state is seldom achieved; however, temperatures in the interior of a neutron star reflect the average accretion rate, not the transients; so pyconuclear reaction rate still apply above shell and flash burning densities.

Calculations of the equation of state of cold and fully catalyzed nuclear matter provide an explicit example of composition discontinuities in a neutron star. In the density range $10^{7}\,\mathrm{g\,cm}^{-3}\lesssim\rho\lesssim\rho_{\mathrm{drip}}$, Salpeter (1961) and later Baym, Pethick, & Sutherland (1971) found that the chemical composition of cold and fully catalyzed matter varies discontinuously with pressure in a series of first-order phase transition. The calculations of Baym, Pethick, & Sutherland differed from those of Salpeter primarily by the inclusion of the effects of the Coulomb lattice, and revealed 11 discrete composition transitions. Within any given region the composition is homogeneous; at certain pressures the energetically stable nucleus changes and the chemical composition of fully catalyzed nuclear matter reflects that change.

A change in chemical composition appears as a density discontinuity in a cold and fully catalyzed neutron star. The star's composition is homogeneous between each discontinuity, and to a slightly perturbed fluid element, pressure equilibrium corresponds to density equality. At the radii where the composition changes, perturbed fluid of one composition crosses into a region of different composition and pressure equilibrium no longer corresponds to density equality; thus, the perturbed fluid element feels a buoyancy force. The resulting non-zero frequency modes are called discontinuity modes.

Naive applications of the usual techniques for calculating g-mode pulsation frequencies fail when applied to discontinuity modes. The remainder of §3 extends the author's slow-motion formalism to permit treatment of discontinuity modes, and develops a physical model of the modes to anticipate the numerical results presented in §4.

3.2. APPROXIMATIONS AND ASSUMPTIONS

The calculations reported in this paper approximate neutron stars as zero-temperature, perfect-fluid spheres composed of fully catalyzed nuclear matter. The calculations were carried out using the slow-motion formalism, described in Finn (1986). Realistic neutron stars are not at zero temperature, they are not composed of fully catalyzed nuclear matter, and they are not perfect-fluid spheres. While large magnetic fields and rapid rotation modify significantly the pulsation spectrum of a neutron star, they do not change the underlying mechanism of the pulsations. In this section, the approximations that neutron stars are

zero-temperature and composed of fully catalyzed nuclear matter are discussed.

This paper is concerned with discontinuity modes, not finite-temperature modes; thus, the direct effect on the g-mode pulsational spectrum of a specific entropy gradient at finite temperature is ignored. A non-zero temperature affects the g-mode pulsational spectrum in another way, however: it causes diffusion across the boundaries separating regions of different composition, altering the chemical composition gradients from those of a zero-temperature star. In the density regime $10^7\,\mathrm{g\,cm^{-3}} \lesssim \rho \lesssim \rho_{\mathrm{drip}}$, the nuclei are tightly bound in a Coulomb lattice and this thermal diffusion is negligible; thus, the composition transitions are well approximated as discontinuous.

Neutron stars are not composed of fully catalyzed nuclear matter; the nuclear processes that change atomic number take place on too long a timescale in neutron stars (Zel'dovich & Novikov 1971). The actual chemical composition of neutron stars at densities below ρ_{drip} depends on the history of the star. Nonetheless, it is reasonable to approximate a neutron star as composed of fully catalyzed nuclear matter at densities $\rho \gtrsim 10^6\,\mathrm{g\,cm^{-3}}$, above the place where nuclear burning of accreted material typically occurs: discontinuity mode character depends only on the fractional density discontinuities and their locations, and in a realistic star these are at least as large as those in a star composed of fully catalyzed nuclear matter.

The assumption that neutron stars are composed of fully catalyzed matter thus avoids features of the discontinuity mode pulsational

spectrum peculiar to particular neutron stars and environments, and draws attention to generic features of the spectrum.

The effect on the pulsation spectrum of a crust with a non-zero elastic shear modulus is also ignored in this paper. Thus far, the formalism for studying fully general-relativistic stellar pulsations has been extended to include an isotropic shear modulus only for torsional (odd-parity) pulsations (Schumaker & Thorne 1983); in a forthcoming paper, I will extend the formalism to permit an isotropic shear modulus in the even-parity pulsation case.

The assumption of perfect fluidity eliminates viscosity as a damping mechanism for the g-mode pulsations. Throughout this paper, all damping mechanisms except for gravitational radiation are ignored. Particularly for g-mode pulsations, gravitational radiation is an ineffective damping mechanism for the pulsations; in more realistic neutron stars, electromagnetic radiation damping (owing to the "shaking" of a magnetic field locked in to the neutron star) and viscous damping are much more significant (for the effects of electromagnetic damping, *cf.* McDermott *et al.* 1984; for the effects of viscosity and thermal conductivity, *cf.* Cutler & Lindblom 1986). The gravitational radiation damping times discussed in later sections are thus not to be interpreted as estimated pulsational damping times for realistic neutron stars. The damping times reported here are significant as a measure of the distribution of pulsational energy between the fluid motion and the gravitational perturbations, and also in the context of gravitational radiation theory, where they provide a non-trivial example

of the productions of weak gravitational radiation in a strong field, compact object.

3.3. BOUNDARY CONDITIONS AND PULSATIONAL ENERGY FOR DISCONTINUITY MODES

The eigenproblem (eigenequations and boundary conditions) for g-mode pulsations in the slow-motion formalism as formulated in Finn (1986) assumes a continuous density distribution and thus requires modification to handle discontinuity modes. In particular, boundary conditions must be specified at the locations of the density discontinuities, and the expression for the pulsational energy (Finn 1986, eq. 19) must be modified. This subsection reviews the slow-motion formalism and extends it to allow the evaluation of g-modes for stars with discontinuous equations of state.

A principal difference between the slow-motion formalism and previous formalisms for studying g-modes is the choice of perturbation variables. The slow-motion formalism recognizes the low-frequency character of g-mode pulsations, and the perturbation variables are chosen accordingly:

$$W \equiv r^2 e^{\lambda/2} \xi^r / Y_{lm} \ , \tag{3.1}$$

$$\beta \equiv \delta p / Y_{lm} = -(\omega^2 e^{-\nu} V + H_0/2)(\rho + p) \ , \tag{3.2}$$

$$J \equiv H_1 - \frac{16\pi e^{\lambda/2}(\rho+p)}{l(l+1)} W \ , \tag{3.3}$$

$$F \equiv H_0 - K \quad . \tag{3.4}$$

The fluid's radial displacement function W and Eulerian pressure perturbation β represent the fluid degrees of freedom. The quantity V appearing in equation (3.2) is related to the transverse displacement of the fluid:

$$V \equiv -r^2 \xi^\theta / \partial_\theta Y_{\ell m}$$

$$= -r^2 \xi^\phi / \sin^2\theta \, \partial_\phi Y_{\ell m} \quad . \tag{3.5}$$

The variables F and J embody the gravitational perturbation. Equations (3.3) and (3.4) express them in terms of the metric perturbations H_0 and K in Regge-Wheeler (1957) gauge: the perturbed line element in Regge-Wheeler gauge, specialized to even-parity perturbations with no anisotropic stresses, is

$$ds^2 = e^\nu (1 + H_0 Y_{\ell m}) dt^2 + \frac{dH_1}{dt} \, dt \, dr - e^\lambda (1 - H_0 Y_{\ell m}) dr^2 - r^2 (1 - K Y_{\ell m}) d\Omega^2 \quad . \tag{3.6}$$

Note that the definition of H_1 used here differs from the Regge-Wheeler definition by a time derivative.

Where the equation of state is discontinuous, some of the perturbation variables are discontinuous; correspondingly, the differential equations that govern the perturbations require boundary conditions in the form of jump conditions on the perturbation variables across the discontinuities:

$$[W] = 0 \quad , \quad [\beta] = \frac{\nu'}{2} [\rho] \frac{e^{-\lambda/2}}{r^2} W \quad ,$$

$$[F]=0 \ , \quad [J]=-[\rho]\frac{16\pi e^{\lambda/2}}{l(l+1)}W \ . \tag{3.7}$$

These conditions are arrived at by straightforward "pillbox" integration of the differential equations (Finn 1986, eqs. 14a-d). The jump condition on the Eulerian pressure perturbation β is equivalent to the continuity of the Lagrangian pressure perturbation across the density discontinuity.

In the slow-motion formalism, the damping time of a pulsational mode owing to gravitational radiation is the ratio of the pulsational energy to the power in gravitational radiation. The pulsational energy is the conserved quantity associated with a variational principle developed for relativistic stellar pulsations by Detweiler & Ipser (1973). The expression for the energy in the pulsations is (Finn 1986 eq. 19):

$$\mathcal{E}(\sigma,\mathcal{R}_\infty,t)\equiv\int_0^{\mathcal{R}_-}|\sigma r|^2 dr\ e^{(\lambda-\nu)/2}\left\{\frac{(\rho+p)}{2}\left(\left|\frac{W}{r^2}\right|^2+l(l+1)\left|\frac{V}{r}\right|^2\right)\right.$$

$$\left.-\frac{l(l+1)e^{-\lambda}}{32\pi r^2}|H_1|^2-\frac{1}{32\pi}\left(2H_0K+|K|^2\right)\right\}$$

$$+\frac{1}{2}\int_0^{\mathcal{R}_-}r^2 dr e^{(\nu+\lambda)/2}\left\{p\gamma_0\left|\frac{\mu}{\rho+p}\right|^2+\frac{e^{-\lambda}}{8\pi}K'(H_0'+\nu'H_0)\right.$$

$$\left.+\frac{\gamma A e^{\lambda/2}}{(\rho+p)^2 p'}\left|\mu+\frac{e^{-\lambda/2}}{r^2}\rho' W\right|^2+H_0\mu\right.$$

$$+\left\{\frac{l(l+1)}{16\pi r^2}-\frac{3}{4}(\rho+p)\right\}|H_0|^2-\frac{e^{-\lambda}}{16\pi}|K'|^2\Bigg]$$

$$+\frac{r^2}{2}\left[\rho\frac{e^{-\lambda/2}}{r^2}WH_0-p'\frac{e^{-\lambda}}{r^4}|W|^2\right]_{r=\mathcal{R}}. \tag{3.8}$$

Here μ is the Eulerian density perturbation

$$\mu\equiv\frac{\rho+p}{\gamma p}\left[\beta+\frac{dp}{dr}\frac{e^{-\lambda/2}}{r^2}W\right]-e^{-\lambda/2}\frac{\rho'}{r^2}W \tag{3.9}$$

and γ is the adiabatic index for the pulsating fluid:

$$\gamma\equiv\frac{\Delta p}{\Delta\rho}\frac{\rho+p}{p}\ , \tag{3.10}$$

where (*cf.* eq. 3.1)

$$\Delta p\equiv\begin{bmatrix}\text{Lagrangian}\\ \text{pressure}\\ \text{perturbation}\end{bmatrix}=\beta+\frac{dp}{dr}\frac{\exp(-\lambda/2)}{r^2}W\ ,\quad \Delta\rho\equiv\begin{bmatrix}\text{Lagrangian}\\ \text{density}\\ \text{perturbation}\end{bmatrix}\ . \tag{3.11}$$

Note that $\gamma\neq\gamma_0$, unless the star is isentropic and chemically homogeneous. The integral is evaluated throughout a sphere of radius $\mathcal{R}_\infty\gg\mathcal{R}$.

At the density discontinuities, ρ' and μ are infinite; hence the integrand of equation (3.8) is infinite and cannot be integrated numerically. At each discontinuity r_i, the singular contributions to the integrand are

$$\lim_{\varepsilon\to 0}\frac{1}{2}\int_{r_i+\varepsilon}^{r_i-\varepsilon} dr\, r^2 e^{(\nu+\lambda)/2}\left[H_0\mu+p\gamma_0\left|\frac{\mu}{\rho+p}\right|^2\right.$$

$$\left.+\frac{\gamma A e^{\lambda/2}}{(\rho+p)^2 p'}\left|\mu+e^{-\lambda/2}\frac{\rho'}{r^2}W\right|^2\right]. \qquad (3.12)$$

A straightforward calculation shows the integrand of equation (3.12) to be a continuous quantity times ρ', which is trivially integrated to give

$$-\frac{1}{2}e^{\nu/2}W\left[\frac{\nu' e^{-\lambda/2}}{2r^2}W+H_0\right][\rho]_{r_i}. \qquad (3.13)$$

This, then, is the contribution to the energy in the pulsations from the singularity at r_i in the integrand of equation (3.8).

The final expression for the energy in the pulsations, valid in the presence of equation of state discontinuities, is thus

$$\mathcal{E}(\sigma,\mathcal{R}_\infty,t)\equiv\sum_{i=1}^{N}-\tfrac{1}{2}e^{\nu/2}W\left[\frac{\nu' e^{-\lambda/2}}{2r^2}W+H_0\right][\rho]_{r_i}$$

$$+\int|\sigma r|^2 dr\; e^{(\lambda-\nu)/2}\left[\frac{(\rho+p)}{2}\left\{\left|\frac{W}{r^2}\right|^2+l(l+1)\left|\frac{V}{r}\right|^2\right\}\right.$$

$$\left.-\frac{l(l+1)e^{-\lambda}}{32\pi r^2}|H_1|^2-\frac{1}{32\pi}(2H_0K+|K|^2)\right]$$

$$+\frac{1}{2}\int r^2 dr e^{(\nu+\lambda)/2}\left[p\gamma_0\left|\frac{\mu}{(\rho+p)}\right|^2+\frac{\gamma A\exp(\lambda/2)}{(\rho+p)^2 p'}\left|\mu+\frac{e^{-\lambda/2}}{r^2}\rho' W\right|^2\right.$$

$$+H_0\mu+\left\{\frac{l(l+1)}{16\pi r^2}-\frac{3}{4}(\rho+p)\right\}|H_0|^2+\frac{e^{-\lambda}}{8\pi}K'(H_0'+\nu'H_0-\frac{1}{2}K')\Bigg]$$

$$+\frac{r^2}{2}\left[\rho\frac{e^{-\lambda/2}}{r^2}WH_0-p'\frac{e^{-\lambda}}{r^4}|W|^2\right]_{r=\mathcal{R}}. \tag{3.14}$$

The N discontinuities in the equation of state are located at r_i, and $\int$ is defined to mean

$$\int \equiv \lim_{\varepsilon\to 0}\left[\int_0^{r_1-\varepsilon}+\int_{r_N+\varepsilon}^{\mathcal{R}_-}+\sum_{i=1}^{N-1}\int_{r_i+\varepsilon}^{r_{i+1}-\varepsilon}\right]. \tag{3.15}$$

Expression (3.14) is also valid in the presence of deviations from isentropy at a finite temperature, in which case A does not vanish. The remainder of this paper is concerned with zero-temperature stars, so A does vanish.

3.4. NUMBER OF G-MODES

In the Cowling approximation, the Newtonian perturbation equations can be cast as a second-order wave equation that is a Sturm-Liouville equation in two different limits. In the limit $\omega^2/\omega_0^2\gg 1$, the equation describes the p-mode regime, and in the limit $\omega_0^2/l\omega^2\gg 1$, it describes the g-mode regime. The Sturm-Liouville nature of the Newtonian perturbation equations permits strong statements about the behavior of pulsation frequencies and eigenfunctions, and many of the qualitative results from the Newtonian analysis should also hold in the relativistic case.

The qualitative nature of the g-mode spectrum in Newtonian stars is understood when the Newtonian convective discriminant A_N is continuous. There are a countable infinity of real frequency (stable) g-modes when anywhere in the star $A_N<0$. This spectrum of stable g-modes has a maximum frequency, and an accumulation point at zero frequency. When anywhere in the star $A_N>0$, there is a countable infinity of imaginary frequency (unstable) g-modes with a maximum growth rate ($|\omega|$ bounded) and an accumulation point at zero growth rate. Finally, there are an infinity of zero-frequency (marginally stable) modes when there is an extended region where $A_N=0$. The proof of these results relies on the Sturm-Liouville character of the Newtonian equations in the Cowling Approximation; the results are generally believed to be true also in the relativistic case, with A_N replaced by A, but a rigorous proof has been given only for the case $A=0$ (Thorne 1966).

This paper is concerned with zero-temperature stars where the chemical composition varies discontinuously but is otherwise homogeneous. Here the relativistic convective discriminant A vanishes everywhere except at the radii r_i, where the composition changes discontinuously. At these radii, the adiabatic index γ (eq. 3.10) remains finite while the index γ_0 (eq. 2.7) vanishes; thus, A is infinite at r_i. If the lower density fluid is above the higher density fluid, then A is negatively infinite at r_i, and it is positively infinite if the fluids are inverted.

In the Newtonian case, it is strictly true that at fixed spherical harmonic order ℓ there is one and only one non-zero frequency g-mode

for each point r_i where A is infinite and negative (Gabriel & Scuflaire 1979); below, I show that this result also holds in the relativistic case.

To begin, consider the Newtonian case. The linearized perturbations of the continuity and Euler equations govern the linear pulsations of a Newtonian zero-temperature, self-gravitating perfect-fluid sphere. To maintain contact with the relativistic case, use analogously defined variables:

$$\beta_N \equiv \delta p / Y_{lm} = \begin{bmatrix} \text{Eulerian pressure} \\ \text{perturbation} \end{bmatrix}, \quad W_N \equiv r^2 \xi^r / Y_{lm}, \quad V_N \equiv r^2 \xi^\theta / \partial_\theta Y_{lm} \ . \tag{3.16}$$

The subscript N reminds us that these perturbation variables are Newtonian analogs of the relativistic slow-motion variables β, W, and V.

Assuming time dependence $\exp(-i\sigma t)$, the linearized continuity equation is

$$\rho \left[\frac{\beta_N}{\Gamma p} - A_N \frac{W_N}{r^2} + \frac{W_N'}{r^2} - \frac{l(l+1)}{r^2} V_N \right] + \frac{\rho' W_N}{r^2} = 0 \ , \tag{3.17}$$

and the linearized Euler equations are

$$-\sigma^2 \rho \frac{W_N}{r^2} = -\beta_N' - g \left[\frac{\rho}{\Gamma p} \beta_N - \rho A_N \frac{W_N}{r^2} \right] \ , \tag{3.18}$$

$$\sigma^2 \rho \frac{V_N}{r^2} = \frac{\beta_N}{r^2} \ . \tag{3.19}$$

The adiabatic index Γ and the Newtonian convective discriminant A_N appearing here are

$$\Gamma \equiv \frac{\rho}{p}\frac{\Delta p}{\Delta \rho} \quad , \quad A_N \equiv \left(\frac{1}{\Gamma_0 p} - \frac{1}{\rho}\frac{\Delta \rho}{\Delta p} \right) \frac{dp}{dr} \quad . \tag{3.20}$$

Note that the adiabatic index Γ differs from the index Γ_0 that characterizes the star's equilibrium distribution:

$$\Gamma_0 \equiv \frac{\rho}{p}\frac{dp/dr}{d\rho/dr} \quad . \tag{3.21}$$

There are three kinds of boundary conditions on equations (3.17-19). At $r=0$, regularity requires that W_N, V_N, and β_N vanish. At $r=\mathcal{R}$ (where $\mathcal{R}$ denotes the surface of the star), the Lagrangian pressure perturbation $\beta_N + W_N p'/r^2$ must vanish. Finally, at each point r_i where the density is discontinuous and A_N is infinite, there are jump conditions on the perturbation variables:

$$[W_N]=0, \text{ and } [\beta_N]=g_N[\rho]W_N/r^2 \quad , \tag{3.22}$$

where g_N denotes the positive Newtonian gravitational acceleration. These jump conditions are analogous to the relativistic jump conditions (eq. 3.7).

The continuity and Euler equations (3.17) and (3.18) combine to form a second-order linear differential equation for β_N:

$$\frac{d}{dr}\left(\frac{d}{dr}\beta_N + \frac{g_N \rho}{\Gamma p}\beta_N \right) = \frac{\sigma^2 + g_N A_N}{\sigma^2}\left(\frac{\ell(\ell+1)}{r^2} - \frac{\rho}{\Gamma p}\sigma^2 \right)\beta_N$$

$$+ \left(\frac{(\sigma^2 + g_N A_N)'}{\sigma^2 + g_N A_N} - \frac{2}{r} - A_N \right)\left(\frac{d}{dr}\beta_N + \frac{g_N \rho}{\Gamma p}\beta_N \right) \quad . \tag{3.23}$$

Restrict attention to the case of a zero-temperature star where A_N vanishes except at a finite number of points where the density changes discontinuously. With the change of variable

$$\beta_N(r)\equiv e^{-\chi(r)}\psi(r)/r \quad , \tag{3.24}$$

$$\chi(r)\equiv\int_0^r \frac{g_N\rho}{\Gamma p}dr \quad , \tag{3.25}$$

equation (3.23) becomes a Sturm-Liouville equation for ψ:

$$\frac{1}{\exp(-\chi)}\frac{d}{dr}\left\{\exp(-\chi)\frac{d\psi}{dr}\right\}=\left\{\frac{\ell(\ell+1)}{r^2}+\frac{\rho}{\Gamma p}\left(\frac{g_N}{r}-\sigma^2\right)\right\}\psi \quad , \tag{3.26}$$

with boundary conditions

$$\psi=0 \tag{3.27}$$

at $r=0$ and $r=\mathcal{R}$, and

$$\left.\begin{aligned}\left[\frac{1}{\rho}\frac{d}{dr}\left[\frac{\psi}{r}\right]\right]&=0\\ [\psi]&=e^{\chi}[\rho]\frac{g_N r}{\sigma^2\rho}\frac{d}{dr}\left[\frac{\psi}{r}\right]\end{aligned}\right\} \tag{3.28}$$

at the discontinuities r_i.

Since ψ satisfies a Sturm-Liouville equation and $g_N>0$, there is a minimum frequency $\sigma_0^2>0$ for which the differential equation and boundary conditions are satisfied. There are also a countable infinity of frequencies $\sigma^2>\sigma_0^2$ for which the differential equations and boundary

conditions are satisfied. If there were no discontinuities in the equation of state ($A_N=0$ everywhere), then the minimum frequency σ_0 would be the f-mode frequency, and the semi-infinite spectrum of eigenfrequencies $\sigma>\sigma_0$ would be the p-mode spectrum. (When $A_N=0$ everywhere, all the g-modes are at zero frequency and correspond to solutions for which the Eulerian pressure perturbation β_N vanishes, but the motion of the fluid does not. For these g-modes $\beta_N=0$ implies $\psi=0$ and the preceding analysis is oblivious of them.)

Return to the case where discontinuities are present. At frequencies $\sigma^2 \lesssim g_N/r$, the coefficient of ψ in equation (3.26) is positive definite, so the behavior of ψ is exponential (as opposed to oscillatory) throughout the star. Expressing the mass of the star as $\mathcal{M}$, the condition $\sigma^2 \lesssim g_N/r$ is equivalent to

$$\sigma^2 \lesssim g_N/r \approx \mathcal{M}/\mathcal{R}^3 \approx \rho_c \quad . \tag{3.29}$$

Thus, the frequency below which ψ is everywhere exponential is of the order of the frequency of the stars f-mode; *i.e.*, ψ is exponential in the g-mode regime. Also, for sufficiently small σ^2, the behavior of ψ determined by the equation (3.26) is independent of σ^2. As a result, the boundary condition at each discontinuity (eq. 3.28) is an equality between a quantity constant in σ^2 ($[\psi]$) and a quantity monotonic in σ^2. Consequently, for each discontinuity in ρ there is only one σ^2, in the regime $\sigma^2<\rho_c$, for which the differential equation and boundary conditions are satisfied, i.e., only one g-mode. (Newtonian discontinuity modes are discussed more completely in Gabriel & Scuflaire 1979.)

Physically, this result is expected. The perturbation equation (3.23) is a wave equation and A_N is part of an effective potential for the waves. Where there are discontinuities in ρ, A_N is a delta function and the effective potential resembles a delta-function potential well. The trapping of modes by a delta-function potential well is a familiar result from elementary quantum mechanics.

More precisely, for σ^2 small compared to ρ_c, the wavefunctions described by equation (3.23) are non-oscillatory: in regions where A_N vanishes, ψ is exponential and has at most one zero. Since the boundary conditions at $r=0$ impose one zero on ψ, unless there is a region in the star where $A_N \leq 0$, ψ does not also vanish at $r=\mathcal{R}$. To develop a second node in the wavefunction, as required by equation (3.27), there must be a region where A_N is sufficiently less than zero over a sufficiently large region. In the present case, A_N is infinitely negative over an infinitesimal distance, and at most one zero of ψ can be fit into the region where A_N is negative (i.e., ψ can have different signs across r_i); correspondingly, there can be at most one eigenfrequency associated with the delta-function in A_N.

The Newtonian perturbation equations also take on Sturm-Liouville form for $\sigma^2 \ll \rho_c$ when A_N is a continuous and non-zero function (e.g., Ledoux & Walraven 1958). The Sturm-Liouville equation is then an eigenequation with eigenvalues $1/\sigma^2$, and a similar analysis shows that when $A_N<0$ over an extended region of the star, then for sufficiently small σ^2 the wavefunction has an arbitrarily large number of nodes in the region $A_N<0$.

The twc principal features of the Newtonian problem that restrict the number of discontinuity modes remain unchanged in the relativistic case. One feature is the local applicability of the convection criterion throughout the star; the other is the delta-function nature of A in the presence of density discontinuities. The local applicability of the relativistic convection criterion guarantees that $A<0$ is a necessary condition for local oscillatory behavior of the wavefunctions. The delta-function nature of A insures that no more than one node forms in the wavefunction per discontinuity in ρ. Both of these features are local phenomena and are independent of spacetime curvature. Thus, because the $A<0$ only at isolated points, and because everywhere A vanishes the wavefunction is exponential, in the relativistic case there is also at most one discontinuity mode associated with each discontinuity in A.

In the late stages of preparation of this paper, I realized that in the relativistic Cowling Approximation (McDermott, Van Horn, & Scholl 1983), the relativistic perturbation equations can be placed in Sturm-Liouville form. Among other things, this will permit a more elegant proof of the above results in the relativistic case. This proof will be included in a paper, currently in preparation, on the relativistic Sturm-Liouville equations.

3.5. ESTIMATED FREQUENCY, ENERGY, AND DAMPING TIMES

To estimate discontinuity-mode frequencies, consider a simpler but analogous problem. In a mixture of two incompressible, immiscible fluids stratified in a uniform gravitational field, there are gravity waves associated with the interface between the fluids. These gravity waves are a simple idealization of the discontinuity modes in a neutron star. The next several paragraphs establish the analogy, which is used throughout the remainder of the paper.

The density discontinuities in neutron stars occur at densities below $\rho_{\rm drip}$. In a typical neutron star these discontinuities are close to the surface of the star: $\rho < \rho_{\rm drip}$ when $1-r/\mathcal{R} \lesssim 1/10$. Consider, as an idealization, a neutron star of radius $\mathcal{R}$ and mass $\mathcal{M}$, with a single density discontinuity at radius r_0. The coordinate distance from the discontinuity to the surface of the star is $\Delta r \equiv \mathcal{R} - r_0$, and for small $\Delta r/\mathcal{R} \ll 1$ the proper distance from the discontinuity to the surface of the star is $h \equiv \Delta r\, e^{\lambda/2} \cong \Delta r\, (1-2\mathcal{M}/\mathcal{R})^{-1/2}$.

Denote the density above and below the density discontinuity as ρ_+ and ρ_-:

$$\rho_+ \equiv \lim_{\varepsilon\to 0} \rho(r_0+\varepsilon) \ , \quad \rho_- \equiv \lim_{\varepsilon\to 0} \rho(r_0-\varepsilon) \ . \tag{3.30}$$

Note that $\rho_+ < \rho_-$. Denote the positive difference in the densities by $\Delta\rho \equiv \rho_- - \rho_+$. The gravitational acceleration in the radial direction measured by a stationary observer at the discontinuity is $-g$, where

$$g \equiv \Gamma^{\hat{r}}_{\hat{t}\hat{t}} \cong g_N \left(1-2\frac{\mathcal{M}}{\mathcal{R}}\right)^{-1/2} \ ,$$

$$g_N \cong \frac{\mathcal{M}}{\mathcal{R}^2} \ . \tag{3.31}$$

The "hats" on the coordinate indices, *e.g.*, $\hat{t}$, refer to the physical components in an orthonormal frame (Misner, Thorne, & Wheeler 1973).

Restrict attention to the discontinuity mode of spherical harmonic order l. The reduced wavelength of the wave pattern in the $\hat{\theta}$ direction is $1/k \cong r_0/L \cong \mathcal{R}/L$, where $L^2 \equiv l(l+1)$.

The stratified-fluid problem is characterized by the boundary conditions on, and the densities of, the upper and lower fluids. Assume the fluids to be infinitely extended in the x and y directions. Since the discontinuity in the neutron star is located much closer to the surface of the star than to the center, take the lower of the two fluids to be infinitely deep, and the upper fluid to have a depth h and a free surface. Let the density of the upper fluid be ρ_+ and the density of the lower fluid be ρ_-. Set $z=0$ at the fluid-fluid interface, let g be the uniform gravitational acceleration in the $-z$ direction, and consider gravity waves of wavenumber k in the x direction on the interface between the two fluids.

In the stratified-fluid problem, the two fluids are incompressible; hence, the velocity field $\vec{v}$ is equal to the gradient of a scalar field ϕ. The space and time dependence of ϕ is $\sim \exp\{i(xk + zk_z - \sigma t)\}$, where the continuity equation relates k and k_z:

$$0 = \vec{\nabla}\cdot\vec{v} = \nabla^2\phi = -(k^2 + k_z^2)\phi \ . \tag{3.32}$$

The frequency of the gravity waves at the fluid-fluid interface of the stratified fluid is readily shown to be (*cf.* Landau & Lifshitz 1959)

$$\sigma_{r_0}^2 = gk\frac{\Delta\rho\exp(-kh)\sinh(kh)}{\rho_+ + \Delta\rho\exp(-kh)\cosh(kh)}. \tag{3.33}$$

The frequency σ_{r_0} is analogous to the frequency of the discontinuity modes as measured by an observer located at the discontinuity in the neutron star, while the frequency calculated in the slow-motion formalism is the frequency observed far from the star (σ_∞). The two frequencies are related by a redshift factor $\alpha \equiv \exp\{\nu(r_0)/2\}$:

$$\sigma_\infty^2 = \sigma_{r_0}^2\alpha^2$$

$$= \alpha^2 gk\frac{\Delta\rho\exp(-kh)\sinh(kh)}{\rho_+ + \Delta\rho\exp(-kh)\cosh(kh)}. \tag{3.34}$$

For small $\Delta r/\mathcal{R}$, the redshift factor is $\alpha \cong (1-2\mathcal{M}/\mathcal{R})^{1/2}$.

In the neutron star, for small $\Delta r/\mathcal{R}$ the proper distance h from the discontinuity to the surface of the star is related to the pressure scale height $h_p \equiv -p/\{p'(1-2\mathcal{M}/\mathcal{R})^{1/2}\}$ at the discontinuity: $h \cong (n+1)h_p$. Here n is the polytropic index effective in the outermost regions of the star, and $n \to 0$ for an incompressible star. Denoting the pressure at the discontinuity by p_0 and recalling $k = L/\mathcal{R}$,

$$kh \cong kh_p(n+1) \cong \frac{L}{\mathcal{R}}\frac{(n+1)p_0}{g\rho_+} \cong (n+1)L\frac{\mathcal{R}}{\mathcal{M}}\frac{p_0}{\rho_+}(1-2\mathcal{M}/\mathcal{R})^{1/2}. \tag{3.35}$$

For small n and l, $kh \ll 1$.

For small kh and $\Delta\rho/\rho_-$, equation (3.34) simplifies to

$$\sigma_\infty^2 \cong \alpha^2 g k \frac{\Delta\rho}{\rho_-} kh$$

$$\cong g_N k \frac{\Delta\rho}{\rho_-} k\,\Delta r \quad . \tag{3.36}$$

Note that the frequency measured at infinity σ_∞ is independent of the surface redshift of the neutron star. Equation (3.36) corresponds to an estimated discontinuity mode period of

$$T = \frac{2\pi}{\sigma_\infty} \cong 5.5 \text{ ms} \left\{ l(l+1) \right\}^{-1/2} \left[\frac{\mathcal{R}}{10\text{km}} \right]^{3/2} \left[\frac{M_\odot}{\mathcal{M}} \frac{1/10}{\Delta\rho/\rho_-} \frac{1/10}{\Delta r/\mathcal{R}} \right]^{1/2} . \tag{3.37}$$

Recall that $M_\odot$=1.477 km is the mass of the sun.

Denote the amplitude of the vertical displacement of a fluid element in the stratified fluid by $\zeta(z)$. When $kh \ll 1$, the ratio $\zeta(0)/\zeta(h)$ is $-\rho_-/\Delta\rho$. The same should hold in the neutron star:

$$\xi^r(r_0)/\xi^r(\mathcal{R}) \cong -\rho_-/\Delta\rho \quad . \tag{3.38}$$

The stratified fluid model approximates the spherical symmetry of the neutron star by plane symmetry. This is valid only when the discontinuity-mode eigenfunctions do not penetrate the star far enough to see significant deviations from plane symmetry. In the region above the discontinuity, the eigenfunctions penetrate a coordinate distance Δr to the surface of the star, and in the region below the discontinuity they penetrate to a distance $1/k$. Consequently, the validity of the stratified-fluid-model estimates is limited by geometrical factors to

applications where $\Delta r/\mathcal{R},\ 1/k\mathcal{R}<1$. The condition $1/k\mathcal{R}\cong 1/\ell<1$ is satisfied for quadrupole (ℓ=2) and higher order modes. The condition $\Delta r/\mathcal{R}\ll 1$ is satisfied in neutron star models with typical masses and reasonable equations of state.

To estimate the energy in a discontinuity mode, consider an approximate expression for the total pulsational energy:

$$\mathcal{E}\cong\tfrac{1}{2}\int dr\, r^2\exp(\lambda/2)\,\alpha\rho\sigma_0^2\{(W/r^2)^2+\ell(\ell+1)(V/r)^2\}\ . \tag{3.39}$$

Here, the factor $dr\, r^2\exp(\lambda/2)$ is the volume element with the angular integral already evaluated; the factor $\tfrac{1}{2}\rho\sigma_0^2\{(W/r^2)^2+\ell(\ell+1)(V/r)^2\}$ is twice the local kinetic energy density (recall $W/r^2=\xi^r/Y_{\ell m}$ and $V/r=\xi^\theta/\partial_\theta Y_{\ell m}$), and σ_0 is the angular frequency measured by a local coordinate stationary observer. The factor of α turns the local kinetic energy into an energy measured by an observer at infinity. Energy associated with the gravitational field is ignored. Below, the value of the energy (3.39) is estimated.

To estimate the transverse displacement of a fluid element V/r, relate it to the Eulerian pressure perturbation β with the help of equations (3.5) and (3.2):

$$\frac{V}{r}\cong -r\frac{\beta}{\rho}\left[\frac{\alpha}{\sigma_\infty r}\right]^2. \tag{3.40}$$

Note that the Lagrangian pressure perturbation vanishes at the surface of the neutron star:

$$\lim_{r\to\mathcal{R}}\left(\beta+\frac{dp}{dr}e^{-\lambda/2}W/r^2\right)=0\ . \tag{3.41}$$

Consequently, near the surface of the star β is proportional to ρ and V/r is constant.

The Eulerian perturbations in a discontinuity-mode pulsation are small, and much smaller at densities $\rho>\rho_-$ than at densities $\rho<\rho_-$; thus, $\beta\cong 0$ at densities $\rho>\rho_-$. Hence, the jump condition (eq. 3.7) on β at r_0 determines β/ρ at densities $\rho<\rho_+$:

$$\frac{\beta}{\rho} \cong -\frac{g}{\alpha}\frac{\Delta\rho}{\rho_-}\frac{e^{-\lambda/2}}{r_0^2}W(r_0). \tag{3.42}$$

The transverse displacement is thus negligible except near the surface, where

$$\frac{V}{r} \cong \mathcal{R}\frac{g}{\alpha}\frac{\Delta\rho}{\rho_-}\left[\frac{\alpha}{\sigma_\infty \mathcal{R}}\right]^2 e^{-\lambda/2}\frac{W(r_0)}{r_0^2} \tag{3.43}$$

$$\cong \frac{1}{l(l+1)}\frac{\mathcal{R}}{h}\frac{W(r_0)}{\mathcal{R}^2} \quad . \tag{3.44}$$

In the stratified-fluid problem, the maximum amplitude of the vertical motion of the fluid occurs at the discontinuity and the amplitude decays exponentially with distance from the discontinuity. The transverse motion V/r is much greater than the vertical motion W/r^2 in the region $\rho<\rho_+$; thus, the only substantial contribution to the pulsation energy comes from V/r. Combining equation (3.39) with (3.43) and (3.36), the estimated pulsation energy is

$$\mathcal{E} \cong \tfrac{1}{2}\mathcal{A}(l+1)\Delta r\,(\rho_+\mathcal{R}^2)\left[\frac{\Delta\rho}{\rho_+}\right]^2(\sigma_\infty\mathcal{R})^{-2}\left\{\frac{g_N W(r_0)}{\mathcal{R}^2}\right\}^2$$

$$\cong 2.2\times 10^{52}\text{ergs}\, l(l+1)\left[\frac{\Delta r/\mathcal{R}}{1/10}\right]\left[\frac{\rho_+}{10^{13}\text{ g cm}^{-3}}\right]\left[\frac{\mathcal{M}}{M_\odot}\right]^2$$

$$\times\left[\frac{T}{10\text{ ms}}\right]^2\left[\frac{10\text{ km}}{\mathcal{R}}\right]\left[\frac{\xi^r(\mathcal{R})/Y_{lm}}{\mathcal{R}}\right]^2 . \qquad (3.45)$$

Discontinuity modes in a zero-temperature, perfect-fluid neutron star are damped by gravitational radiation, and the damping times are long compared to the period of the pulsations. In the slow-motion formalism, the damping time is twice the ratio of the pulsational energy to the power in gravitational radiation. It is natural to estimate the power in gravitational radiation from a multipole formula:

$$\frac{dE}{dt} = \frac{1}{32\pi}\left[\frac{d^{l+1}I^{lm}}{dt^{l+1}}\right]^2 . \qquad (3.46)$$

In the Newtonian limit of weak fields and slow motion, I^{lm} is the l^{th} multipole moment of the time-dependent mass distribution

$$I^{lm} = \frac{16\pi}{(2l+1)!!}\left[\frac{(l+1)(l+2)}{2(l-1)l}\right]^{1/2}\int r^2 dr\, d\Omega Y^*_{lm}\,\delta\rho\, r^l \qquad (3.47)$$

($\delta\rho$ is the Eulerian density perturbation). Derivations of the multipole formula (eq. 3.46) that identify I^{lm} with integrals over the mass distribution (*e.g.*, Thorne 1980) all assume weak fields and slow motion. While the gravitational field is not weak in neutron stars, to the accuracy desired of rule-of-thumb estimates equations (3.46) and (3.47) reasonably approximate the power in gravitational radiation.

To estimate I^{lm} for an idealized neutron star with a single density discontinuity, evaluate the angular integral in equation (3.47) and integrate the radial terms by parts

$$I^{lm} = \frac{16\pi}{(2l+1)!!}\left[\frac{(l+1)(l+2)}{2(l-1)l}\right]^{1/2}\int_0^{\mathcal{R}} r^2 dr\,(r^2\mu)$$

$$= -\frac{16\pi}{(2l+1)!!}\left[\frac{(l+1)(l+2)}{2(l-1)l}\right]^{1/2}\int_0^{\mathcal{R}} dr\; l r^{l-1}\int_0^{r} dx\; x^2\mu \quad . \tag{3.48}$$

Recall that μ is the radial Eulerian density perturbation in the star.

For small $\Delta r/\mathcal{R}$, use equations (3.9) and (3.42) to estimate μ:

$$\mu \cong \begin{cases} 0 & \text{for} \quad r < r_0 \\ \delta(r-r_0)\,\Delta\rho\, e^{-\lambda/2} W/r^2 & \text{for} \quad r = r_0 \\ \rho\beta/\gamma p & \text{for} \quad r > r_0 \end{cases} . \tag{3.49}$$

With μ estimated this way,

$$0 = \int_0^{\mathcal{R}} dx\; x^2\mu = \lim_{\varepsilon\to 0}\int_{r_0-\varepsilon}^{\mathcal{R}} dx\; x^2\mu \quad , \tag{3.50}$$

and

$$\lim_{\varepsilon\to 0}\int_{r_0-\varepsilon}^{r} dx\; x^2\mu = e^{-\lambda/2}\Delta\rho\, W(r_0) - \int_{r_0}^{r} dx\; g\,\rho W e^{-\lambda/2}\frac{\rho}{\gamma p}\frac{\Delta\rho}{\rho_+} \tag{3.51}$$

is monotonic for $r > r_0$; thus, equation (3.48) becomes

$$I^{lm} \lesssim \frac{16\pi}{(2l+1)!!}\left[\frac{(l+1)(l+2)}{2(l-1)l}\right]^{1/2} l\Delta\rho\,\mathcal{R}^{l-1}\Delta r\, e^{-\lambda/2} W(r_0) \quad . \tag{3.52}$$

Using equations (3.46) and (3.45) for the gravitational radiation power

and the pulsational energy, the discontinuity mode damping time is

$$\tau \gtrsim \frac{\{(2l+1)!!\}^2}{8\pi}\,\frac{l-1}{l+2}\,\mathcal{R}\,(\sigma_\infty \mathcal{R})^{-2(l+2)}\left[\frac{\mathcal{M}}{\mathcal{R}}\right]^2\left[\frac{\mathcal{R}}{\Delta r}\right](\rho_+\mathcal{R}^2)^{-1}\alpha^{-2}\ . \tag{3.53}$$

For quadrupole ($l=2$) modes

$$\tau \gtrsim 2.3\times10^{10}\ \mathrm{s}\left[\frac{10\,\mathrm{km}}{\mathcal{R}}\right]^{11}\left[\frac{T}{5\,\mathrm{ms}}\right]^{8}\left[\frac{\mathcal{M}}{M_\odot}\right]^2 \times\left[\frac{10^{12}\,\mathrm{g\,cm^{-3}}}{\rho_+}\right]\left[\frac{1/10}{\Delta r/\mathcal{R}}\right]\left[1-\frac{2\mathcal{M}}{\mathcal{R}}\right]^{-1}\ . \tag{3.54}$$

4. Numerical Results

4.1. INTRODUCTION

I have applied the slow-motion formalism, as extended in §3.3, to the numerical study of discontinuity modes in zero-temperature perfect-fluid neutron stars. Only results for quadrupole ($l=2$) discontinuity modes are reported here, and the relativistic convective discriminant A (eq. 2.5) has been assumed to vanish everywhere except at those isolated points where the composition changes discontinuously.

Section 4.2 presents results for idealized stellar models with a single discontinuity in the equation of state. These models are made from a modified polytropic equation of state that allows much control over the properties that determine the discontinuity-mode spectrum. I

have studied such models extensively, both to validate the numerical code and to gain insight into the more realistic but more complicated case of stars with many discontinuities. The value of the simple physical estimates of discontinuity-mode frequency and energy (§3.5) is particularly apparent in these models.

Section 4.3 discusses the numerical results for stars whose low-density equation of state is that of cold and fully catalyzed nuclear matter (Baym, Pethick, & Sutherland 1971). The first several high-frequency discontinuity modes are presented for one model, and the highest frequency discontinuity mode is calculated for several models with different high-density equations of state.

4.2. SINGLE-DISCONTINUITY STARS

4.2.1. *Equation of State*

To validate the numerical code and further develop the insights of §3.5, neutron star models with a single density discontinuity were built. The equation of state used was of the form

$$p = \begin{cases} K\rho^{\Gamma_0} & \text{for } \rho > \rho_+ + \Delta\rho \\ K(1+\Delta\rho/\rho_+)^{\Gamma_0}\rho^{\Gamma_0} & \text{for } \rho < \rho_+ \end{cases} . \tag{4.1}$$

At ρ_+ the density increases discontinuously by a fractional amount $\Delta\rho/\rho_+$. The parameter K was chosen so that model stars with central densities $\sim 10^{15}$ g cm^{-3} had radii and masses typical of neutron stars. The appropriate value of K for a given Γ_0 was estimated by noting that to

order of magnitude

$$\mathcal{R} \cong \frac{p_c}{p'} \cong \frac{K \rho_c^{\Gamma_0}}{g \rho_c} \quad . \tag{4.2}$$

Estimating $g \cong \mathcal{M}/\mathcal{R}^2 \cong \mathcal{R}\rho_c$ ($\mathcal{M}$ the mass of the star),

$$K(\rho_c, \mathcal{R}, \Gamma_0) \cong \mathcal{R}^2 \rho_c^{2-\Gamma_0}. \tag{4.3}$$

In the calculations described below, K was taken from equation (4.3).

The equation of state (4.1) is patched together from two polytropic equations of state with the same index Γ_0 in such a way that the properties of the high density ($\rho > \rho_+$) region are independent of ρ_+ and $\Delta\rho$. This is intentional.

Model stars built from a simple equation of state like (4.1) have a discontinuity mode that depends only on the index Γ_0, the central density of the star ρ_c, the density at the discontinuity ρ_+, the size of the discontinuity $\Delta\rho$, and K. When equation of state (4.1) is used, the radial location of the discontinuity r_0 is independent of $\Delta\rho$; additionally, when $\rho_+ \ll \rho_c$, the mass $\mathcal{M}$ and radius $\mathcal{R}$ of stellar model depend only on ρ_c. In particular, the mass and radius are independent of ρ_+ and $\Delta\rho$. Thus, the effect on the discontinuity mode of ρ_c, ρ_+, and $\Delta\rho$ may be studied separately as long as $\rho_+ \ll \rho_c$.

The regime $\rho_+ \ll \rho_c$ is the physically relevant regime for neutron stars. In realistic neutron stars, the density discontinuities all occur near the surface at low densities ($\rho_+ < \rho_{\rm drip} \ll \rho_c$), while the mass and radius are determined by the high density ($\rho > \rho_{\rm drip}$) equation of state.

4.2.2. *Parameter Space*

Discontinuity-mode eigenfrequencies, eigenfunctions, energies, and damping times have been evaluated for 120 model neutron stars constructed from the equation of state (4.1). The models represent two different indices Γ_0 and (for each Γ_0) six different central densities ρ_c. For each Γ_0 and ρ_c, there were ten models that explored different combinations of ρ_+ and $\Delta\rho/\rho_+$.

The two different indices investigated were $\Gamma_0=2$ and $\Gamma_0=5/3$. For each index, K in equation (4.1) was fixed by equation (4.3) evaluated for a 10 km radius star with a central density of 10^{15} g cm^{-3}. Under these conditions, equation (4.3) estimates $K = 100$ km^2 for $\Gamma_0 = 2$, and $K = 9$ km$^{4/3}$ for $\Gamma_0 = 5/3$. My calculations adopt these values.

For each Γ_0, six different values of ρ_+ were investigated. At $\rho_+ = 1$ and 10×10^{13} g cm^{-3}, fractional discontinuities of 10%, 5%, and 2% were investigated. At $\rho_+ = 2$ and 20×10^{13} g cm^{-3}, a fractional discontinuity of 5% was investigated, and at $\rho_+ = 5$ and 50×10^{13} g cm^{-3}, a fractional discontinuity of 2% was investigated. This parameter subspace was repeated for central densities of 1, 2, 5, 10, 20, and 50×10^{14} g cm^{-3}.

For the models built from the $\Gamma_0 = 5/3$ equation of state, the radii ranged from 24. to 9.0 km, the masses ranged from 0.42 to 1.1 $M_\odot$, and the surface redshifts ranged from $z = 0.026$ to $z = 0.26$. For the models built from the $\Gamma_0 = 2$ equation of state, the radii ranged from 12. to 7.8 km, the masses ranged from 0.12 to 1.3 $M_\odot$, and the surface redshifts ranged from $z = 0.014$ to $z = 0.43$.

The discussion of §3.5 shows that the important quantities for determining the pulsation eigenfrequencies are $\Delta\rho/\rho_+$ and $\Delta r/\mathcal{R}$. The parameter space investigated here covers the typical $\Delta\rho/\rho_+$ and $\Delta r/\mathcal{R}$ found in model stars based on the Baym, Pethick, & Sutherland (BPS) equation of state. For the constant Γ_0 stars investigated, $\Delta\rho$ and ρ_+ are several decades larger than in stellar models based on the BPS equation of state. The central densities explored are typical of realistic neutron stars.

4.2.3. *Numerical Results*

The discontinuity-mode eigenfrequencies, pulsational energies, damping times, and eigenfunctions were numerically evaluated for the 120 models described in §4.2.2. Here, the results of those calculations are compared with the analytic estimates of §3.5. All the numerical calculations were carried out using the slow-motion formalism; in the discussion that follows, a quantity with a subscript SM denotes the quantity as computed in the slow-motion formalism, and a quantity with the subscript EST denotes the estimate made in §3.5.

Figure 1 illustrates how the fraction $T_{\rm SM}/T_{\rm EST}$ varies with $\Delta r/\mathcal{R}$. Each model is represented by a + in Figure 1 and all 120 models are shown. The curves drawn through the points distinguish the sixty $\Gamma_0=5/3$ models from the sixty $\Gamma_0=2$ models. The periods themselves range from 5.3 to 50. ms for the $\Gamma_0=5/3$ models, and from 11. to 88. ms for the $\Gamma_0=2$ models.

The period estimate (eq. 3.37) does an impressive job in predicting the periods of the discontinuity modes over all the parameter space. As expected, the agreement is best for small $\Delta r/\mathcal{R}$; however, in all cases investigated, $T_{\rm EST}$ always agrees with the $T_{\rm SM}$ to within a factor of two. The variation with Γ_0 is also understandable: the discussion of §3.5 was confined to incompressible fluids, and $1/\Gamma_0$ is a dimensionless measure of the compressibility of the neutron star fluid.

Figure 2 shows the fraction $\mathcal{E}_{\rm SM}/\mathcal{E}_{\rm EST}$ as a function of $\Delta r/\mathcal{R}$ for all 120 models. Each model is shown by a + in Figure 2, and the two curves drawn through the points distinguish the sixty $\Gamma_0=5/3$ models from the sixty $\Gamma_0=2$ models. The energies range from 1.9×10^{51} to 7.9×10^{53} ergs for the $\Gamma_0=5/3$ models, and from 2.5×10^{50} to 4.87×10^{53} for the $\Gamma_0=2$ models.

The pulsation energy estimate (eq. 3.45) accurately predicts the energy of the discontinuity modes when $\Delta r/\mathcal{R}\ll 1$. Its accuracy rapidly deteriorates when $\Delta r/\mathcal{R}\gtrsim 1/10$.

The numerically calculated damping times range over 15.5 orders of magnitude, from 5×10^{10} to 2×10^{23} s for $\Gamma=2$, and from 1×10^{8} to 2×10^{19} s for $\Gamma=5/3$. In all cases, equation (3.54) correctly gives a lower bound on the numerically calculated damping time. For small $\Delta r/\mathcal{R}\lesssim 10^{-1}$ the estimated lower bound is roughly a factor of 10 lower than the calculated damping time. The $\Gamma=2$, $\rho_c=5\times10^{15}$ g cm^{-3} models are an exception to this rule; for these models the numerically calculated damping times are anomalously small: a factor of 10 lower than expected from extrapolation of damping times at lower central

densities, and just a factor of 2 greater than the lower bound of equation (3.54).

In the regime $\Delta r/\mathcal{R} \gtrsim 10^{-1}$, equation (3.54) underestimates the numerically calculated damping times by up to a factor of 10^3.

Table 1 gives the results of the slow-motion calculations for typical models. It describes the ten $\Gamma_0 = 5/3$, $\rho_c = 10^{15}$ g cm^{-3} models. Each model has a radius of $\mathcal{R}$=14.1 km and a mass of $\mathcal{M}$=0.937 $M_\odot$. The first three columns give the fractional radial distance from the surface of the star to the discontinuity $\Delta r/\mathcal{R}$, the density at the discontinuity ρ_+, and the fractional density discontinuity $\Delta\rho/\rho_+$. The next two columns give the numerically calculated period $T_{\rm SM}$ and the estimated period $T_{\rm EST}$. The following two columns give the the numerically calculated energy $\mathcal{E}_{\rm SM}$ and the estimated energy $\mathcal{E}_{\rm EST}$, and the final column gives the damping time τ calculated by the slow-motion formalism.

The analogy developed in §3.5 extends to the qualitative features of the eigenfunctions; in particular, the relation between $\xi^r(\mathcal{R})$ and $\xi^r(r_0)$ predicted in §3.5 (eq. 3.38) is reproduced numerically for small $\Delta r/\mathcal{R}$. Figure 3 shows the quantity $\Delta\rho\xi^r(r_0)/\rho_+\xi^r(\mathcal{R})$ plotted against $\Delta r/\mathcal{R}$ for all 120 models, with lines drawn through the points to differentiate between models of different Γ_0. The ratio $\xi^r(r_0)/\xi^r(\mathcal{R})$ ranged from -7.6 to $-49.$ among the 120 models investigated.

Figure 4 shows the radial dependence of the physical fluid variables ξ^r and β versus $\log(1-r/\mathcal{R})$ for a model with small $\Delta r/\mathcal{R}$. The model shown has $\rho_c = 10^{15}$ g cm^{-3}, $\rho_+ = 9.5\times10^{11}$ g cm^{-3}, and $\Delta\rho/\rho_+ = 10\%$. The

radial location of the discontinuity is obvious. Note the magnitude of the discontinuity in β (*cf.* eq. 3.7), and note also how the radial displacement of the fluid is of significant amplitude only around the discontinuity. The transverse displacement of the fluid (not shown) is a step-function at the discontinuity: approximately 0 for $\rho > \rho_+$, and constant for $\rho < \rho_+$, as expected for small $\Delta r/\mathcal{R}$.

To summarize, for $\Delta r/\mathcal{R} < 1/10$ the analytic estimates of §3.5 describe very accurately the magnitude and functional dependence of discontinuity-mode periods and energies, and the ratio of the radial perturbation at the discontinuity to the radial perturbation at the star's surface. The lower bound on the estimated damping time (eq. 3.54) is always satisfied, and for small $\Delta r/\mathcal{R} < 1/10$ is roughly an order of magnitude below the numerically calculated damping time.

The agreement of the numerical calculations with the analytic predictions gives confidence that the numerical code is a correct implementation of the slow-motion formalism for stars with composition discontinuities.

4.3. DISCONTINUITY MODES FROM THE BPS EQUATION OF STATE

4.3.1. *Equation of State*

The equation of state of fully catalyzed nuclear matter in the range 1.0×10^4 g cm$^{-3} \leq \rho \leq 4.3\times10^{11}$ g cm^{-3} was found by Baym, Pethick, & Sutherland (1971). They found 11 composition transitions, and correspondingly 11 density discontinuities, in the equation of state. The

tabulated equation of state (BPS Table 5) does not explicitly contain the discontinuities; these are given in BPS Table 2 to a lower precision than the tabulated equation of state. Since the discontinuity-mode eigenproblem has boundary conditions at the discontinuities, the equation of state must be extended to define explicitly the density discontinuities. Rather than reproduce the calculations of BPS, I have chosen to modify the tabulated equation of state, in the manner explained below, to define explicitly these boundaries.

For each density discontinuity in BPS Table 2, I made two new entries in the tabulated equation of state (BPS Table 5): one at density ρ_+ and the other at $\rho_-=\rho_++\Delta\rho$. The pressure at these two points was determined from the neighboring points in the tabulated equation of state. The pressure from the nearest tabulated point of density $\rho>\rho_-$ was logarithmically extrapolated at constant adiabatic index to ρ_-. Likewise, the pressure at density $\rho<\rho_+$ was extrapolated to ρ_+. These two pressures were averaged to give the pressure at the discontinuity.

In several instances, tabulated points of the BPS equation of state fell between ρ_+ and ρ_-; these points were deleted from the equation of state. The points were present because of the arbitrary use of the lower-precision BPS Table 2 to determine the location of the density discontinuities*.

The details of the modification of the BPS equation of state are not important to the discontinuity-mode spectrum. The estimates of §3.5

* Baym, private communication.

and the numerical results of §4.2 show that the discontinuity-mode frequencies are sensitive to the equation of state only through the fractional density discontinuity.

Properties of the density discontinuities are summarized in Table 2. Each discontinuity reflects a change in which nucleus is stable at a given pressure. The first column shows the change in nuclear species as the density increases. The second column shows the density ρ_+ where the discontinuity occurs, and the third column indicates the fractional discontinuity $\Delta\rho/\rho_+$. The fourth column gives the pressure calculated at the discontinuity. The first four columns are properties of the BPS equation of state. The remaining column gives the radial coordinate depth from the surface of the star to the discontinuity for a model star. The model star is based on Arnett & Bowers' (1974) equation-of-state model B, which uses the BPS equation of state. It has a central density of 10^{15} g cm^{-3}, a radius of 9.83 km, and a mass of $0.52\,\mathcal{M}_\odot$.

The BPS equation of state describes the regime 1.0×10^4 g cm^{-3} $\lesssim\rho\lesssim 4.3\times10^{11}$ g cm^{-3} of cold and fully catalyzed nuclear matter. The equation of state appropriate at higher densities is more controversial; however, the discontinuity-mode spectrum is sensitive to the high density equation of state only through the star's total mass and radius.

4.3.2. *Numerical Results*

As a test of the slow-motion computer code, f-mode periods and damping times have been calculated for several different stars and compared with equivalent results from Lindblom & Detweiler (1983). The stars were built around different equations of state, but all had a central density $\rho_c = 10^{15}$ g cm^{-3}. The equations of state differed only in the high density $\rho > \rho_{drip}$ region; in the low density region the BPS equation of state was always used.

Table 3 shows the periods and damping times for the f-mode in four model stars with different equations of state. The first column indicates the equation of state used, and refers to the models studied by Arnett & Bowers (1974). These four equations of state span a range of stiffness; in order of increasing stiffness, B < D < A < C.

The next two columns of Table 3 show the mass and radius of the model star. The next two columns give the f-mode period, first as calculated by the slow-motion formalism and second as calculated by Lindblom & Detweiler (1983), using the exact formalism for non-radial pulsations of relativistic stars. The f-mode damping times follow, first as calculated by the slow-motion formalism and second as calculated by Lindblom & Detweiler.

Since the fundamental mode is an acoustic mode, a star's f-mode period and damping time are not affected by the small discontinuities. The near-agreement of the f-mode periods and damping times calculated here with the calculations of Lindblom & Detweiler is taken

as a crude test of the slow-motion numerical code. The differences are attributable to the weakness of the slow-motion approximation in the f-mode regime, and are discussed more fully in Finn 1986.

Figure 5 shows the proper radial displacement ξ^r for the first four discontinuity modes of a model star constructed from Arnett and Bowers' (1974) model B with central density 10^{15} g cm^{-3}. Table 4 accompanies Figure 5 and gives the periods, energies, and damping times of the modes. Note how the number of nodes increases with increasing period.

The discontinuity modes become more and more difficult to find numerically as the period increases. In its present incarnation, the slow-motion formalism can find the frequencies of the next several modes, but not with sufficient precision to determine their damping times.

The first discontinuity mode, g_1, of model stars based on Arnett & Bowers' equation-of-state models A, B, C, and D have been compared. The proper radial displacement ξ^r is qualitatively the same for all four models; it is strongly peaked about the discontinuity associated with the ^{78}Ni$\rightarrow^{76}$Fe transition and does not seem significantly affected by the presence of the other discontinuities. This suggests that the g_1 mode is strongly associated with the ^{78}Ni$\rightarrow^{76}$Fe transition and is decoupled from the other discontinuities in the star. The period and energy estimates of §3.5 should apply to this mode.

Table 5 compares the estimates of the period and energy with the

numerical calculations for the g_1 mode in several model stars. The estimates were made using the formulae of §3.5, as if the $^{78}Ni \rightarrow ^{76}Fe$ transition were the only discontinuity in the star. The results shown in Table 5 are for stars with a central density $\rho_c = 10^{15}$ g cm^{-3}. Column one shows the equation of state used to build the model; columns two and three show the radius and mass of the star. The fractional radial depth of the density discontinuity is given in the fourth column. The next two columns show the period calculated with the slow-motion formalism and the estimated period. The final two columns show the energy calculated with the slow-motion formalism and the estimated energy.

The estimate of the period is in close agreement with the period calculated by the slow-motion formalism; the energy estimate is roughly a uniform factor of five high.

5. Conclusions

Chemical inhomogeneities present in neutron stars perturb g-modes away from zero frequency. In realistic neutron stars, the chemical composition varies discontinuously, and associated with each discontinuity there is a single g-mode, referred to as a discontinuity mode.

Discontinuity modes are physically analogous to gravity waves in a mixture of two incompressible, immiscible fluids stratified in a uniform gravitational field. The periods, energies, and qualitative features of the wavefunctions in the discontinuously stratified fluid problem are estimates of the corresponding aspects of discontinuity modes. The

analogy also provides a lower-bound estimate of the gravitational radiation damping time of discontinuity modes.

Numerical calculations with the slow-motion approximation, extended to study discontinuity modes, show that the frequency and energy estimates provided by the stratified-fluid model apply to model neutron stars over a wide range of conditions. The gravitational radiation damping time estimate is not as widely applicable, but is still a useful rule-of-thumb guide. Clearly, the stratified-fluid analogy captures the important physics of discontinuity modes in neutron stars and provides a simple conceptual framework for investigating the modes and their properties.

McDermott, Van Horn, & Scholl (1983) studied the high frequency g-modes perturbed by deviations from isentropy at finite temperature. The lowest g-mode periods they found were $\sim$ 50 ms. Typical discontinuity-mode periods in neutron stars made from fully catalyzed nuclear matter are $\sim$ 5 ms. Discontinuity modes thus appear to be more important than finite-temperature modes in determining the high frequency g-mode spectrum of neutron stars.

Acknowledgements

Kip S. Thorne provided the initial motivation for studying discontinuity modes in neutron stars. I am especially thankful to Kip, and to E. Sterl Phinney, for a critical reading of an early version of the manuscript. This research was supported by National Science Foundation grants NSF 84-51725 and AST 85-14126.

References

Arnett, W. D. & Bowers, R. L. 1974. *Neutron Star Structure: A Survey*, Austin, The University of Texas at Austin.

Baym, G., Pethick, C. & Sutherland, P. 1971. *Astrophys J.*, **170**, 299.

Cowling, T. G., 1941. *Mon. Not. R. astr. Soc.*, **101**, 367.

Cox, J. P. 1980. **Theory of Stellar Pulsations**, Princeton University Press, Princeton (New Jersey).

Cutler, C. & Lindblom, L. 1986. Preprint.

Detweiler, S. L. & Ipser, J. R. 1973. *Astrophys. J.*, **185**, 685.

Detweiler, S. L. 1975. *Astrophys. J.*, **197**, 203.

Finn, L. S. 1986. *Mon. Not. R. astr. Soc.*, **222**, 393

Fujimoto, M. Y., Tomoyuki, H., Iben, I. & Richardson, M. B. 1984. *Astrophys. J.*, **278**, 813.

Gabriel, M. & Scuflaire, R. 1979. **Nonlinear and Nonradial Stellar Pulsation: proceedings of a workshop held at the University of Arizona in Tuscon, March 12-16, 1979**, eds. Hill, H. A., & Dziembowski, W. A., Springer-Verlag, Berlin, p. 478,

Landau, L. D., & Lifshitz, E., M. 1959. **Fluid Mechanics** Pergammon Press, Oxford.

Ledoux, P., & Walraven, Th. 1958. **Handbuch der Physik, 51**, ed. Flügge, S., Springer-Verlag, Berlin, p. 353.

Lindblom, L. & Detweiler, S. L. 1983. *Astrophys. J.*, **53**, 73.

McDermott, P. N., Van Horn, H. M. & Scholl, J. F. 1983. *Astrophys. J.*, **268**, 837.

McDermott, P. N., Savedoff, M. P., Van Horn, H. M., Zweibel, E. G. & Hansen, C. J. 1984. *Astrophys. J.*, **281**, 746

McDermott, P. N., Hansen, C. J., Van Horn, H. M. & Buland, R. 1985. *Astrophys. J.*, **297**, L37.

Meltzer, D. W. & Thorne, K. S. 1966. *Astrophys. J.*, **145**, 514.

Misner, Thorne, K. S. & Wheeler, J. H. 1973. **Gravitation**, Freeman, San Francisco.

Press, W. H., Flannery, B. P., Teukolsky, S. A., & Vetterling, W. T. 1986. **Numerical Recipes**, Cambridge University Press, New York.

Regge, T. & Wheeler, J. A. 1957. *Phys. Rev.*, **108**, 1063.

Salpeter, E. E. 1961. *Astrophys. J.*, **134**, 669.

Salpeter, E. E. & Van Horn, H. M. 1969. *Astrophys. J.* **155**, 183.

Schumaker, B. L. & Thorne, K. S. 1983. *Mon. Not. R. astr. Soc.*, **203**, 457.

Thorne, K. S. 1966. *Astrophys. J.*, **144**, 201.

Thorne, K. S. 1969. *Astrophys. J.*, **158**, 1.

Thorne, K. S. 1980. *Rev. Mod. Phys.*, **52**, 299.

Tsuruta, S. 1979. *Physics Reports*, **56**, 237.

Van Horn, H. M. 1980. *Astrophys. J.*, **236**, 899.

Zel'dovich, Ya. B., & Novikov, I. D. 1971. **Relativistic Astrophysics, Vol. I**, eds. Thorne, K. S., & Arnett, W. D., University of Chicago Press, Chicago, pg 178 ff.

Appendix A -- Numerical Techniques

The details of my computer implementation of the slow-motion formalism are contained in Appendix A of Finn (1986). The extension of that code to discontinuity-mode calculations was not straightforward. The eigenfunctions of a discontinuity mode are sharply peaked about the discontinuity and the stability of numerical integration near discontinuities in the equation of state is a delicate issue.

In the slow-motion formalism, the four eigenfunctions satisfy a fourth order homogeneous system of ordinary differential equations. The original version of the slow-motion formalism assumed a continuous equation of state; boundary conditions were posed only at the center and the surface of the star. Alone, the core boundary conditions determine one two-parameter family of solutions to the differential equations, and the surface boundary conditions another. Only at an eigenfrequency is it possible to satisfy the surface and core boundary conditions simultaneously with eigenfunctions smooth throughout the star.

The original computer implementation of the slow-motion formalism found the eigenfrequencies and eigenfunctions of the system by shooting. A guess was made for the eigenfrequency, and the two-parameter family of surface solutions was numerically integrated to a midpoint in the star. Similarly, the two-parameter family of core solutions was numerically integrated to the same midpoint. The trial eigenfrequency was considered a true eigenfrequency when a linear combination of the surface solutions could be matched smoothly to a

linear combination of the core solutions.

Consideration of discontinuity modes adds boundary conditions inside the star. Since the eigenfunctions of a discontinuity mode are sharply peaked near the discontinuities, the stability of numerical integration of solutions near discontinuities is delicate.

For simplicity, consider an idealized star with a single discontinuity in its equation of state. The discontinuity-mode eigenfunctions are strongly peaked about the discontinuity; however, of the two surface (or core) solutions, one is strongly peaked about the discontinuity and the other decays as the discontinuity is approached. Since the eigenfunctions are strongly peaked about the discontinuity, integration of the system toward the discontinuity is stable, while integration away from the discontinuity is not.

In a star with multiple discontinuities, integration toward one discontinuity is always integration away from another. What is appropriate in this circumstance is always to integrate toward the *nearest* discontinuity. The appropriate definition of *nearest* can be a subtle issue; in the author's slow-motion code these subtleties have been ignored, and *nearest* is defined by physical proximity.

In the slow-motion code, the algorithm for determining discontinuity modes goes as follows. Given a trial frequency, the two-parameter family of solutions satisfying the core boundary conditions is integrated from the center of the star to its midpoint. (In all the cases considered, the innermost discontinuity is at $r > \mathcal{R}/2$.) Also as

before, a two-parameter family of solutions is integrated from the surface of the star toward the outermost discontinuity; however, at the outermost discontinuity, integration of the surface solutions stops.

At the midpoint between each adjacent pair of discontinuities, a four-parameter family of solutions is introduced. These solutions are integrated from the midpoint toward the discontinuities. The integration is monitored to insure a minimum spatial resolution in this region, and stops at the discontinuities. Similarly, in the region between the innermost discontinuity and the star's midpoint, a four-parameter family of solutions is integrated toward the midpoint and toward the innermost discontinuity. A trial frequency is an eigenfrequency if a linear combination of the many solutions can be found that satisfies the boundary conditions at the discontinuities and is otherwise smooth throughout the star. By this technique, integration always proceeds toward the *nearest* discontinuity.

A disadvantage of this algorithm is that it requires the solution of a large system of equations. If there are N discontinuities in the star, then a system of $4(N+1)$ homogeneous algebraic equations in $4(N+1)$ variables must be solved. The numerical solution of such a large system is delicate. In numerical code described here, an initial solution to the system is found by singular-value decomposition and improved by iteration (*cf.* Press *et al.* 1986). The degree to which the solution of this system does not satisfy the system is monitored in a norm where all the equations have equal weight.

Table Captions

Table 1. Discontinuity modes are analogous to gravity waves in a discontinuously stratified fluid. This table compares quadrupole discontinuity-mode period and energy estimates based on this analogy (§3.5) with detailed numerical calculations made with the slow-motion formalism. Each row in this table is for a different model star. All the models have a central density $\rho_c = 10^{15}$ g cm^{-3}. The equation of state is given by equation (4.1) with $\Gamma_0=5/3$ and $K=9$ km$^{4/3}$. The density ρ_+ at the discontinuity and the fractional density discontinuity $\Delta\rho/\rho_+$ are shown in the table. All of the models have a radius of $\mathcal{R}=14.1$ km and a mass of $\mathcal{M}=0.95$ M$_\odot$. The first column shows the fractional coordinate distance of the discontinuity from the surface of the star. The fourth and fifth columns show the true and estimated period of the discontinuity mode, and the sixth and seventh column show the true and estimated pulsational energy. The energy is normalized to $\xi^r/\mathcal{R}=1$ at the surface of the star, where ξ^r is the radial coordinate displacement of a perturbed fluid element from its equilibrium position. The eighth column shows the gravitational radiation damping time of the pulsations calculated by the slow-motion formalism.

Table 2. Properties of the density discontinuities in the Baym, Pethick, & Sutherland (1971) equation of state. The first three columns show the nature of the composition change, the density at which it occurs, and the fractional density discontinuity. The next column gives the estimated pressure at the discontinuity, which is not given by Baym, Pethick, & Sutherland. The technique used to estimate the pressure at

the discontinuities is described in the text. The final column shows the fractional coordinate depth at which the discontinuity occurs for a particular stellar model. The model is based on equation of state model B of Arnett & Bowers (1974). In the low-density regime, model B uses the BPS equation of state. The central density of the model is $\rho_c = 10^{15}$ g cm^{-3}, the mass is 0.52 $M_\odot$, and the radius is 9.8 km.

Table 3. A comparison of quadrupole f-mode characteristics calculated by Lindblom & Detweiler (1983) using the exact theory of nonradial pulsations, and those calculated in this paper using the slow-motion formalism. In the present work, discontinuities in the equation of state are explicitly taken into account. The discontinuities do not affect the f-modes; rather, they perturb g-modes away from zero frequency. Model stars built from four different equations of state are compared in this table. The first column shows the Arnett & Bowers (1974) designation of the equation of state used to build the model. All the models had central density $\rho_c = 10^{15}$ g cm^{-3}. Columns designated SM refer to slow-motion formalism calculations; columns designated LD refer to the exact-formalism calculations of Lindblom & Detweiler (1983).

Table 4. Properties of the first four quadrupole discontinuity modes of a particular model star, based on equation of state model B of Arnett & Bowers (1974). The low-density equation of state is that of Baym, Pethick & Sutherland (1971). The central density of is $\rho_c = 10^{15}$ g cm^{-3}; the radius of the model is $\mathcal{R}$=9.83 km, and the mass is $\mathcal{M}$=0.522 $M_\odot$. The properties tabulated below were calculated using the slow-motion formalism. The energy is normalized to $\xi^r/\mathcal{R}$=1 at the surface of the

star, and scales as $(\xi^r/\mathcal{R})^2$.

Table 5. Properties of the first quadrupole discontinuity mode of four model stars. Each model has a central density of 10^{15} g cm^{-3}. All the models have the same low-density equation of state (Baym, Pethick, & Sutherland 1971), but each has a different high-density equation of state. Arnett & Bowers (1974) give the complete equation of state for each model; the first column of the table refers to the equation of state as designated in Arnett & Bowers. The next three columns show the fractional coordinate distance from the surface to the discontinuity associated with the first (g_1) quadrupole discontinuity mode, the radius $\mathcal{R}$, and mass $\mathcal{M}$ of the star. (The g_1 mode of the star is associated with the transition ^{78}Ni$\rightarrow^{76}$Fe at a density $\rho=1.6\times10^{11}$ g cm^{-3}). Section 3.5 develops estimates for the period and pulsational energy of the g_1 mode; the next four columns compare the slow-motion formalism calculations of the period and energy with these estimates. The slow-motion formalism calculations are in the columns headed SM. The energy is normalized to $\xi^r/\mathcal{R}=1$ at the surface of the star, and scales as $(\xi^r/\mathcal{R})^2$. The final column gives the gravitational-radiation damping time of the mode as calculated by the slow-motion formalism. The fact that the ratio of the Est to SM columns is independent of the high-density equation of state (model A, B, C, D) shows that the properties of the g_1 mode are determined by just the physical location of the density discontinuity, its fractional size, and the overall mass and radius of the star.

Figure Captions

Figure 1. Section 3.5 develops estimates for discontinuity-mode periods, energies, and eigenfunctions based on an analogy between discontinuity modes and ordinary gravity waves in a two-component, incompressible fluid. To investigate the accuracy of these estimates, 120 different model stars were constructed (§4.2), each model with a single discontinuity in the equation of state. The models represented varying adiabatic index, central density, density at the discontinuity, and density discontinuity. The discontinuity-mode period, energy, damping time, and eigenfunctions were computed with the slow-motion formalism. In this figure, the ratio between the computed and estimated periods are compared. The abscissa is the logarithmic fractional depth of the discontinuity in the star. The fractional depth must be small for the the simple model to approximate the conditions in a neutron star. Each of the 120 models is represented by a cross, and lines through the crosses indicate the two different adiabatic indices sampled. For more details, see §3.5 and §4.2.

Figure 2. The ratio of the pulsation energy computed in the slow-motion formalism to the estimated energy as a function of the logarithmic fractional depth of the discontinuity. See caption of Figure 1 for further explanation.

Figure 3. The ratio of the amplitude of the radial motion of a fluid element at the discontinuity to the predicted amplitude as a function of the logarithmic fractional depth of the discontinuity. See caption of Figure 1 for further explanation.

Figure 4 Typical fluid-variable eigenfunctions in an idealized neutron star model with a single discontinuity in its equation of state. The proper radial displacement of a fluid ξ^r and its Eulerian pressure perturbation β are shown as a function of the logarithmic fractional depth in the star. The equation of state is given by equation (4.1), with $\Gamma_0=5/3$ and $K=9\,\mathrm{km}^{4/3}$. The model had central density $10^{15}\,\mathrm{g\,cm}^{-3}$, density at the discontinuity $10^{12}\,\mathrm{g\,cm}^{-3}$, and fractional density discontinuity 10%. For more details see §4.2.

Figure 5 The Baym, Pethick, & Sutherland equation of state has 11 density discontinuities, and associated with each is a discontinuity mode. This figure shows the proper radial displacement of a perturbed fluid element for the first four discontinuity modes of a particular model star. The star was built from equation of state model B of Arnett & Bowers and the central density of the model was $10^{15}\,\mathrm{g\,cm}^{-3}$. The abscissa shows the logarithmic fractional depth in the star. For more details see §4.3.

Table 1.

$\Delta r/\mathcal{R}$	ρ_+	$\Delta\rho/\rho_+$	Period		Energy		Damping Time
%	10^{12} g cm^{-3}	%	ms		10^{52}ergs		sec
			SM	Est.	SM	Est.	SM
16.	45.	2	8.49	8.1	45.3	54.	1.15(10)
10.	19.	5	7.41	6.2	8.93	11.	7.10(09)
6.6	8.1	10	7.11	5.4	2.21	2.8	1.22(10)
6.1	8.1	5	10.2	7.6	4.26	5.4	2.42(11)
5.8	8.1	2	16.3	12.	10.4	13.	1.08(13)
3.9	4.3	2	20.5	14.	5.81	7.4	1.62(14)
2.3	1.8	5	17.5	12.	1.07	1.3	1.43(14)
1.7	.95	10	15.2	10.	.303	.39	1.16(14)
1.5	.95	5	21.8	14.	.579	.71	2.28(15)
1.5	.95	2	34.8	23.	1.41	1.8	1.01(17)

Table 2.

Composition	ρ_+	$\Delta\rho/\rho_+$	p_0	$\Delta r/\mathcal{R}$
-	g cm^{-3}	%	dyne cm^{-2}	%
^{56}Fe→^{62}Ni	8.1(6)	2.9	5.3(23)	0.22
^{62}Ni→^{64}Ni	2.7(8)	3.1	6.9(25)	1.0
^{64}Ni→^{84}Se	1.2(9)	7.9	4.9(26)	1.8
^{84}Se→^{82}Ge	8.2(9)	3.5	5.8(27)	3.2
^{82}Ge→^{80}Zn	2.2(10)	3.8	2.1(28)	4.4
^{80}Zn→^{78}Ni	4.8(10)	4.1	5.6(28)	5.5
^{78}Ni→^{76}Fe	1.6(11)	4.6	2.6(29)	7.6
^{76}Fe→^{124}Mo	1.8(11)	2.2	2.9(29)	7.8
^{124}Mo→^{122}Zr	1.9(11)	3.1	3.0(29)	7.8
^{122}Zr→^{120}Sr	2.7(11)	3.3	4.6(29)	8.5
^{120}Sr→^{118}Kr	3.7(11)	3.5	6.7(29)	9.2

Table 3.

Model	Radius	Mass	f-mode			
			Period		Damping Time	
-	(km)	($M_\odot$)	(ms)		(sec)	
			LD	SM	LD	SM
A	10.0	0.812	0.494	0.507	0.314	0.335
B	9.83	0.522	0.525	0.528	0.638	0.649
C	12.0	1.32	0.531	0.562	0.214	0.223
D	11.1	1.06	0.514	0.533	0.251	0.268

Table 4.

Mode	Period	Energy	Damping Time
-	(ms)	(10^{48} erg)	(sec)
g_1	5.13	25.2	1.09(12)
g_2	10.5	4.14	9.56(15)
g_3	14.2	4.14	1.93(16)
g_4	15.3	1.04	2.46(17)

Table 5.

Model	$\mathcal{R}$	$\mathcal{M}$	$\Delta r/\mathcal{R}$	Period		Energy		τ
-	km	$M_\odot$	%	(ms)		(10^{49} erg)		(sec)
				SM	Est.	SM	Est.	SM
A	10.0	.812	4.7	5.70	5.7	4.80	28.	1.02(13)
B	9.83	.522	7.6	5.13	5.8	2.52	14.	1.09(12)
C	12.0	1.32	3.2	7.41	7.1	13.4	81.	4.12(13)
D	11.1	1.06	3.9	6.57	6.5	8.50	51.	2.18(13)

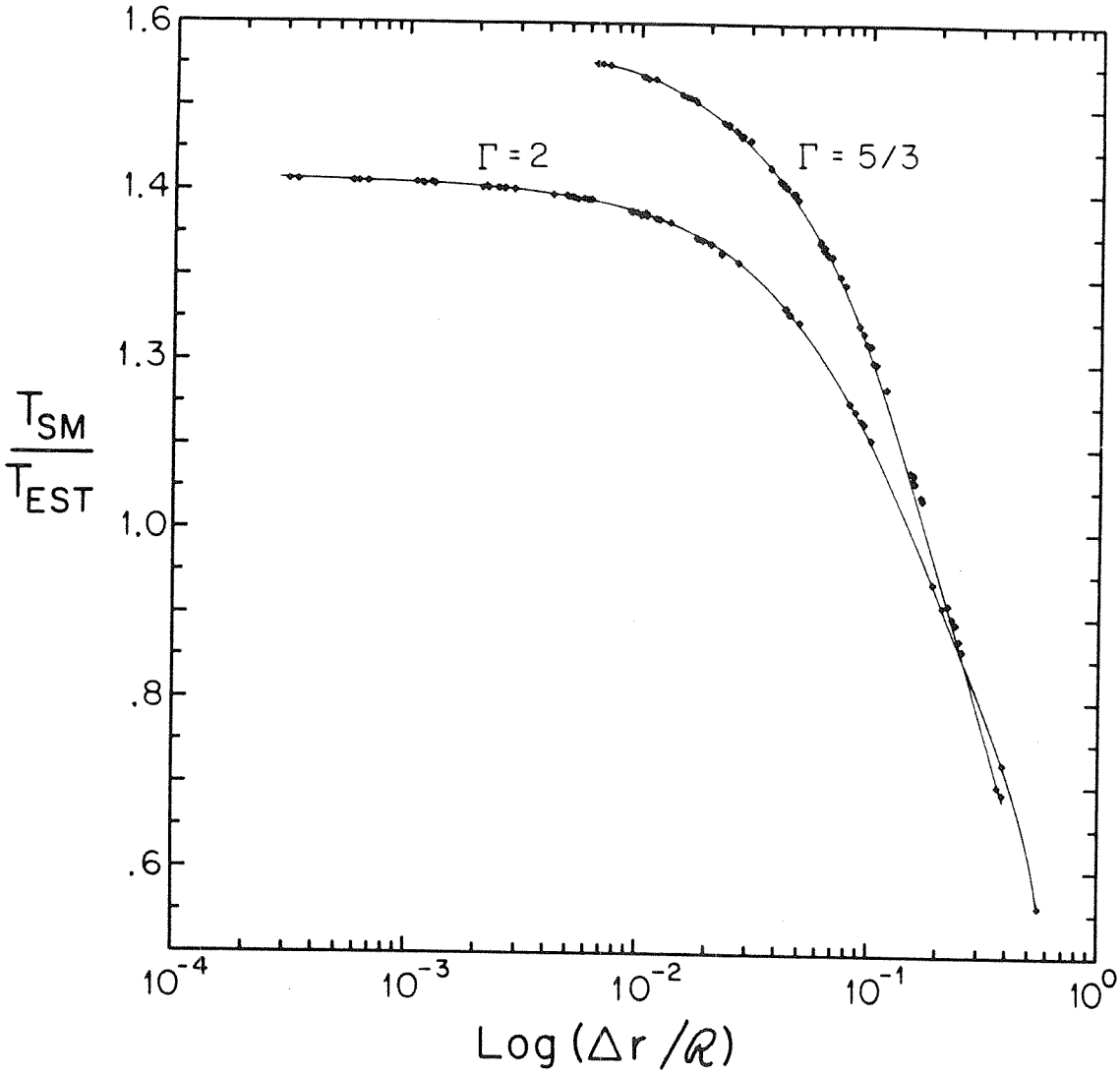

Figure 1

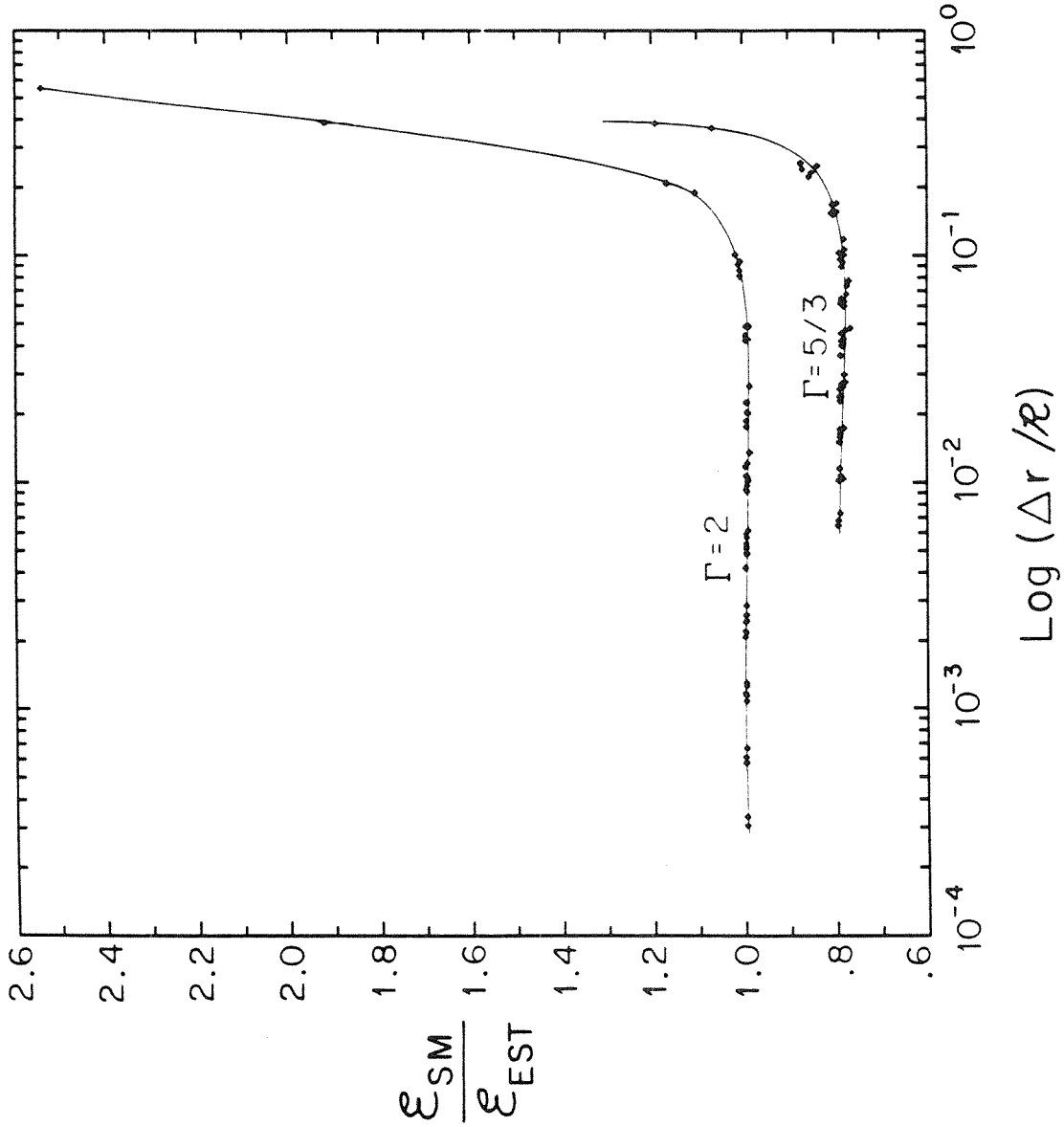
2.6
2.4
2.2
2.0
1.8
1.6
1.4
1.2
1.0
.8
.6
$\frac{\varepsilon_{SM}}{\varepsilon_{EST}}$
10^{-4}
10^{-3}
10^{-2}
10^{-1}
10^{0}
Log (Δr /$\mathcal{R}$)
$\Gamma = 2$
$\Gamma = 5/3$

Figure 2

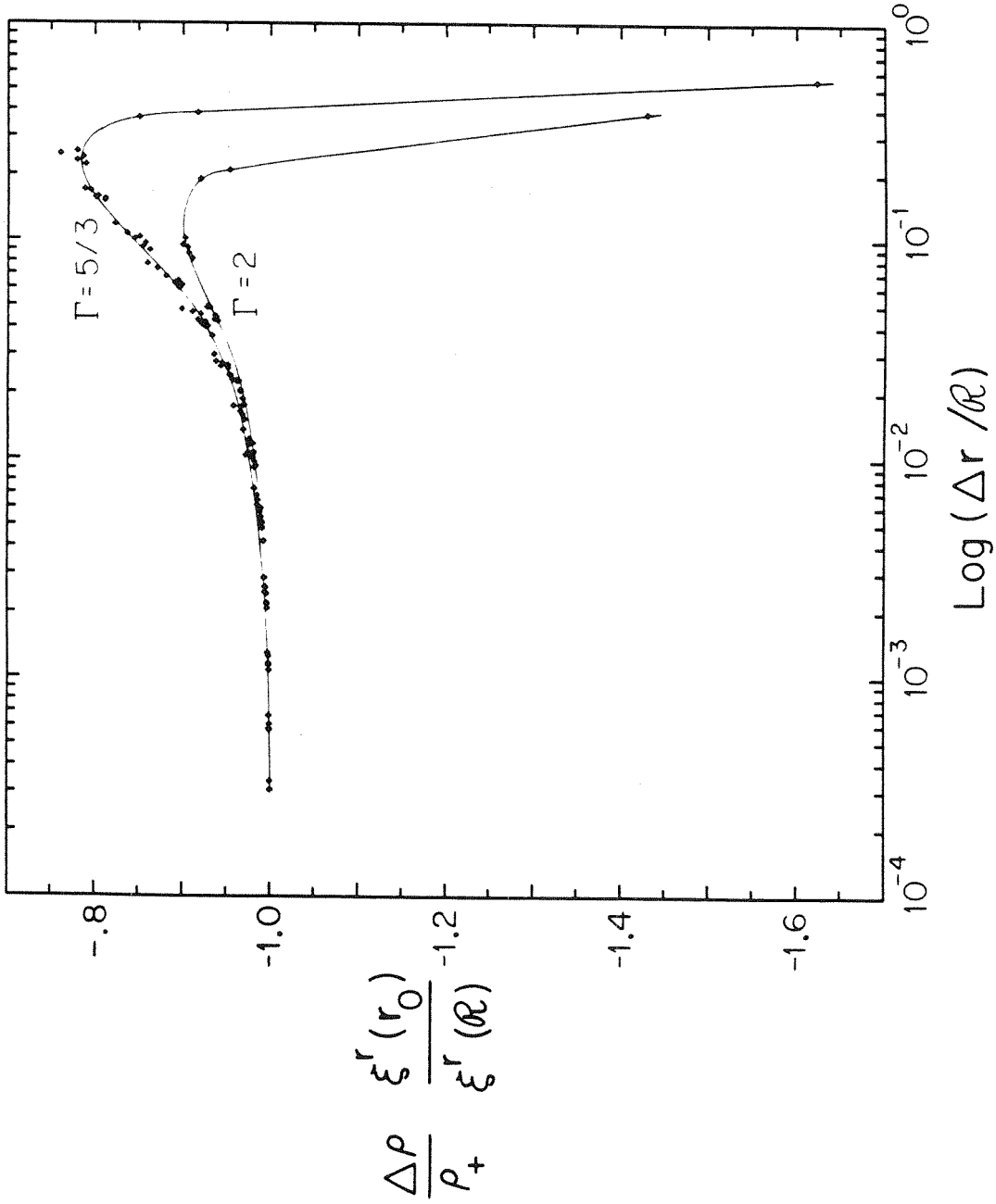
Γ = 5/3
Γ = 2
-.8
-1.0
-1.2
-1.4
-1.6
10^{-4}
10^{-3}
10^{-2}
10^{-1}
10^{0}
$\frac{\Delta\rho}{\rho_+} \quad \frac{\xi^r(r_0)}{\xi^r(\mathcal{R})}$
Log (Δr /ℛ)

Figure 3

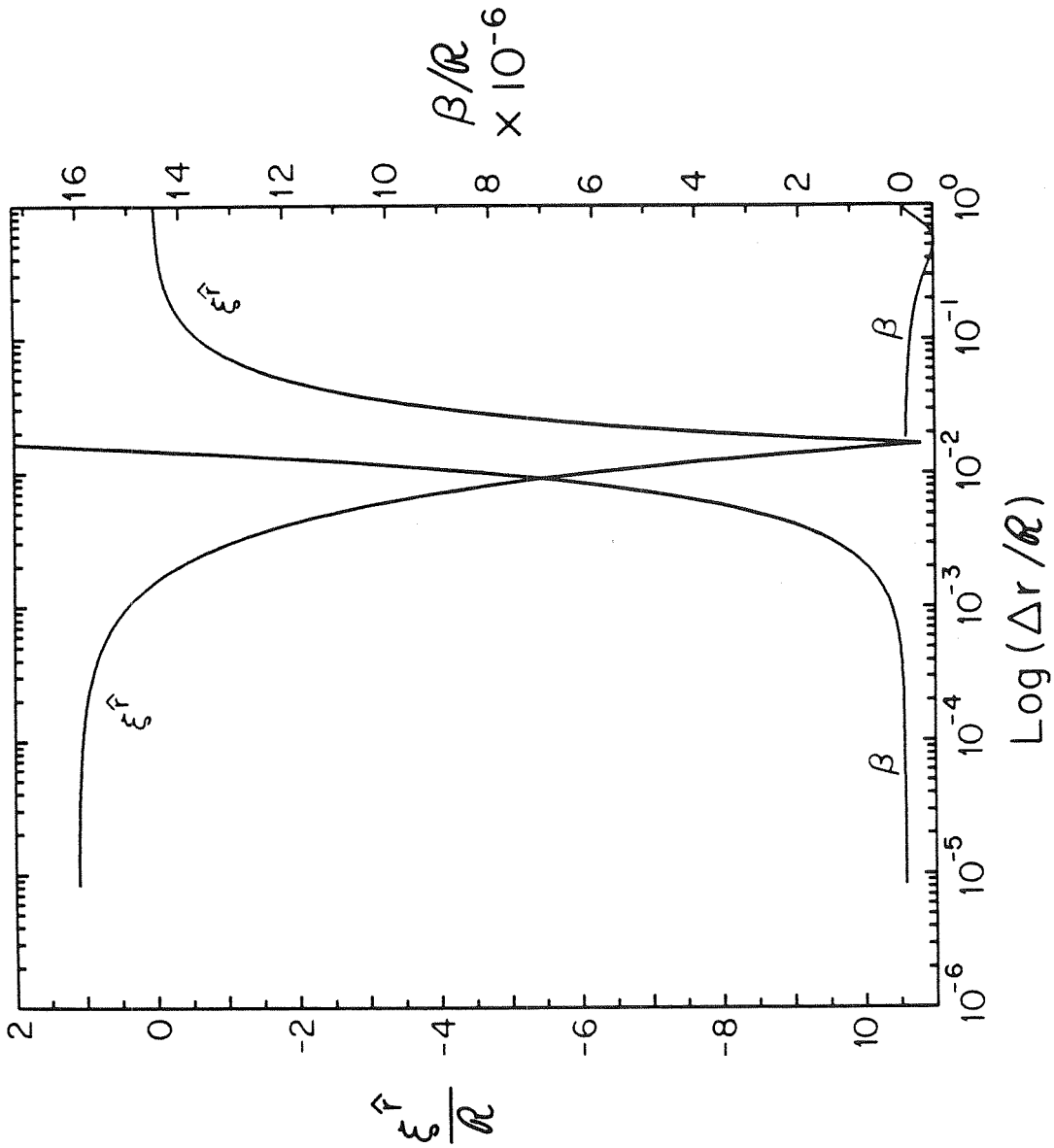

Figure 4

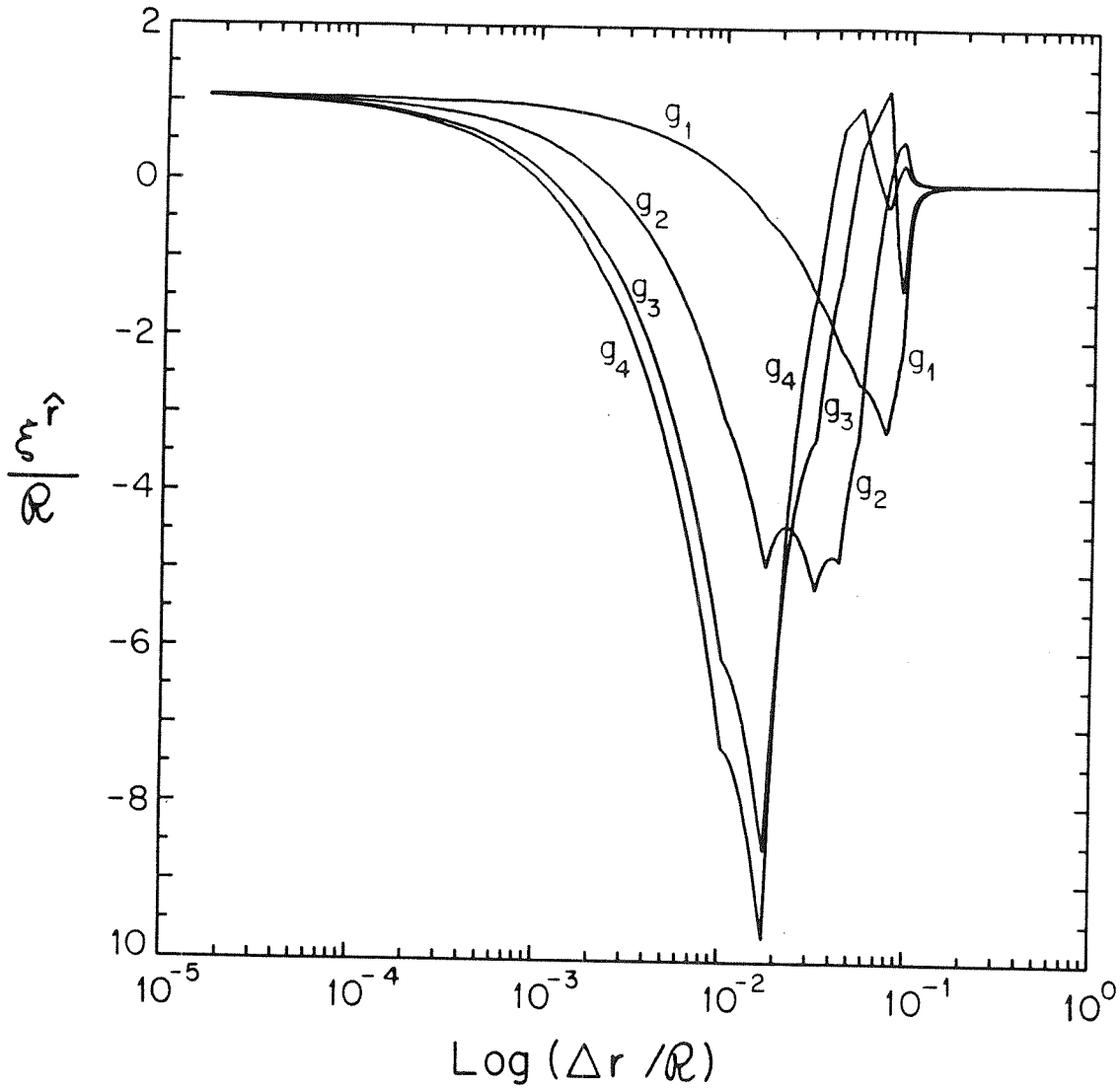
2
0
-2
-4
-6
-8
10
$\hat{r}$
ξ
$\mathcal{R}$
g_1
g_2
g_3
g_4
g_4
g_3
g_2
g_1
10^{-5}
10^{-4}
10^{-3}
10^{-2}
10^{-1}
10^{0}
Log (Δr /$\mathcal{R}$)

Figure 5

Chapter 4

Relativistic Stellar Pulsations in the Relativistic Cowling Approximation

Submitted to *Monthly Notices of the Royal Astronomical Society.*

Abstract

Much that is known about the general pulsational properties of non-rotating Newtonian stars is traceable to the fact that in the Cowling approximation, the stellar pulsation equations can be cast in a nearly Sturm-Liouville form. In this paper, the relativistic Cowling approximation (an approximation scheme first introduced by McDermott, Van Horn, & Scholl [1983] and analogous to the Newtonian Cowling Approximation) is investigated, and it is shown that in this approximation the equations for non-radial relativistic stellar pulsations are also of nearly Sturm-Liouville character. The consequences of this are discussed as a series of theorems regarding the eigenfrequencies, and eigenfunctions of g-modes, f-modes, and p-modes in relativistic stars.

1. Introduction

1.1. Motivation

In 1941, Cowling realized that with the neglect of the Eulerian perturbation of the gravitational potential, the linearized non-radial stellar pulsation problem for non-rotating stars is Sturm-Liouville in both the high- and low-frequency limits. It was this limiting character of the pulsational equations that led Cowling to separate the pulsational spectrum into three parts: at fixed spherical harmonic order l, he identified the high-frequency p-mode spectrum and the low-frequency g-mode spectrum, separated by the single f-mode.

Owing to the nearly Sturm-Liouville nature of the equations describing Newtonian stellar pulsations, a great deal is known about the pulsational spectra of Newtonian stars; for example, the theory provides necessary and sufficient conditions for the existence of stable and unstable g-modes, the number of such modes, and (when the number is infinite) their asymptotic period separation (see Gabriel & Scuflaire 1979 for a complete treatment of the Newtonian equations in the Cowling approximation).

In 1983, McDermott, Van Horn, & Scholl proposed that an approximation analogous to the Newtonian Cowling approximation could be applied to the relativistic non-radial stellar pulsation problem. In this paper, their relativistic Cowling approximation is made precise and is put into a form where the same techniques used to analyze the Newtonian equations can be applied with the same results: theorems about the number of pulsational modes and their stability, about the asymptotic behavior of the pulsational eigenfrequencies, and about the correlation between eigenfrequencies and nodes of their eigenfunctions. These results will be derived for the special case of non-rotating perfect-fluid relativistic stars.

The remainder of §1 describes the conventions and notations used throughout the paper. In §2 the Cowling approximation is discussed for both Newtonian and relativistic stars, and the relativistic Cowling approximation is given a precise formulation. Section 3 introduces the nearly Sturm-Liouville form of the relativistic perturbation equations and discusses the physical content of several theorems related to the system. The conclusions are presented in §4.

1.2. Conventions and Notation

The relativistic non-radial stellar pulsation problem is formulated in terms of a general perturbation about an exact solution of the Einstein Field Equations; the line element of the exact solution is

$$ds_0^2 = e^{\nu}dt^2 - e^{\lambda}dr^2 - r^2 d\Omega^2, \tag{1.1}$$

where

$$d\Omega^2 = d\theta^2 + \sin^2\theta d\phi^2. \tag{1.2}$$

The functions $\nu(r)$ and $\lambda(r)$ are defined by the equations of stellar structure:

$$\frac{d\nu}{dr} = \frac{2(m + 4\pi r^3 p)}{r(r-2m)}, \tag{1.3}$$

$$e^{-\lambda} = 1 - \frac{2m}{r}, \tag{1.4}$$

and

$$m(r) = \int_0^r 4\pi r^2 \rho dr. \tag{1.5}$$

The perturbations about this exact solution are resolved into spherical harmonic angular dependence Y_{lm} and exponential time dependence $\exp(-i\omega t)$ with complex frequency $\omega \equiv \sigma - i/\tau$ (σ and τ real). The metric perturbations are expressed in Regge-Wheeler (1957) gauge; for fixed spherical harmonic order l and m, the

perturbed metric is expressed in terms of three functions, H_0, H_1, and K (see Thorne & Campolattaro 1967, but note the difference in the definition of H_1):

$$ds^2 \equiv ds_0^2 + \left(e^{\nu} H_0 dt^2 + 2\frac{dH_1}{dt} dt\, dr + e^{\lambda} H_0 dr^2 + r^2 K d\Omega^2 \right) Y_{lm}. \tag{1.6}$$

The fluid degrees of freedom are expressed in terms of the radial coordinate displacement of a fluid element from its equilibrium location and the Eulerian pressure perturbation. Denoting the coordinate displacement of a fluid element from its equilibrium location as $\vec{\xi}$, the fluid perturbations are W and β, where

$$\xi^r \equiv r^{-2} e^{-\lambda/2} W Y_{lm}, \tag{1.7}$$

$$\delta p \equiv \beta Y_{lm}, \tag{1.8}$$

and

$$\delta p \equiv \left(\begin{array}{c} \text{Eulerian} \\ \text{pressure} \\ \text{perturbation} \end{array} \right). \tag{1.9}$$

In general, a quantity prefixed by δ (Δ) indicates its Eulerian (Lagrangian) perturbation.

For completeness, the angular components of the fluid displacement are expressed in terms of the radial function V:

$$\begin{aligned} \xi^{\theta} &\equiv -\frac{V}{r^2}\frac{dY_{lm}}{d\theta}, \\ \xi^{\phi} &\equiv -\frac{V}{r^2 \sin^2\theta}\frac{dY_{lm}}{d\phi}. \end{aligned} \tag{1.10}$$

The subscript N on a relativistic quantity is used to indicate its Newtonian limit, or a Newtonian quantity analogous to the relativistic quantity, and subscripted square brackets are used to indicate a discontinuity in a quantity; *e.g.*,

$$[\rho]_r \equiv \lim_{\epsilon \to 0} \{\rho(r+\epsilon) - \rho(r-\epsilon)\}. \tag{1.11}$$

2. The Cowling Approximation

2.1. Introduction

This subsection is a brief introduction to the Newtonian Cowling approximation and its validity. The knowledgeable reader may wish to skip this subsection and proceed directly to §2.2, where the version of the relativistic Cowling approximation proposed in this paper is presented.

The Newtonian Cowling approximation (Cowling 1941) neglects the Eulerian perturbation of the Newtonian gravitational potential in the linearized pulsation equations. In Newtonian theory, the Eulerian perturbation $\delta\Phi$ of the gravitational potential Φ is determined by the Poisson equation

$$\nabla^2\delta\Phi = 4\pi\delta\rho_N, \tag{2.1}$$

where $\delta\rho_N$ is the Eulerian perturbation of the rest-mass density ρ_N. For large radial-wavenumber k_r or spherical harmonic order l, equation (2.1) becomes in order of magnitude

$$\delta\Phi \simeq -4\pi\delta\rho_N \left[k_r^2 + l(l+1)/R^2\right]^{-1}, \tag{2.2}$$

where R is the radius of the star. Consequently, for high radial- or angular-order modes, $\delta\Phi$ is negligible compared to $R^2\delta\rho_N$.

Similarly, in the Newtonian Cowling approximation, the radial displacement function W_N (where $\xi^r \equiv W_N Y_{lm}/r^2$) is described by the radial Euler equation. The radial and angular Euler equations and the continuity equation can together be simplified to yield a first-order equation for W_N:

$$\frac{dW_N}{dr} = -\frac{r^2}{dp/dr}\left(\frac{1}{\Gamma p}\frac{dp}{dr} + \frac{d\Phi}{dr}\frac{l(l+1)}{(\sigma r)^2}\right)\beta_N + \frac{1}{\Gamma p}\frac{dp}{dr}W_N, \tag{2.3}$$

where

$$\beta_N \equiv \begin{pmatrix} \text{Eulerian perturbation of} \\ \text{the Newtonian pressure} \end{pmatrix}, \tag{2.4}$$

$$\Gamma \equiv \frac{\Delta p}{\Delta \rho_N} \frac{\rho_N}{p}, \tag{2.5}$$

and

$$\Delta p = \begin{pmatrix} \text{Lagrangian} \\ \text{pressure} \\ \text{perturbation} \end{pmatrix}, \qquad \Delta \rho_N = \begin{pmatrix} \text{Lagrangian} \\ \text{rest-mass-density} \\ \text{perturbation} \end{pmatrix}. \tag{2.6}$$

(For a derivation of [2.3] see §3.2 below; also, *cf.* Ledoux & Walraven 1958 eq. [79.4] — but beware the difference in notation). Here and below, σ represents the angular frequency of a pulsational mode.

High-order modes (corresponding to either large l or n) can correspond to either high- or low-frequency (*i.e.*, to either p- or g-modes). For high-order, high-frequency modes (*i.e.*, $kR \gg 1$ and $[\sigma R]^2 \gg 1$, corresponding to p-modes), the frequency σ is related to the wavenumber k through the sound speed $c_{s,N}$:

$$\sigma^2 \simeq \left(\frac{\Gamma p}{\rho_N}\right)^2 k^2 \equiv c_{s,N}^2 k^2 \tag{2.7}$$

(*cf. e.g.*, Cox eq. [17.95]); while for high order, low-frequency modes (*i.e.*, $kR \gg 1$ and $[\sigma R]^2 \ll 1$, corresponding to g-modes), the frequency is related to the wavenumber through the Newtonian Brunt-Väisälä frequency n_N:

$$\sigma^2 \simeq -\frac{1}{p}\frac{dp}{dr}\left(\frac{1}{\Gamma_0} - \frac{1}{\Gamma}\right)\frac{d\Phi}{dr}\frac{l(l+1)}{(kR)^2} \equiv n_N^2 \frac{l(l+1)}{(kR)^2} \tag{2.8}$$

(*cf. e.g.*, Cox eq. [17.96]). Both of these dispersion relations are valid in either of the limits $n/l \to \infty$ or $l/n \to \infty$; in the former limit, the wavenumber $|k|$ is asymptotic to n/R, while in the latter limit, the wavenumber is asymptotic to $[l(l+1)]^{1/2}/R$. In equation (2.8), the index Γ_0 is defined

$$\Gamma_0 \equiv \frac{dp/dr}{d\rho_N/dr}\frac{\rho_N}{p}. \tag{2.9}$$

(Note the difference between the index Γ_0 eq. [2.9] and the adiabatic index Γ eq. [2.5]: the former describes the relationship between pressure and density in the equilibrium stellar model, while the latter describes their relationship in the pulsating fluid.)

Together with (2.3), the dispersion relations show that for high-frequency and high-order modes

$$\frac{W_N}{R^3} \simeq \frac{1}{kR}\frac{\beta}{\Gamma p}, \tag{2.10}$$

while for low-frequency and high-order modes

$$\frac{W_N}{R^3} \simeq \frac{kR}{n_N^2 R^2}\frac{\beta_N}{\rho_N}. \tag{2.11}$$

Thus, for p- and g-modes of sufficiently high order kR, $\delta\Phi$ is negligible compared to either W_N/R^3 or $R^2\delta\rho_N$ and the Cowling approximation is valid. Physically, the mass motion is incoherent for high-order modes and this suppresses the gravitational perturbation. A more compact way of saying this is that high-order modes are strictly local phenomenon.

Actually, the Newtonian Cowling approximation is good for for all g-modes, since for these modes the Eulerian rest-mass-density perturbation (the source of $\delta\Phi$) is negligible compared to the fluid displacement regardless of the order.

This discussion is strictly correct only in the asymptotic limits $n/l \to \infty$ and $l/n \to \infty$; however, some justification can be had for neglecting $\delta\Phi$ even when both n and l are small (Cowling 1941), and experience has shown that the Cowling approximation gives an accurate description of high-order monopole and dipole modes, and of all modes with $l \geq 2$ in Newtonian stars (Deubner & Gough 1984).

In general relativity, metric perturbations are the analog of the Newtonian gravitational perturbation $\delta\Phi$, and a "relativistic" Cowling approximation neglects certain Eulerian perturbations of the metric. The question of which metric perturbations to neglect, and the determination of the approximation's regime of validity

is delicate, however: in general relativity, the metric perturbations are intertwined with the fluid perturbations through both initial value and dynamical equations; and in the limit of high frequency the gravitational field is radiative (for $l \geq 2$) inside a compact star. In the next subsection, a modification of the relativistic Cowling approximation proposed by McDermott, Van Horn, & Scholl (1983) is introduced; and in the final subsection the regime of validity of the approximation is discussed.

2.2. The Relativistic Cowling Approximation

A relativistic analog of the Newtonian Cowling approximation involves the neglect or approximation of the gravitational (or metric) perturbations. As a way of determining an appropriate approximation for the metric perturbation, consider the zero frequency limit of the Newtonian and relativistic equations of stellar pulsations. In the limit of zero frequency, the Eulerian perturbation $\delta\Phi$ of the Newtonian gravitational field vanishes and the Newtonian Cowling approximation agrees exactly with the full Newtonian theory of stellar pulsations. Similarly, in the relativistic theory of stellar pulsations, the zero frequency limit of the complete equations for $l \geq 2$ admits solutions of the form (Finn 1986a eqs. [7a–d] and eq. [9b])

$$\begin{aligned} \beta = H_0 = K = 0, \\ H_1 = \frac{16\pi(\rho + p)e^{\lambda/2}}{l(l+1)} W, \end{aligned} \tag{2.12}$$

where ρ and p are the total energy density (as distinguished from the rest-mass density ρ_N) and pressure measured in the rest-frame of the fluid, respectively; and the radial function W is given by

$$W(r,t) = \mathcal{W}(r)t, \qquad \text{where} \quad \mathcal{W}(r) \equiv \begin{pmatrix} \text{arbitrary piecewise} \\ \text{continuous function} \end{pmatrix}. \tag{2.13}$$

The function $\mathcal{W}$ vanishes at $r = 0$, R, and in regions where the star is not neutrally stable against convection. Just as $\delta\Phi$ vanishes in the limit of zero frequency, so the

relativistic metric perturbations H_0 and K vanish; however, the metric perturbation $g_{tr} = dH_1/dt$ remains finite and can be large. The non-vanishing of H_1 suggests that in the Newtonian limit it is not completely determined by the Newtonian gravitational perturbation $\delta\Phi$.

In fact, the metric perturbation H_1 has no Newtonian analog: it represents the gravitational effects of the radial momentum density due to the fluid motion. In the Newtonian limit of slow-motion and weak fields, the metric perturbations H_0, H_1, and K are expressed in terms of Newtonian quantities as follows (Thorne 1969, eqs. [20a–b] — but beware the different definition of H_1):

$$\begin{aligned} H_0 &= K = -2\delta\Phi, \\ H_1 &\simeq \frac{1}{l(l+1)}\left(16\pi\rho_N W_N - 4r^2\frac{d\delta\Phi}{dr}\right), \end{aligned} \tag{2.14}$$

(recall that $W_N \equiv r^2\xi^r/Y_{lm}$ is the Newtonian radial displacement function). Thus, in the straightforward extension of the Newtonian Cowling approximation we expect H_0 and K to vanish, but not H_1.

Equation (2.14) should not be taken to mean that in the Newtonian limit the relativistic equations do not agree with the Newtonian equations; on the contrary, in the Newtonian limit

$$r^2(\rho + p) \lesssim M/R \simeq \|\Phi\| \ll 1, \tag{2.15}$$

and so

$$H_1 \lesssim \|\Phi\|\xi^r \ll \xi^r \sim W_N/R^2 \tag{2.16}$$

(M is the mass of the star). In the Newtonian limit, H_1 is thus negligible compared to W_N/R^2; only in compact stars where M/R is not small is H_1 not negligible.

With the insights provided by the zero frequency solutions and the Newtonian limits of the relativistic equations of stellar pulsations, the following set of equations correspond to a more accurate version of the relativistic generalization of the

Cowling approximation proposed by McDermott, Van Horn, & Scholl (see below for the detailed origin of these equations):

$$\left(e^{-\nu/2}\frac{d}{dr}-\frac{1}{\gamma p}\frac{dp}{dr}\right)\left\{e^{\nu/2}\gamma p\left[\frac{l(l+1)}{r^2}V+\frac{e^{-\lambda/2}}{r^2}\left(\frac{dW}{dr}+\frac{dp}{dr}\frac{1}{\gamma p}W\right)\right]\right\} + \sigma^2(\rho+p)e^{-\nu}\left(\frac{e^{\lambda/2}}{r^2}W-H_1\right)+\frac{1}{r^2}AW=0, \tag{2.17}$$

$$\sigma^2(\rho+p)e^{-\nu}V=\gamma p\left[\frac{l(l+1)}{r^2}V+\frac{e^{-\lambda/2}}{r^2}\left(\frac{dW}{dr}+\frac{1}{\gamma p}\frac{dp}{dr}W\right)\right], \tag{2.18}$$

$$\beta=-\gamma p\left[\frac{l(l+1)}{r^2}V+\frac{e^{-\lambda/2}}{r^2}\left(\frac{dW}{dr}+\frac{1}{\gamma p}\frac{dp}{dr}W\right)\right], \tag{2.19}$$

$$H_1=\frac{16\pi(\rho+p)e^{\lambda/2}}{l(l+1)}W. \tag{2.20}$$

In these relativistic equations, the angular pulsation frequency σ is in radians per unit Schwarzschild time t, and the relativistic convection discriminant A is given by (Finn 1986b eq. [2.6])

$$A=\frac{1}{p}\frac{dp}{dr}\left(\frac{1}{\gamma_0}-\frac{1}{\gamma}\right)e^{-\lambda/2}, \tag{2.21}$$

where

$$\gamma\equiv\frac{\Delta p}{\Delta\rho}\frac{\rho+p}{p},\quad \gamma_0\equiv\frac{dp/dr}{d\rho/dr}\frac{\rho+p}{p}. \tag{2.22}$$

The adiabatic index γ describes the pulsating fluid, while the index γ_0 describes the equilibrium model. Recall that Δp and $\Delta\rho$ are the Lagrangian pressure and energy-density perturbations.

The origins of equations (2.17)–(2.20) are as follows: Equations (2.17) and (2.18) are the radial and angular components of the relativistic Euler equations ($\delta T^{j\mu}{}_{;\mu}=0$, where j is r or θ, and $T^{\alpha\beta}$ is the stress energy tensor) in the limit that K and H_0 vanish; equation (2.19) is the relativistic continuity equation ($\nabla\cdot$

$[n\vec{u}] = 0$, where n is the number density of baryons and $\vec{u}$ is the 4-velocity) in the limit $K = H_0 = 0$; and equation (2.20) is the initial-value equation that defines the metric perturbation H_1 ($\delta G^{rt} = 8\pi\delta T^{rt}$, where $G^{\alpha\beta}$ is the Einstein tensor) in the limit that K and H_0 vanish. The remaining initial value and dynamical Einstein Field Equations are discarded in the relativistic Cowling approximation. For comparison, the full set of perturbed Einstein Field Equations together with the equations of motion can be found in Detweiler & Ipser (1973) equations (8c)–(9d); however, note two typographical errors in those equations: in equation (9c), the factor $-(2/r - 3\nu'/2 - \lambda'/2)H_0'$ should read $-(2/r + 3\nu'/2 - \lambda'/2)H_0'$, and the factor $-\exp(\nu/2)\nabla\delta p$ should read $-\exp(\nu/2)\nabla\delta p$.

With the the neglect of H_0 and K, the gravitational degree of freedom vanishes from the relativistic equations and there is no gravitational radiation. In the absence of other damping or driving forces, the square of the pulsation frequency is thus real.

The boundary conditions in the relativistic Cowling approximation are an abbreviation of the boundary conditions for the fully relativistic pulsation problem (Finn 1986a §2.2):

$$\begin{aligned} &\text{at } r = 0 \qquad W = \beta = 0, \\ &\text{at } r = R \qquad \beta + \frac{e^{-\lambda/2}}{r^2}\frac{dp}{dr}W = 0. \end{aligned} \tag{2.23}$$

Equation (2.23) arises from the requirements of regularity at the origin and vanishing of the Lagrangian pressure perturbation at the surface of the star. Furthermore, if the composition of the star changes discontinuously on shells at radii r_i, there are additional jump boundary conditions on W and β at the discontinuities (Finn 1986b §3.3):

$$\begin{aligned} [\beta]_{r_i} &= [\rho]_{r_i}\frac{1}{2}\frac{d\nu}{dr}\frac{e^{-\lambda/2}}{r^2}W, \\ [W]_{r_i} &= 0. \end{aligned} \tag{2.24}$$

These jump conditions represent the requirements of continuity of the Lagrangian pressure perturbation and radial fluid displacement across a discontinuity in the density of the unperturbed star.

Since the Einstein Field Equations consist of both dynamical and initial-value equations, it is important to make the relativistic Cowling approximation *before* any of the field equations are simplified. If this precaution is not taken, then equations that are later discarded might inadvertently be used before being discarded to eliminate H_1 from some or all of the the remaining equations, thereby leading to various inconsistent approximations.

For exactly this reason, the relativistic Cowling approximation described above differs from that proposed by McDermott, Van Horn, & Scholl (1983): They derived their approximation by setting $H_0 = K = 0$ in a set of equations from which H_1 had already been eliminated — eliminated not using the exact version of equation (2.20), but rather using one of the equations that the Cowling approximation discards. It turns out that their approximation can be obtained from the above by setting H_1 equal to zero in equations (2.17)–(2.19) and discarding equation (2.20). Thus, their equations differ from the above by fractional errors of order

$$\frac{H_1}{W/R^2} \simeq \frac{16\pi R^2(\rho + p)}{l(l+1)}. \tag{2.25}$$

All of the modes studied in McDermott, Van Horn, & Scholl have significant radial displacements only in the outermost regions of the star where the energy density ρ and pressure p are small; consequently, the errors committed by neglecting H_1 are insignificant in their numerical work. The role of H_1 in the relativistic Cowling approximation is discussed in more detail in §3.3 below.

For dipole ($l = 1$) perturbations, the story is a little different but the bottom line is the same. Dipole pulsations do not give off gravitational radiation; in terms of the perturbation equations, the gravitational degree of freedom present in the

Regge-Wheeler gauge for $l \geq 2$ becomes a coordinate gauge freedom in the case $l = 1$. Campolattaro & Thorne (1970) exploited this $l = 1$ gauge freedom to find a unique coordinate gauge where the gravitational (metric) perturbations vanish outside the star and expressed the pulsation equations in this gauge.

In the relativistic Cowling approximation proposed above, the gravitational degree of freedom has already been eliminated by the neglect of the perturbations H_0 and K; consequently, in the $l = 1$ limit of the relativistic Cowling approximation there is no gauge freedom remaining to exploit and the equations posed above for $l \geq 2$ are also the correct ones for $l = 1$. It is straightforward to verify directly that the equations above agree with those that are obtained in the Campolattaro-Thorne gauge under the assumption that the only non-vanishing metric perturbation is $H_1 = 8\pi(\rho + p)\exp(\lambda/2)W$. Throughout the remainder of this paper all results hold for $l = 1$ as well as for $l \geq 2$ unless otherwise noted.

2.3. Regimes of Validity

The relativistic Cowling approximation expressed in equations (2.17)–(2.18) agrees with the full relativistic equations in the limit of small frequency; consequently, by construction the approximation is valid in the low-frequency limit.

In the high-frequency limit, the justification of the approximation for $l \geq 2$ is complicated by the radiative nature of the gravitational field: In pulsating stars, the f-mode frequency (which is always less than the p-mode frequencies) is $\sigma_f^2 \simeq l\rho_c$ (where ρ_c is the central density), so that

$$(\sigma_p R)^2 > (\sigma_f R)^2 \simeq l\frac{M}{R} \quad \text{for fixed } l \tag{2.26}$$

(σ_p is any p-mode frequency). For ultra-relativistic stars $M/R \sim 1/4$, which means that even for low-l f-modes and low-l, low-radial-order p-modes, the star extends

nearly into the wave-zone of the gravitational field. For higher-order p- or f-modes, most of the star is in the wave zone.

The gross dependence of K, H_0, H_1, and W on kR is unaffected by the transition from weak to strong fields; so, to estimate the order of magnitude of the gravitational perturbations for high-order modes, consider the weak-field (but not slow-motion) limit of the full field equations. Thorne (1969) explores the weak-field limit of the relativistic equations and finds

$$\left(r\frac{d}{dr}+\frac{l(l+1)}{2}-1\right)(H_0-K)\simeq-\left[8\pi r^2\beta+(\sigma r)^2K\right], \tag{2.27}$$

$$\left(\sigma^2-\frac{l(l+1)}{r^2}\right)K+\frac{1}{r^2}\frac{d}{dr}\left(r^2\frac{dK}{dr}\right)-\frac{2}{r^2}(H_0-K)=8\pi\delta\rho_N. \tag{2.28}$$

(equations [2.27] and [2.28] are from Thorne 1969 eqs. [10b] and [10a], respectively). For fixed l and large kR, corresponding to high-order modes, the high (p-mode) pulsation frequency σ and the wavenumber k are related through the sound speed $c_{s,N}$ (*cf.* eq. [2.7]):

$$\sigma^2\simeq k^2c_{s,N}^2\simeq k^2\frac{p}{\rho_N}\simeq k^2\frac{M}{R}; \tag{2.29}$$

consequently,

$$K\simeq-\frac{8\pi R^2\delta\rho_N}{(kR)^2} \tag{2.30}$$

and

$$H_0-K\simeq\frac{1}{kR}8\pi R^2\beta\frac{c_{s,N}^2}{1-c_{s,N}^2}. \tag{2.31}$$

Thus, for sufficiently large kR, the gravitational perturbations H_0 and K are negligible compared to the Eulerian density and pressure perturbations.

It remains to compare the gravitational perturbations to the fluid perturbation W/R^3. In the weak field (but not slow-motion) limit

$$W=-r^2\frac{d\beta}{dr}\frac{1}{\rho_N\sigma^2}+r^2\frac{\delta\rho_N}{\rho_N\sigma^2}\frac{4\pi r^3\rho_N-m}{r^2}-r^2\frac{1}{\sigma^2}\frac{d}{dr}(K-\frac{1}{2}H_0) \tag{2.32}$$

(from Thorne 1969 equation [10c]), and for large kR this becomes

$$\frac{W}{R^3} \simeq \frac{\beta}{\gamma p}\frac{1}{kR} \simeq \frac{\delta\rho_N}{\rho_N}\frac{1}{kR}. \tag{2.33}$$

Consequently, for large kR

$$\frac{W/R^3}{K} \simeq \frac{kR}{8\pi}\frac{R}{M} \gg 1 \tag{2.34a}$$

and

$$\frac{W/R^3}{H_0 - K} \simeq \frac{1}{8\pi}\frac{1}{R^2\rho_N}\frac{\rho_N}{\gamma p}\frac{1-c_{s,N}^2}{c_{s,N}^2} \simeq \frac{1}{8\pi}\left(\frac{R}{M}\right)^2\frac{1-c_{s,N}^2}{c_{s,N}^2}. \tag{2.34b}$$

Thus, for sufficiently large kR, the fluid displacement perturbation W is always much greater than the gravitational perturbation K. By contrast, the perturbations W and H_0 scale identically with kR for high-frequency modes and it is only when $M/R \ll 1$ that H_0 is negligible compared to W/R^3.

The similarity in the scaling of W/R^3 and H_0 for high frequency and large kR is related to a pathological, gauge-induced $\sim r$ divergence of H_0 for large r. As discussed by Price & Thorne (1969), when one switches from the Regge-Wheeler gauge, which is poorly suited to the wave zone but is good in the near zone, to radiative-type gauges (*e.g.,* the TT gauge), the metric perturbations all die out as $1/r$ at large r. This suggests that by a suitable change of gauge the Cowling approximation might be brought into a form valid for all high-frequency modes. This has not been attempted as yet.

To summarize, the relativistic Cowling approximation is a reasonable approximation for all g-modes and for high-order p-modes in stars that are not too relativistic. (Equation [2.34] suggests that $M/R \lesssim 1/6$ might be sufficient for high-order $[n/l \to \infty$ or $l/n \to \infty]$ modes, and this is satisfied for all but the most compact neutron stars; however, see the discussion of $l = 1$ modes in §3.3.) Analogy with the Newtonian Cowling approximation suggests that it would be reasonable to

investigate numerically the accuracy of the relativistic Cowling approximation for low-order modes (both small n and small l).

3. Analysis of Relativistic Perturbation Equations

3.1. Introduction

The analysis of the properties of solutions to the relativistic equations in the Cowling approximation is identical to the rigorous analysis of the Newtonian Cowling approximation given by Gabriel & Scuflaire (1979). For this reason, no proofs are presented here; instead, this section stresses the similarities and differences between stellar pulsations in the relativistic and Newtonian Cowling approximations. In §3.2, a canonical form of the Newtonian equations is shown, and the analogous form of the relativistic equations is introduced. Subsection 3.3 discusses the principal difference between the Newtonian and relativistic equations, and §3.4 discusses properties held in common by solutions of the Newtonian and relativistic equations.

3.2. Sturm-Liouville Form of The Perturbation Equations

The relativistic Cowling approximation reduces to second-order the linearized non-radial stellar pulsation equations. Eliminating V and H_1 from the relativistic Cowling approximation equations (2.17)-(2.18) yields a second-order system of first-order equations for W and β:

$$\begin{aligned}\frac{d\beta}{dr} &= \left(\frac{1}{\gamma p}\frac{dp}{dr} - \frac{1}{2}\frac{d\nu}{dr}\right)\beta \\ &\quad + \left\{-\frac{dp}{dr}Ae^{-\lambda/2} + \sigma^2 e^{-\nu}(\rho+p)\left[1 - \frac{16\pi r^2(\rho+p)}{l(l+1)}\right]\right\}\frac{e^{\lambda/2}}{r^2}W, \qquad (3.1)\\ \frac{dW}{dr} &= -\frac{r^2 e^{\lambda/2}}{dp/dr}\left[\frac{1}{\gamma p}\frac{dp}{dr} + \frac{d\nu}{dr}\frac{l(l+1)}{(\sigma r)^2 e^{-\nu}}\right]\beta - \frac{1}{\gamma p}\frac{dp}{dr}W.\end{aligned}$$

In the Newtonian limit these equations reduce to those of the Newtonian Cowling approximation (*cf. e.g.,* Ledoux & Walraven 1958 eqs. [79.4] and [79.5]):

$$\begin{aligned}\frac{d\beta_N}{dr} &= -\frac{1}{\Gamma p}\frac{dp}{dr}\beta_N + \left(-\frac{dp}{dr}A_N + \sigma^2\rho_N\right)\frac{1}{r^2}W_N, \\ \frac{dW_N}{dr} &= -\frac{r^2}{dp/dr}\left(\frac{1}{\Gamma p}\frac{dp}{dr} + \frac{d\Phi}{dr}\frac{l(l+1)}{(\sigma r)^2}\right)\beta_N + \frac{1}{\Gamma p}\frac{dp}{dr}W_N\end{aligned} \tag{3.2}$$

Here and below, the subscript N reminds us that these are Newtonian quantities.

Most discussions of the Newtonian Cowling approximation are in terms of the variables v_N and w_N (first defined for constant Γ and Γ_0 by Ledoux & Walraven eq. [79.7] and later modified by Gabriel & Scuflaire 1979 eq. [1]-[4] for variable Γ and Γ_0):

$$\begin{aligned}v_N &= \exp\left(\int_0^r dr\,\frac{1}{\Gamma p}\frac{dp}{dr}\right)W_N \equiv f_{1,N}W_N \\ w_N &= \exp\left(\int_0^r dr\,A_N\right)\frac{\beta_N}{\rho_N} \equiv f_{2,N}\frac{\beta_N}{\rho_N}.\end{aligned} \tag{3.3}$$

Here, the Newtonian convection discriminant A_N is

$$A_N \equiv \frac{1}{p}\frac{dp}{dr}\left(\frac{1}{\Gamma_0} - \frac{1}{\Gamma}\right), \tag{3.4}$$

and the indices Γ_0 and Γ are defined by[1]

$$\Gamma_0 \equiv \frac{\rho_N}{p}\frac{dp}{d\rho_N} \quad \text{and} \quad \Gamma \equiv \frac{\rho_N}{p}\frac{\Delta p}{\Delta\rho_N}. \tag{3.5}$$

[1] The index Γ (and later, γ) cannot be defined by strictly thermodynamic considerations. The index Γ (γ) parameterizes the equation of state that governs the pulsating fluid in Newtonian (relativistic) stars. That equation of state may be a function of the frequency of the pulsations due to heat transfer into or out of a fluid element in the course of a pulsation [and, in neutron stars, due to nuclear reactions (*e.g.,* neutronization) that may proceed with timescales on the order of the pulsation period]. If one wishes to describe such situations, then one must define Γ (and γ) in terms of the physical Lagrangian perturbations Δp and $\Delta\rho$ in the pulsating fluid, and then compute them self-consistently with the pulsation frequencies on which they depend.

In terms of v_N and w_N, the Newtonian equations (3.2) take the form

$$\frac{dv_N}{dr} = \left(\frac{\sigma_c^2}{\sigma^2} - 1\right) \frac{r^2}{c_{s,N}^2} \frac{f_{1,N}}{f_{2,N}} w_N \equiv a_N w_N, \tag{3.6a}$$

$$\frac{dw_N}{dr} = \frac{1}{r^2} \left(\sigma^2 - n_N^2\right) \frac{f_{2,N}}{f_{1,N}} v_N \equiv b_N v_N. \tag{3.6b}$$

The sound speed $c_{s,N}$, Brunt-Väisälä frequency n_N, and acoustic cut-off frequency $\sigma_{c,N}$ are

$$\begin{aligned} c_{s,N}^2 &= \frac{\Gamma p}{\rho_N}, \\ \sigma_{c,N}^2 &= \frac{l(l+1)}{r^2} c_{s,N}^2, \\ n_N^2 &= -A_N \frac{d\Phi}{dr}. \end{aligned} \tag{3.7}$$

In addition to the boundary conditions expressed in Newtonian limits of equations (2.23) and (2.24), it is clear that $f_{1,N}$ is continuous throughout the star and that at each r_i where there is a density discontinuity,

$$\left[\frac{f_{2,N}}{\rho_N}\right]_{r_i} = 0. \tag{3.8}$$

Either v_N or w_N may be eliminated from equation (3.6) to yield equivalent second-order equations:

$$\frac{d}{dr}\left[\frac{f_{2,N}}{\left(\frac{l(l+1)}{\sigma^2} - \frac{r^2\rho_N}{\Gamma p}\right) f_{1,N}} \frac{dv_N}{dr}\right] = \frac{1}{r^2}\left(\sigma^2 - n_N^2\right) \frac{f_{2,N}}{f_{1,N}} v_N, \tag{3.9a}$$

$$\frac{d}{dr}\left[\frac{r^2 f_{1,N}}{(\sigma^2 - n_N^2) f_{1,N}} \frac{dw_N}{dr}\right] = \left[\frac{l(l+1)}{\sigma^2} - \frac{r^2\rho_N}{\Gamma p}\right] \frac{f_{1,N}}{f_{2,N}} w_N. \tag{3.9b}$$

In the limit of large σ^2, (3.9a) is a Sturm-Liouville equation with eigenvalues σ^2; and in the limit of large σ^{-2}, (3.9b) is a Sturm-Liouville equation with eigenvalues σ^{-2}. This observation was first made (in the case where Γ and Γ_0 are constant) by Cowling (1941); the above, more general discussion is due to Ledoux & Walraven (1958), and is elaborated on by Gabriel & Scuflaire (1979).

In the relativistic case, we can define variables v and w that are analogous to v_N and w_N:

$$\begin{aligned} v &= \exp\left(\int_0^r dr \frac{1}{\gamma p}\frac{dp}{dr}\right) W \equiv f_1 W, \\ w &= \exp\left(\int_0^r dr A e^{\lambda/2}\right) \frac{\beta}{\rho + p} \equiv f_2 \frac{\beta}{\rho + p}, \end{aligned} \tag{3.10}$$

where the relativistic convection discriminant A is

$$A \equiv \frac{1}{p}\frac{dp}{dr}\left(\frac{1}{\gamma_0} - \frac{1}{\gamma}\right) e^{-\lambda/2} \tag{3.11}$$

and the relativistic indices γ_0 and γ are defined by[2]

$$\gamma_0 \equiv \frac{\rho + p}{p}\frac{dp/dr}{d\rho/dr} \quad \text{and} \quad \gamma \equiv \frac{\rho + p}{p}\frac{\Delta p}{\Delta \rho}. \tag{3.12}$$

In terms of v and w, the relativistic equations (3.1) take the same form as the Newtonian equations:

$$\frac{dv}{dr} = \frac{f_1}{f_2}\left(\frac{\sigma_c^2}{\sigma^2} - 1\right)\frac{r^2}{c_s^2} e^{\lambda/2} w \equiv aw, \tag{3.13a}$$

$$\frac{dw}{dr} = \frac{e^{\lambda/2}}{r^2}(\alpha\sigma^2 - n^2)\frac{f_2}{f_1} e^{-\nu} v \equiv bv, \tag{3.13b}$$

where

$$\alpha \equiv 1 - \frac{16\pi r^2(\rho + p)}{l(l+1)}, \tag{3.13c}$$

and the relativistic sound speed c_s, acoustic cut-off frequency σ_c, and Brunt-Väisälä frequency n are defined as follows:

$$\begin{aligned} c_s^2 &= \frac{\gamma p}{\rho + p}, \\ \sigma_c^2 &= \frac{l(l+1)}{r^2} c_s^2 e^{\nu}, \\ n^2 &= -\frac{1}{2}\frac{d\nu}{dr} A e^{-\lambda/2} e^{\nu} \end{aligned} \tag{3.14}$$

---

[2] See footnote 1.

(the relativistic Brunt-Väisälä frequency n is in radians per unit Schwarzschild time t, *cf.* Finn 1986b eq. [2.8]). In addition to the boundary conditions expressed in equations (2.23) and (2.24), it is clear that f_1 is continuous throughout the star and that at each r_i where there is a density discontinuity, f_2 satisfies a jump condition:

$$\left[\frac{f_2}{\rho + p}\right]_{r_i} = 0. \tag{3.15}$$

The principal difference between the relativistic equations and the Newtonian equations is the appearance of the factor α (eq. [3.13c]) in the definition of the coefficient b. This factor originates with the proportionality between H_1 and W in the relativistic Cowling approximation (eq. [2.20]); if this factor is everywhere positive, there are only trivial differences between the mathematical character of the Newtonian and relativistic equations.

As in the Newtonian equations, either v or w may be eliminated from (3.13) to produce two equivalent second-order equations in Liouville form:

$$\begin{aligned} \frac{d}{dr}\left\{\frac{f_2}{\left[\frac{l(l+1)}{\sigma^2 e^{-\nu}} - r^2\frac{\rho+p}{\gamma p}\right] e^{\lambda/2} f_1}\frac{dv}{dr}\right\} &= \frac{e^{\lambda/2}}{r^2}(\alpha\sigma^2 - n^2)\frac{f_2}{f_1}e^{-\nu}v, \\ \frac{d}{dr}\left[\frac{r^2 f_1 e^{\nu}}{e^{\lambda/2} f_2(\alpha\sigma^2 - n^2)}\frac{dw}{dr}\right] &= \frac{f_1}{f_2}\left[\frac{l(l+1)}{\sigma^2 e^{-\nu}} - \frac{r^2(\rho+p)}{\gamma p}\right] e^{\lambda/2} w. \end{aligned} \tag{3.16}$$

In particular, in the limit of large σ^2, the first of equations (3.16) is a Sturm-Liouville equation with eigenvalues σ^2, and in the limit of large σ^{-2} the second is a Sturm-Liouville equation with eigenvalues σ^{-2}.

3.3. Discussion

The gross properties of a second-order system such as equations (3.13) are determined by the sign of ab. To understand how this occurs, consider the special case where a and b are constant:

$$\frac{d^2 v}{dr^2} = abv. \tag{3.17}$$

Where ab is greater than zero, v is an exponential function and can have at most one zero; where ab is less than zero, v is oscillatory and can have multiple zeros. Since the boundary conditions on v require it to vanish at $r = 0$ and R, it is clear that there are non-trivial solutions satisfying the boundary conditions only when ab is less than zero. This discussion can be generalized to the general case where ab is not constant (*cf.* Swanson, 1968).

For the Newtonian system described by equations (3.6) the sign of ab is determined solely by the ratio of σ^2 to $\sigma^2_{c,N}$ and n^2_N. If both $\sigma^2_{c,N}$ and n^2_N are non-negative, then ab is everywhere positive for negative σ^2 and there are no unstable modes; only for positive σ^2 can ab be negative and admit solutions of the Newtonian eigenequations.

The situation in relativistic stars is complicated by the factor of α (eq. [3.13c]) in the definition of b. The factor α originates with the non-vanishing of H_1 in the relativistic Cowling approximation (eq. [2.20]), and the role played by H_1 in the relativistic radial Navier-Stokes equation (eq. [2.17]). As long as α is everywhere positive, then the gross behavior of the relativistic Cowling equations is no different from that of the Newtonian Cowling equations; however, if α is negative somewhere in a star, then for positive n^2 and σ^2_c the product ab is negative for some σ^2 less than zero and correspondingly there are unstable pulsational modes. These modes have no Newtonian analog; they are a purely relativistic phenomenon.

For $l \geq 2$ and realistic equations of state, the factor α is always positive. To see this, consider the equations of relativistic stellar structure in the form introduced by Bondi (1964):

$$\begin{aligned} \frac{dx}{dr} &= \frac{x[2(\gamma-1)(1-2y)-\gamma(x+y)]}{r(1-2y)}, \\ \frac{dy}{dr} &= \frac{x-(\gamma-1)y}{r(\gamma-1)}, \end{aligned} \tag{3.18}$$

where

$$y \equiv \frac{m(r)}{r} \quad \text{and} \quad x \equiv 4\pi r^2 p. \tag{3.19}$$

In high-density regions, which is the only place where α is in any danger of being zero or negative, the equation of state is well approximated by

$$p = (\gamma - 1)\rho \tag{3.20}$$

with constant γ, $1 \leq \gamma \leq 2$; consequently,

$$16\pi r^2(\rho + p) = \frac{4\gamma}{\gamma - 1}x. \tag{3.21}$$

Hence, $16\pi r^2(\rho + p)$ is maximized when x is maximized. Since x is non-negative and vanishes at $r = 0$ and R, x is maximized when dx/dr vanishes:

$$\max(x) = \frac{1}{\gamma}(2(\gamma - 1) - (5\gamma - 4)y). \tag{3.22}$$

The density is a monotone decreasing function of radius; therefore, at any radius r

$$m(r) > \frac{4}{3}\pi r^3 \rho(r), \tag{3.23}$$

so that where x is maximized,

$$y(r) > \frac{\max(x)}{3(\gamma - 1)}. \tag{3.24}$$

For realistic equations of state of the form given by equation (3.20), γ lies in the range $1 < \gamma < 2$. The lower bound represents the limit of a pressureless gas and the upper bound is imposed by causality and the dominant energy condition (for $\gamma > 2$, the sound speed is greater than the speed of light and the pressure exceeds the energy density). Combining this constraint with equations (3.21), (3.22), and (3.24) we obtain

$$\max\left[\frac{16\pi r^2(\rho + p)}{l(l+1)}\right] < \frac{4}{l(l+1)}. \tag{3.25}$$

Since α is always positive for $l \geq 2$, the signs of a and b are determined by the ratio of σ^2 to the relativistic acoustic cutoff frequency σ_c^2 and Brunt-Väisälä frequency n^2 in the same way that the signs of a_N and b_N are determined by the ratio of σ^2 to $\sigma_{c,N}^2$ and n_N^2.

For $l = 1$, however, it is easy to find cases where the factor α vanishes or becomes negative. In such stars, there is a spectrum of solutions to the relativistic Cowling equations that are dynamically unstable.

In the high-radial-order limit, the dispersion relation for Cowling modes is given by equation (3.17):

$$-k^2 = ab = \left(\frac{\sigma_c^2}{\sigma^2} - 1\right)(\alpha\sigma^2 - n^2)\frac{e^{\lambda-\nu}}{c_s^2}. \tag{3.26a}$$

Reexpressed in terms of σ^2, (3.26a) is

$$\sigma^2 = \frac{1}{2\alpha}\left\{\alpha\sigma_c^2 + n^2 + k^2c_s^2e^{\nu-\lambda} \pm \left[(\alpha\sigma_c^2 + n^2 + k^2c_s^2e^{\nu-\lambda})^2 - 4\alpha\sigma_c^2n^2\right]^{1/2}\right\}. \tag{3.26b}$$

The two branches of the square root correspond to the p-mode and g-mode spectra. The low-frequency g-mode spectrum has a dispersion relation that is independent of α ([3.26b] with near cancellation of the two parts),

$$\sigma^2 \simeq \frac{l(l+1)}{(kR)^2}n^2, \tag{3.27}$$

while the high-frequency p-mode spectrum has a dispersion relation that depends on α:

$$\sigma^2 \simeq \sigma_c^2 + \frac{n^2 + k^2c_s^2}{\alpha}. \tag{3.28}$$

As α decreases from 1 towards 0, the g-mode frequencies are unchanged; however, the p-modes are pushed to higher and higher frequencies until, when α passes through 0 and becomes negative, new modes emerge from $\sigma^2 = -\infty$ and move

toward 0 frequency. The $l = 1$ relativistic-Cowling-approximation instability is associated with these p-modes.

It is important to emphasize that, although it is a real instability in the relativistic Cowling approximation, this instability is not to be found in nature: Detweiler (1975) has found a variational principle for relativistic $l = 1$ non-radial pulsational modes and has used this principle to show that for positive n^2 there are no unstable dipole modes in perfect-fluid relativistic stars. The presence of this instability in the relativistic Cowling approximation marks a catastrophic breakdown of the approximation for dipole high-radial-wave-number p-modes in relativistic stars with $8\pi r^2(\rho + p) > 1$ somewhere in the star.

Some idea of how compact a star must be before this catastrophic breakdown of the Cowling approximation occurs can be found by examining homogeneous (constant energy density, $\rho = \rho_0$) stars. Considering only those models with central pressure p_c less than energy density ρ_0, we obtain

$$\min(\alpha_{l=1}) \simeq \alpha_{l=1}(R) = 1 - 8\pi R^2 \rho_0 = 1 - 6M/R. \tag{3.29}$$

This suggests that for high-radial-wave-number, $l = 1$ p-modes the Cowling approximation breaks down if the surface of the star is within the radius of the last stable circular orbit of the Schwarzschild potential.

The $l = 1$ case is also noteworthy in the Newtonian Cowling approximation. As discussed below, the Cowling approximation predicts that the f-mode frequency separates the g-mode and p-mode spectra; however, a full treatment of $l = 1$ pulsations shows that the f-mode resides at zero frequency regardless of the presence of positive frequency g-modes (see, *e.g.,* Cox 1980 §17.8). For $l = 1$, the gravitational perturbations are crucial to the understanding of some pulsational modes even in the Newtonian limit where the Cowling approximation provides an otherwise reasonable understanding of dipole modes.

The remainder of this paper is concerned with relativistic stars for which $\alpha > 0$ everywhere.

3.4. Properties of The Relativistic Equations

Gabriel & Scuflaire have given a rigorous treatment of the properties of the Newtonian Cowling approximation. Their treatment introduced two auxiliary functions Ψ_N and Θ_N which characterized the (v_N, w_N) plane:

$$v_N = \Psi_N \cos\Theta_N, \quad \text{and} \quad w_N = \Psi_N \sin\Theta_N. \tag{3.30}$$

Using these definitions, Gabriel & Scuflaire were able to prove that the Newtonian equations in the Cowling approximation, even though not precisely Sturm-Liouville themselves, have a number of properties in common with Sturm-Liouville systems. These properties are summarized below.

First, consider solutions with positive σ^2. Corresponding to a given solution with eigenfunction $v_N(r)$ and eigenvalue σ^2 is an integer j that characterizes the number of nodes in v_N in the following way: at each node in v_N, count $+1$ if $d\Theta_N/dr$ is positive and -1 if $d\Theta_N/dr$ is negative; the sum is j.

Restrict attention momentarily to the case where there are no density discontinuities in the star.

If n_N^2 is positive in some finite region of the star, then for each j, $-\infty < j < \infty$, there is a unique mode with positive σ^2. Denoting the eigenfunction and eigenvalue associated with each j by $v_{j,N}$ and σ_j^2, the following properties hold:

$$\sigma_{j-1}^2 < \sigma_j^2, \tag{3.31}$$

$$\lim_{j\to-\infty} \sigma_j^2 = 0, \tag{3.32}$$

and

$$\lim_{j\to+\infty} \sigma_j^2 = \infty. \tag{3.33}$$

The p-modes all correspond to $j \geq 1$, the real-frequency g-modes (g^+ modes) to $j \leq -1$, and the f-mode to $j = 0$.

If $n_N^2 \leq 0$ throughout the star (the star is everywhere either marginally stable or unstable to convection), then there are no modes with $j < 0$ and $\sigma_j^2 > 0$; *i.e.,* there are no real-frequency g-modes.

Consider now the case where there are N "stable" ($[\rho_N]_{r_i} < 0$) density discontinuities. If the star has a finite sized, convectively stable region ($n_N^2 > 0$), then none of the previous results are changed. On the other hand, if the star is everywhere either marginally stable or unstable to convection ($n_N^2 \leq 0$), then for each j, $-N \leq j \leq 0$, there is an eigenfunction $v_{j,N}$ with eigenvalue $\sigma_j^2 > \sigma_{j-1}^2 > 0$. There are exactly N of these stable "discontinuity" modes: no more and no less.

Now consider solutions with negative σ^2, and at first restrict attention to the case where there are no density discontinuities in the star. If the star is everywhere stable against convection ($n_N^2 \geq 0$), then there are no such solutions; *i.e.,* there are no imaginary-frequency g-modes (g^- modes).

If the star has at least one finite sized, convectively unstable region ($n_N^2 < 0$), then for each j, $0 < j < \infty$, there is a unique mode with eigenfunction $v_{j,N}$ and $\sigma_j^2 < 0$; and

$$0 > \sigma_j^2 > \sigma_{j-1}^2, \tag{3.34}$$

$$\lim_{j \to \infty} \sigma_j^2 = 0. \tag{3.35}$$

Consider now a star with N "unstable" discontinuities ($[\rho_N]_{r_i} > 0$). If the star has a finite sized convectively unstable region, then none of the above results are changed. If the star is everywhere marginally or fully stable against convection, then for each j, $1 \leq j \leq N$, there is exactly one mode $v_{j,N}$ with eigenfrequency $\sigma_j^2 < 0$, and $\sigma_j^2 < \sigma_{j-1}^2$. These are the "unstable" discontinuity modes.

In exactly the same way that Ψ_N and Θ_N are defined for the Newtonian equations (eq. [3.30]), Ψ and Θ can be defined for the relativistic equations; and all the proofs of Gabriel & Scuflaire go through for these relativistic quantities with only trivial generalizations. Thus, *as long as $\alpha > 0$, all of the above results that hold for Newtonian stars in the Cowling approximation hold also for relativistic stars in the relativistic Cowling approximation.*

Exactly the same theorems also verify what was conjectured above: that when $\alpha < 0$ somewhere in the star, the relativistic Cowling approximation for $l = 1$ has a semi-infinite spectrum of unstable p-modes as solutions (modes that signal a breakdown of the approximation).

4. Conclusions

Our understanding of the properties of Newtonian stellar pulsation eigenfunctions and eigenfrequencies has benefited greatly from the introduction of the Cowling approximation. The relativistic Cowling approximation, an approximation similar to the Newtonian Cowling approximation and first introduced in a different form by McDermott, Van Horn, & Scholl (1983), was shown here to yield similar benefits.

In this paper, the relativistic Cowling approximation was reformulated in a manner consistent with the low-frequency limit of the relativistic stellar pulsation equations. The approximation is valid for all g-mode pulsations, and is expected to be valid for p-mode pulsations in mildly (but not highly) relativistic stars.

In the relativistic Cowling approximation, the relativistic equations form a second order, nearly Sturm-Liouville system. The same techniques that are used to analyze the Newtonian pulsation equations in the Newtonian Cowling approximation were here applied to the relativistic equations. The same conclusions that hold

for the Newtonian equations were shown to hold also for the relativistic equations, giving greater confidence that many other results and intuitions developed in the study of Newtonian stellar pulsations can also be applied in the study of relativistic stellar pulsations.

Acknowledgments

It is a pleasure to thank Kip Thorne for his many useful comments on an early version of the manuscript. This research was supported in part by NSF 84-51725 and AST 85-14126.

References

Bondi, H. 1964. *Roy. Soc. London Proc., A,* **281**, 39.

Campolattaro, A. & Thorne, K. S. 1970. *Astrophys. J.,* **159**, 847.

Cowling, T. G. 1941. *Mon. Not. R. astr. Soc.,* **101**, 367.

Cox, J. P. 1980. **Theory of Stellar Pulsation,** Princeton University Press, Princeton (New Jersey).

Detweiler, S. L., & Ipser, J. R. 1973. *Astrophys. J.,* **185**, 685.

Detweiler, S. L. 1975. *Astrophys. J.,* **201**, 440.

Deubner, F. L., & Gough, D. 1984. *Ann. Rev. Astr. Astrophys.,* **22**, 593.

Finn, L. S. 1986a. *Mon. Not. R. astr. Soc.,* **222**, 393.

Finn, L. S., 1986b. *California Institute of Technology, GRP-081 preprint.*

Gabriel, M. & Scuflaire, R. 1979. *Acta Astr.,* **29**, 135.

Ledoux, P. & Walraven, Th. 1958. *Handuch der Physik,* **51**, 353.

McDermott, P. N., Van Horn, H. M., & Scholl, J. F. 1983. *Astrophys. J.,* **268**, 837.

Price, R., & Thorne, K. S. 1969. *Astrophys. J.,* **155**, 163.

Regge, T. & Wheeler, J. A. 1957. *Phys. Rev.,* **108**, 1063.

Swanson, C. A. 1968. **Comparison and Oscillations Theory of Linear Differential Equations,** Academic Press, New York.

Thorne, K. S. 1969. *Astrophys. J.,* **158**, 997.

Thorne, K. S., & Campolattaro, A. 1967. *Astrophys. J.,* **149**, 591.

Chapter 5

Non-radial Relativistic Pulsation in Stars with a Shear Modulus

Within hours after its formation in the collapse of a normal star or a white dwarf, the outer layer of a neutron star solidifies to form a solid crust (*cf.* Shapiro & Teukolsky 1983). This crust, which extends from a density of approximately $10^6\,\mathrm{g\,cm^{-3}}$ to nuclear densities (ρ_{nuc} approximately $4 \times 10^{14}\,\mathrm{g\,cm^{-3}}$), makes it possible for a neutron star to support toroidal, torsional-mode oscillations, where the restoring force is due to the shear stress in the crust. The theory of *torsional modes* in neutron stars has been developed by Schumaker & Thorne (1983).

The influence of a solid crust on the pulsational modes of a neutron star does not end with torsional modes, however: g-modes (*cf.* Chapter 2–3; McDermott, Van Horn, & Scholl 1983) are expected to be greatly affected by the solidification of the crust. [The effect of a solid crust on p-modes is not expected to be as significant because in p-modes the compressional forces (owing to the bulk modulus and much greater than the shear modulus) are dominant, whereas in g-modes the much smaller gravitational force is dominant, permitting the shear modulus to act in a significant manner]. An important step in the study of neutron star g-modes is thus the extension of the non-radial pulsation theory to encompass stars that can support shear stresses.

This chapter reports on work-in-progress toward extending the theory of non-radial relativistic stellar pulsations to encompass stars with an isotropic shear modulus. In the first subsection, the shear strain is derived in terms of the Thorne-Campolattaro perturbation variables and the shear stress is introduced in the Einstein field equations and equations of motion (the Euler equations) for the pulsating fluid. In the second subsection, a Lagrangian density describing the pulsations is derived from the field equations and the Euler equations, and a variational principle is stated that can be used to investigate the eigenfunctions and eigenfrequencies.

The metric conventions used below are the same as used in the TECHNICAL INTRODUCTION (Chapter 1); other notations used in Chapters 2 and 3 are used here also.

SHEAR STRESS IN NON-RADIAL STELLAR PULSATIONS

Carter & Quintana (1972) extended the standard theory of elastic solids to general relativity. They showed that the standard non-relativistic equation for the time rate of change of the shear strain $\Sigma_{\mu\nu}$ in terms of the expansion rate θ, the shearing rate $\sigma_{\mu\nu}$, and the shear strain itself can be written relativistically as (Carter & Quintana equation 6.3):

$$[\Sigma_{\mu\nu}]^{\cdot} = \frac{2}{3}\theta\Sigma_{\mu\nu} + \sigma_{\mu\nu}. \tag{1.1}$$

The time derivative $[]^{\cdot}$ in this expression is the proper time derivative co-moving with the shearing matter (the *convected time derivative* of Carter & Quintana), and it is presumed that the spatial frame is the rest frame of the fluid. For the fully covariant tensor $\Sigma_{\mu\nu}$, which resides in the three-space orthogonal to the flow lines, this time derivative reduces to the Lie derivative along the material flow-lines U. The tensor $\perp_{\mu\nu}$ projects onto this spacelike hypersurface and is given in terms of the material flow-lines U_μ and the spacetime metric $\mathsf{g}_{\mu\nu}$,

$$\perp_{\mu\nu} \equiv \mathsf{g}_{\mu\nu} - \mathsf{U}_\mu \mathsf{U}_\nu, \tag{1.2}$$

and the rate of expansion and the rate of shear are given by projections of the divergence of the 4-velocity U_μ:

$$\begin{aligned} \theta &\equiv \mathsf{U}^{\mu}{}_{;\mu}, \\ \sigma_{\mu\nu} &\equiv \frac{1}{2}(\perp^{\alpha}_{\mu} \mathsf{U}_{\nu;\alpha} + \perp^{\alpha}_{\nu} \mathsf{U}_{\mu;\alpha}) - \frac{1}{3} \perp_{\mu\nu} \theta. \end{aligned} \tag{1.3}$$

We assume that the equilibrium background upon which the non-radial pulsations are a small perturbation has no shear strain, shear strain rate, or expansion

strain rate of its own; consequently, the shear strain, shear strain rate, and expansion strain rate are all of the order of the perturbation and the term $\theta\Sigma$ in equation (1.1) is negligible. Similarly, the deviations of the fluid four-velocity from rest in the equilibrium Schwarzschild spacetime are also of the order of the perturbation, so that the convected time derivative in equation (1.1) becomes $\exp(-\nu/2)d/dt$. In our first-order perturbation theory, the relation between the shear strain rate σ and the shear strain Σ takes on an especially simple form:

$$\Sigma_{\mu\nu} = e^{\nu/2}\int_0^t dt\,\sigma_{\mu\nu}. \tag{1.4}$$

The absence of a constant of integration reflects the vanishing of the shear strain in the absence of a perturbation.

Our assumption that the shear vanishes in the unperturbed background is almost certainly incorrect; however, the background shear strain $\Sigma^{(0)}$ will be only a small contribution to the stress-energy of the equilibrium solution $\mathbf{T}^{(0)}$. In the limit of small perturbations, but smaller background shear, our approximation of vanishing background shear is valid.

The 4-velocity of the non-radially pulsating material is given by

$$\begin{aligned}
\mathsf{U}^t &= e^{-\nu/2}(1-\frac{1}{2}H_0Y_{lm}),\\
\mathsf{U}^r &= \frac{e^{-(\nu+\lambda)/2}}{r^2}\partial_t W\,Y_{lm},\\
\mathsf{U}_\theta &= e^{-\nu/2}\partial_t V\,\partial_\theta Y_{lm},\\
\mathsf{U}_\phi &= e^{-\nu/2}\partial_t V\,\partial_\theta Y_{lm}.
\end{aligned} \tag{1.5}$$

Using the 4-velocity and equation (1.4), it is straightforward but tedious to calculate the shear strain tensor:

$$\Sigma^t_\mu = \Sigma^\mu_t = 0, \tag{1.6a}$$

$$\Sigma^r_r \equiv AY_{lm} = \frac{1}{3}\left[K - H_2 + \frac{e^{-\lambda/2}}{r^2}\left(2W' - \frac{6}{r}W\right) - \frac{l(l+1)}{r^2}V\right]Y_{lm}, \tag{1.6b}$$

$$\Sigma^r_A \equiv \mathcal{B}\partial_A Y_{lm} = \frac{1}{2}\left[\frac{e^{-\lambda/2}}{r^2}W + \exp(-\lambda)\left(\frac{2}{r}V - V'\right)\right]\partial_A Y_{lm}, \tag{1.6c}$$

$$\begin{aligned}\Sigma^A_B &\equiv \mathcal{C}Y_{lm}{}^{|A}{}_B + \mathcal{D}\delta^A_B Y_{lm} \\ &= VY_{lm}{}^{|A}{}_B \\ &\quad + \frac{1}{6}\delta^A_B\left[H_2 - K + \frac{e^{-\lambda/2}}{r^2}\left(\frac{6}{r}W - 2W'\right) - 2\frac{l(l+1)}{r^2}V\right]Y_{lm}.\end{aligned} \tag{1.6d}$$

In the above, the latin indices A and B run over the coordinates θ and ϕ, the vertical bar (as in $Y_{lm}{}^{|A}{}_B$) indicates a covariant derivative on the sphere with *negative definite* line element $ds^2 = -r^2(d\theta^2 + \sin^2\theta\, d\phi^2)$, and δ^A_B is the Kronecker delta. The remaining elements of $\Sigma_{\mu\nu}$ can be found by raising and lowering indices with the projection tensor $\perp_{\mu\nu}$ (*cf.* equation 1.2). Note that the trace (with respect to $\perp^\nu_\mu$) of Σ^μ_ν vanishes:

$$\mathcal{A} + \frac{l(l+1)}{r^2}\mathcal{C} + 2\mathcal{D} = 0. \tag{1.7}$$

Note also that we now distinguish between H_0 and H_2: the presence of anisotropic stresses breaks the degeneracy that was implicitly assumed in Chapters 2–4.

Carter & Quintana give a quasi-Hookean relationship between the shear strain and the shear stress an isotropic solid, and in the limit of a first-order perturbation theory the shear stress is directly proportional to the shear strain: $\delta\mathbf{T}^{\text{shear}} = -2\mu\boldsymbol{\Sigma}$. The constant of proportionality μ is the isotropic shear modulus.

Thorne & Zimmerman (1967) give the perturbed Einstein field equations in the Regge-Wheeler gauge for non-radial pulsations without any assumptions on the source stress-energy tensor; together with the stress-energy tensor of the perturbed perfect fluid (Thorne & Campolattaro 1967), we can write down the field equations for the perturbation of a spherical star with an isotropic shear modulus:

$r^2 \begin{bmatrix} t \\ t \end{bmatrix}$:

$$e^{-\lambda} r^2 K'' + (3 - r\lambda'/2) e^{-\lambda} r K' - \frac{(l+2)(l-1)}{2} K - e^{-\lambda} r H_2{}' - \left[(1 - r\lambda') + \frac{l(l+1)}{2} \right] H_2 = 8\pi r^2 \alpha, \tag{1.8a}$$

$2r^2 e^{\lambda} \begin{bmatrix} r \\ t \end{bmatrix}$:

$$l(l+1) H_{1,t} + 2r \left[H_{2,t} - e^{\nu/2} \left(e^{-\nu/2} r K_{,t} \right)' \right] = 16\pi(\rho + p) e^{\lambda/2} W_{,t}, \tag{1.8b}$$

$2r^2 e^{(\nu+\lambda)/2} \begin{bmatrix} A \\ t \end{bmatrix}$:

$$\left[e^{(\nu-\lambda)/2} H_{1,t} \right]' - e^{(\nu+\lambda)/2} \left(K_{,t} + H_{2,t} \right) = -16\pi e^{(\nu+\lambda)/2} (\rho + p) V_{,t}, \tag{1.8c}$$

$r^2 \begin{bmatrix} r \\ r \end{bmatrix}$:

$$(1 + r\nu'/2) e^{-\lambda} r K' - e^{-\nu} r^2 K_{,tt} - \frac{(l+2)(l-1)}{2} K - e^{-\lambda} (1 + r\nu') H_2 + \frac{l(l+1)}{2} H_0 - e^{-\lambda} r H_0{}' + 2r e^{-(\nu+\lambda)} H_{1,tt} = -8\pi r^2 (\beta + 2\mu \mathcal{A}), \tag{1.8d}$$

$2r^2 \begin{bmatrix} A \\ r \end{bmatrix}$:

$$r^{-1}(1+r\nu'/2)H_2 - r^{-1}(1-r\nu'/2)H_0 + {H_0}' - K' - e^{-\nu}H_{1,tt} = -32\pi\mu e^{\lambda}\mathcal{B}, \tag{1.8e}$$

$2 \begin{bmatrix} A \\ B \end{bmatrix}$:

$$H_0 - H_2 = 32\pi\mu\mathcal{C}, \tag{1.8f}$$

$2e^{-\lambda} \begin{bmatrix} A \\ B \end{bmatrix}$:

$$\begin{aligned} K'' - {H_0}'' &+ 2e^{-\nu+\lambda/2}r^{-1}\left[e^{-\lambda/2}rH_{1,tt}\right]' \\ &- r^{-1}\left[1+r(\nu'-\lambda'/2)\right]{H_1}' - r^{-1}(1+r\nu'/2){H_2}' \\ &+ r^{-1}\left[2+r(\nu'-\lambda')/2\right]K' - e^{\lambda-\nu}(K+H_2)_{,tt} \\ &+ r^{-2}\left\{r\lambda' + r\nu'\left[r(\lambda'-\nu')/2-1\right] - r^2\nu''\right\}H_2 \\ &- e^{\lambda}\frac{l(l+1)}{r^2}(H_2-H_0) = -16\pi e^{\lambda}(\beta+2\mu\mathcal{D}). \end{aligned} \tag{1.8g}$$

The notation $\begin{bmatrix} \mu \\ \nu \end{bmatrix}$ indicates that the equation corresponds to the field equation $\delta\mathsf{G}^{\mu}_{\nu} = 8\pi\delta\mathsf{T}^{\mu}_{\nu}$ (where $\delta\mathbf{G}$ is the perturbed Einstein tensor and $\delta\mathbf{T}$ is the perturbed stress-energy tensor) with appropriate spherical harmonic dependence factored out. The radial dependence of the Eulerian density perturbation $\delta\rho$ is defined to be α:

$$\delta\rho \equiv \alpha Y_{lm}. \tag{1.9}$$

Equations (1.9f) and (1.9g) correspond to different types of spherical harmonic dependence: the angular dependence factored out of equation (1.9f) is ${Y_{lm}}^{;A}{}_{B}$, and the dependence factored out of equation (1.9g) is Y_{lm}.

The continuity equation [$\nabla \cdot (n\mathbf{U}) = 0$, where n is the baryon number density] determines the relationship between the Eulerian pressure perturbation β and the other perturbation variables of the Thorne-Campolattaro formalism:

$$\beta = \gamma p \left[\frac{1}{2} H_2 + K - \frac{l(l+1)}{r^2} V - \frac{e^{-\lambda/2}}{r^2} \left(W' + \frac{p'}{\gamma p} W \right) \right],$$

where γ relates the Lagrangian perturbations in pressure (Δp) and baryon number density (Δn) through

$$\frac{\gamma p}{\Delta p} \equiv \frac{n}{\Delta n} \tag{1.10}$$

(definition of γ).

The divergence of the stress-energy tensor for a perfect fluid undergoing non-radial pulsations is also given in Thorne & Zimmerman. We can calculate the divergence of the additional terms introduced by the shear stress-energy tensor to get the Euler equations (*i.e.*, the equations of motion) for the solid-crust star:

$$\begin{aligned} \delta \mathrm{T}_r : \quad & - e^{-\nu/2} \left(e^{\nu/2} \beta \right)' + \frac{p'}{\gamma p} \beta - \omega^2 e^{-\nu} (\rho + p) \left[\frac{e^{\lambda/2}}{r^2} W_{,tt} - H_{1,tt} \right] \\ & - \frac{1}{2} (\rho + p) {H_0}' + \frac{p'}{\gamma p} \frac{e^{-\lambda/2}}{r^2} WS + 2\mu e^{\lambda} \frac{l(l+1)}{r^2} \mathcal{B} \\ & + \frac{2\mu}{r} \left[\frac{l(l+1)}{r^2} \mathcal{C} + 2\mathcal{D} \right] - 2 \frac{(\mu r^2 e^{\nu/2} \mathcal{A})'}{r^2 e^{\nu/2}} = 0, \end{aligned} \tag{1.11a}$$

$$\begin{aligned} \delta \mathrm{T}_A : \quad & - \beta - \omega^2 e^{-\nu} (\rho + p) V - \frac{1}{2} (\rho + p) H_0 \\ & - 2\mu \mathcal{D} - \frac{2\mu}{r^2} [l(l+1) - 1] \mathcal{C} - 2 \frac{[\mu r^2 e^{(\nu+\lambda)/2} \mathcal{B}]'}{r^2 e^{(\nu+\lambda)/2}} = 0, \end{aligned} \tag{1.11b}$$

where S is the relativistic Schwarzschild discriminant

$$S \equiv p' - \frac{\gamma p}{\rho + p}\rho', \tag{1.12}$$

and $\delta\mathsf{T}_\mu$ represents the equation of motion $\delta\mathsf{T}^\nu_{\mu;\nu}$ with the spherical harmonic dependence (Y_{lm} for eq. [1.12a], $Y_{lm;A}$ for eq. [1.12b]) factored out. Equation (1.9) has been used to simplify the Euler equations.

Lagrangian Density for Non-radial Pulsations

From the Einstein field equations (eqs. [1.8]) and the equations of motion (eqs. [1.11]), it is possible to construct a Lagrangian density from which the eigenfunctions and eigenfrequencies can be derived by a variational principle.

That a Lagrangian density for the pulsations exists is evident from the existence of the Hilbert action for general relativity. The Lagrangian density for our first-order perturbation theory could be obtained by a second variation of the Hilbert action (Taub 1969; Moncrief 1974). Instead, I have chosen to reconstruct the Lagrangian from the field equations and the equations of motion in the manner described by Schumaker & Thorne (1983, Appendix B). Intuitively, the steps required to construct the Lagrangian are simple to understand from an understanding of the Hilbert variational principle.

The Hilbert variational principle, from which the Einstein field equations with source can be obtained by variation, is

$$I = \int_\Omega d^4x \left[\frac{1}{16\pi}(-g)^{1/2}R + \mathcal{L}_{\text{matter}}\right]. \tag{2.1}$$

Here, R is the scalar curvature of spacetime, $\mathcal{L}_{\text{matter}}$ is the Lagrangian density describing other matter fields, and g is the determinant of the fully covariant metric $\mathsf{g}_{\alpha\beta}$. The Lagrangian density describing the gravitational field is identified as

$\mathcal{L}_{\rm geom} = (-g)^{1/2}R/16\pi$. The Hilbert action is identified as the action associated with the "geometry":

$$I_{\rm geom} = \int_\Omega d^4x\, \mathcal{L}_{\rm geom} = \frac{1}{16\pi}\int_\Omega d^4x\, (-g)^{1/2}R. \tag{2.2}$$

When the variation of the action δI with respect to the metric $\mathbf{g}$ vanishes (integration over a compact region of spacetime Ω, and with variations $\delta \mathsf{g}_{\alpha\beta}$ vanishing at the boundary), then the metric is a solution to the Einstein field equations. In particular,

$$\delta I = \frac{1}{16\pi}\int_\Omega d^4x\, (-g)^{1/2}\left(\mathsf{G}^{\alpha\beta} - 8\pi\mathsf{T}^{\alpha\beta}\right)\delta\mathsf{g}_{\alpha\beta}, \tag{2.3}$$

where $\delta\mathsf{g}_{\alpha\beta}$ is the variation of the metric (*cf.* §21.2 of Misner, Thorne, & Wheeler 1973, henceforth denoted MTW). In order to obtain this expression from the action (eq. [2.1]), we are forced to integrate by parts. Since the variation vanishes on the boundary, however, the surface terms so obtained vanish.

In order to derive the field equations from the action above, one is forced to vary the entire metric. The formalism developed for non-radial pulsations is specialized to a particular gauge where the coordinates are chosen so that some of the metric perturbations vanish. Consequently, the action cannot be reconstructed from just the field equations given above; additional information related to the chosen gauge is needed. An indication of where the additional information comes from is given by considering the special class of metric variations corresponding to coordinate gauge transformations. For these metric variations, the variation of the Hilbert action $I_{\rm geom}$ vanishes separately and can be written

$$\begin{aligned}\delta I_{\rm geom} &= -\frac{1}{8\pi}\int_\Omega d^4x\, (-g)^{1/2}\mathsf{G}_{\alpha\beta}{}^{;\beta}\zeta^\alpha \\ &= -\int_\Omega d^4x\, (-g)^{1/2}\mathsf{T}_{\alpha\beta}{}^{;\beta}\zeta^\alpha,\end{aligned} \tag{2.4}$$

where ζ is the generator of the gauge transformation ($\delta\mathsf{g}_{\alpha\beta} = \zeta_{\alpha;\beta} + \zeta_{\beta;\alpha}$; *cf.* box 18.2 of MTW), and the second equality follows from the field equations.

All of this suggests that the Lagrangian density for the non-radial pulsations might be reconstructable from the perturbed field equations and equations of motion by forming a sum of the products of perturbation quantities with either a field equation or an equation of motion.

The technique used to reconstruct the Lagrangian density involves *i)* the introduction for each perturbation quantity (*e.g.*, W) an analogous quantity denoted by the same symbol but with a superscript dagger (*e.g.*, $W^\dagger$) and complex-conjugate angular dependence; *ii)* construction of the quantity

$$(-g)^{1/2}\left[\delta \mathsf{g}^\dagger{}_{\alpha\beta}\left(\delta \mathsf{G}^{\alpha\beta}-\delta \mathsf{T}^{\alpha\beta}\right)-16\pi\xi^{\dagger\alpha}\delta \mathsf{T}_\alpha{}^\beta{}_{;\beta}\right] \tag{2.5}$$

accurate to second order in the perturbation and where ξ is the Eulerian coordinate displacement of a pulsating fluid element; and *iii)* the addition to this quantity of a pure divergence to make expression (2.5) symmetric in daggered and "undaggered" quantities. That result, with the distinction between daggered and undaggered quantities dropped, is the desired Lagrangian density (*cf.* Schumaker & Thorne). The resulting Lagrangian density (integrated over all angles) is

$$\begin{aligned}
\mathcal{L} =& r^2(\rho+p)e^{-(\nu-\lambda)/2}\left(\frac{W_{,t}}{r^2}\frac{W_{,t}}{r^2}+\frac{l(l+1)}{r^2}V_{,t}V_{,t}\right)+2\mu r^2 e^{(\nu+\lambda)/2}\Sigma^{\mu\nu}\Sigma_{\mu\nu}\\
&-r^2e^{(\nu+\lambda)/2}\frac{\beta^2}{\gamma p}+\frac{e^{(\nu-\lambda)/2}}{r}\frac{p'}{\gamma p}SWW-2(\rho+p)e^{-\nu/2}H_{1,t}W_{,t}\\
&+\frac{e^{(\nu+\lambda)/2}}{16\pi}(l+2)(l-1)K(H_2-H_0)+\frac{r^2e^{(\nu-\lambda)/2}}{16\pi}\left(K'-2H_0{}'\right)K'\\
&-r^2e^{(\nu+\lambda)/2}H_0\alpha+\frac{e^{(\nu+\lambda)/2}}{16\pi}\left[8\pi r^2(\rho+p)-l(l+1)\right]H_0H_2\\
&+\frac{re^{(\nu-\lambda)/2}}{8\pi}H_0{}'H_2-\frac{r^2e^{-(\nu-\lambda)/2}}{16\pi}\left[K_{,t}K_{,t}+2H_{2,t}K_{,t}\right]\\
&+\frac{e^{-(\nu+\lambda)/2}}{16\pi}\left[4rH_{1,t}H_{2,t}+l(l+1)H_{1,t}H_{1,t}\right]\\
&+\frac{re^{(\nu-\lambda)/2}}{8\pi}\left[\left(1-\frac{r\nu'}{2}\right)H_0K'-\left(1+\frac{r\nu'}{2}\right)H_2K'\right]\\
&-\frac{re^{-\lambda/2}}{4\pi}\left(e^{-\nu/2}rK_{,t}\right)'H_{1,t}+\frac{e^{(\nu-\lambda)/2}}{16\pi}(1+r\nu')H_2H_2.
\end{aligned} \tag{2.6}$$

In this Lagrangian, S is the relativistic Schwarschild convection discriminant,

$$S = p' - \gamma p \rho' / (\rho + p), \tag{2.7}$$

and β is the Eulerian pressure perturbation (*cf.* [1.9]).

In terms of this Lagrangian density, the eigenmodes of a star with an isotropic shear modulus satisfy the variational equation

$$\delta \int_\Omega dt\, dr\, \mathcal{L} = 0, \tag{2.8}$$

where the integration is over a compact region of spacetime Ω and the perturbation is held fixed on the boundary $\partial\Omega$. Corresponding to the variation of the Lagrangian with respect to a given metric or fluid perturbations is a given field equation or equation of motion. In particular,

Variation with respect to	H_0	leads to equation	(1.8a),
	H_1		(1.8b),
	H_2		(1.8d),
	W		(1.11a),
	V		(1.11b),

and variation with respect to K leads to a linear combination of equations (1.8f) and (1.8g). When attempting to obtain the Einstein field equations or the equations of motion from the Lagrangian, or when using the variational principle to find the eigenmodes of a neutron star, it is important that β be expanded in terms of the Thorne-Campolattaro perturbation variables H_0, H_1, H_2, K, W, and V *before* the variation is made; in the context of the Lagrangian (eq. [2.6]), β is a shorthand for the linear combination of perturbation variables given in equation (1.9).

Conclusions

The initial steps toward a theory of non-radial relativistic stellar pulsations for stars with an isotropic shear modulus have been taken with the introduction of the

shear-stress tensor in the Einstein field equations, the introduction of the forces due to the shear stress in the Euler equations, and the derivation of a Lagrangian and an associated variational principle for calculating the eigenmodes of a pulsating star.

Since the modes most likely to be affected by the presence of a solid crust in a neutron star are the g-modes, the slow-motion formalism (Chapter 2) should be extended to encompass the presence of an isotropic shear modulus. Part of that extension will be the calculation of a conserved energy for the pulsations from the Lagrangian density presented here, and the remainder will involve the appropriate choice of perturbation variables (bearing in mind that the degeneracy between H_0 and H_2 is broken by the presence of a shear modulus).

Additionally, the Lagrangian density presented here may be used to investigate the stability and pulsation frequencies of eigenmodes of relativistic stars with an isotropic shear modulus.

REFERENCES

Carter, B., & Quintana, H. 1972. *Proc. R. Soc. Lond. A.*, **331**, 57.

McDermott, P.N., Van Horn, H.M., & Scholl, J.F. 1983. *Astrophys. J.*, **268**, 837.

Misner, C.A., Thorne, K.S., Wheeler, J.A. 1973. **Gravitation,** Freeman, San Francisco.

Moncrief, V. 1974. *Annals of Physics,* **88**, 343.

Schumaker, B.L., & Thorne, K.S. 1983. *Mon. Not. R. astr. Soc.,* **203**, 457.

Shapiro, S.L., & Teukolsky S.A. 1983. **Black Holes, White Dwarfs, and Neutron Stars,** John Wiley & Sons, New York

Taub, A.H. 1969. *Commun. Math Phys.,* **15**, 235.

Thorne, K.S., & Campolattaro, A. 1967. *Astrophys. J.,* **149**, 591.

Thorne, K.S., & Zimmerman, B.A. 1967. *Grape-Aid Technical Report,* California Institute of Technology.

Chapter 6

Gravitational Radiation from Solar Oscillations: Proposal for a Transition-Zone Test of General Relativity

Originally appeared in *Classical and Quantum Gravity,* **2,** 381–402 (1985).

Abstract

Observed oscillations of the sun with five to ten minute periods are a predicted source of gravitational radiation with a strain at the earth of $\sim 10^{-26}$. In the transition zone ($2\pi r \sim \lambda$; inner part of the solar system), the dynamical character of the gravitational field emerges as a phase shift of the oscillatory tidal force relative to the phase of the solar oscillations. The phase shift is sensitive to the spin of the gravitational field, suggesting a test of the spin composition of relativistic gravity. This paper investigates and compares the transition-zone phase shift for three pure-spin theories: Nordstrøm's theory (a spin 0 theory), a vector theory analogous to electromagnetism (spin 1), and general relativity (spin 2); and for Jordan-Brans-Dicke Theory in which gravity is a mixture of spins 2 and 0. The solar gravitational waves might be detectable, near the turn of the century, by optically linked gravitational antennae flown in space. Such detection would permit a direct measurement of the spin composition of relativistic gravity.

1. Introduction

1.1. *Motivation*

Experimental validation of general relativity lags far behind its theoretical development. Except for the indirect evidence of gravitational radiation from the binary pulsar (Taylor *et al.* 1979), current experimental knowledge of gravitation is confined to "gravito-statics": the laws of motion of test bodies in static gravitational fields. Instrumentation is just now approaching the precision where the predicted "gravito-magnetic" (*e.g.*, Lense-Thirring effect) and "gravito-dynamic" (gravitational radiation) phenomena are measurable. The direct detection of gravitational radiation offers the first opportunity for a detailed examination of the dynamical characteristics of gravity.

The most powerful and decisive tests of gravitation thus far have been conducted in the solar system, and it is only natural to look to the solar system for a source that can be studied in concert with the gravitational field. The observationally well-established five-minute solar oscillations (which have periods ranging from four to ten minutes) provide such a source of gravitational radiation. An estimate based on the theoretical structure of a ten-minute period oscillation predicts a strain of magnitude 10^{-26} at the earth's orbit. Waves of this period and magnitude might be detectable following the turn of the century.

The idea of looking for gravitational effects of solar oscillations was first discussed by Douglass (1979). Douglass focussed on the possibility of measuring the oscillating Newtonian quadrupole moment of the sun

via doppler-tracking of a solar probe at a distance of $4R_{\odot}$. Following up on this work, Johnson *et al.* (1980) made more detailed calculations of the time-varying solar quadrupole moment. Since the solar probe would not be in the wave zone of the gravitational field, the prospect of detecting gravitational radiation was not considered feasible. In this paper the possibility of testing general relativity by measuring the oscillatory gravitational field in the transition zone, where it is becoming radiation, is discussed. We shall refer to this transition-zone field as "radiation" even though it is not fully radiative.

Detecting the solar gravitational radiation will take a significant effort: it cannot be done on the surface of the earth because seismic noise debilitates earth-bound detectors at periods $\gtrsim 1$ sec (*e.g.*, Weiss 1979). The only hope is a detection system consisting of several spacecraft capable of doppler tracking each other at optical frequencies (optical heterodyning). An advantage of investigating solar gravitational radiation is its accessible transition zone (region where $\lambda \leqq 2\pi r \lesssim 7\lambda$; earth is at $\approx \lambda$).

The transition-zone tidal force of a radiating source contains structure found in neither the wave zone ($2\pi r \gtrsim 7\lambda$) nor the near zone ($2\pi r < \lambda$). One aspect of this structure is related to the polarization of the wave-zone field. In the near zone the gravitational field looks Newtonian — *i.e.*, it is both scalar and instantaneous. All viable theories of gravity must predict identical Newtonian near-zone fields; however, wave-zone predictions are not so constrained. The wave-zone fields predicted by various theories of gravity have polarizations that depend

on the spin of the field. These identical Newtonian near-zone fields match to the distinct wave-zone fields in the transition zone.

In general, the details of the matching of near zone to wave zone depend critically on the available polarization states of the radiation – or equivalently, on the spin of the field (for a discussion of the relationship between polarization states and field spin see Eardley *et al.* 1973). A consequence of the development of polarization with increasing radius is an emerging phase shift between the oscillations of the sun and the tidal acceleration in the transition zone: a phase shift that is sensitive to the spin structure of gravity, to distance from the sun, and to the orientation of the detector. In the near zone there is no phase shift relative to instantaneous action-at-a-distance (the phase shift is $\propto (\omega r)^5$ for quadrupolar waves) regardless of spin; in the wave zone the phase shift is ωr + (a constant of order unity) (speed of light propagation) regardless of spin; but in the transition zone the phase shift depends strongly on spin.

This paper explores the transition-zone phase shift for weakly gravitating, slow-motion sources, focusing on solar oscillations as a specific source. The remainder of §1 establishes notation and conventions. Section 2 provides background on the five-minute solar oscillations and describes a gravitational-wave detector suitable for measuring the radiation. In §3 the relative phase between the tidal acceleration and the motion of the sun is calculated for a spin 0 theory (the linearized Nordström theory), a spin 1 theory (analogous to electromagnetism), a spin 2 theory (linearized General Relativity), and

a mixed spin 2/spin 0 theory (Jordan-Brans-Dicke). Section 3 concludes with a discussion of the transition-zone phase shift, focusing on a comparison of the differing predictions of Jordan-Brans-Dicke and general relativity and on the precision of measurement needed to distinguish experimentally between them beyond present-day knowledge. Section 4 summarizes the conclusions.

1.2. *Conventions*

Throughout this paper geometrized units are used ($G=c=1$) (*cf.* Box 1.8 of Misner *et al.* 1973). The metric and Riemann tensor conventions are those of Misner *et al.* (1973). The remaining notation is that of Thorne (1980 pp. 307–308), some of which is summarized below.

Unless otherwise noted, all calculations are carried out in the context of the linearized approximation to the gravitation theory of interest. In particular this means that all tensor indices are raised and lowered with the Minkowski metric $\eta_{\mu\nu} \equiv \text{diag}(-1, +1, +1, +1)$.

The coordinates $(t, x, y, z) = (x^0, x^1, x^2, x^3)$ are treated as Minkowski coordinates in flat space (x, y, z are Cartesian). Commas denote partial derivatives with respect to (t, x, y, z). Greek indices run from 0 to 3 and latin indices from 1 to 3. Repeated latin down indices are to be summed as though $\eta^{jk}=\delta_{jk}$ were present. The radial vector of length r is denoted $\mathbf{x}$, and $\mathbf{n}$ denotes the unit radial vector. The tensor product of l radial vectors is given the shorthand notation

$$N_{A_l} \equiv n_{a_1} n_{a_2} \cdots n_{a_l}, \quad X_{A_l} \equiv x_{a_1} x_{a_2} \cdots x_{a_l} .$$

Multiple indices on a tensor are abbreviated similarly:

$$S_{A_l} \equiv S_{a_1 a_2 \cdots a_l} \ .$$

The fields are described in terms of multipole moments of the sun's mass distribution. The multipole moment of order l is symmetric on all its indices, and trace-free on any pair of indices ("STF"). The fully symmetrized and trace-free part of an arbitrary tensor is denoted with a superscript STF. Capital script letters denote symmetric trace-free tensors:

$$\mathcal{I}_{A_l} \equiv \left[I_{A_l} \right]^{\mathrm{STF}} \ .$$

Spherical Hankel functions play a large role in this work. To distinguish between tensors with coordinate indices and functions with order indices, wherever possible, coordinate indices on tensors are written as subscripts and order indices on functions as superscripts. This leads to the unconventional notation for the spherical Bessel and Hankel functions:

$$\begin{aligned} j^l(x) &\equiv \left[\begin{array}{l} \text{Spherical Bessel function} \\ \text{of the first kind} \end{array} \right] \\ y^l(x) &\equiv \left[\begin{array}{l} \text{Spherical Bessel function} \\ \text{of the second kind} \end{array} \right] \\ h^l(x) &\equiv \left[\begin{array}{l} \text{First spherical Hankel} \\ \text{function of the first kind} \end{array} \right] = j^l(x) + i\, y^l(x) \ . \end{aligned}$$

The terms near zone, transition zone and wave zone refer to three regions of space surrounding a weakly gravitating slow-motion source

(the sun). If ω is the characteristic angular frequency of the radiation emitted by the source, r the distance from the source, and L the size of the source, then the three regions are defined as follows (*cf.* Figures 1–4; also Thorne 1980 pp. 315–316):

Near zone: $\omega L < \omega r \lesssim 1$,
Transition zone: $1 \lesssim \omega r \lesssim 7$,
Wave zone: $\omega r \gtrsim 7$.

Physically, the field in the near zone is instantaneous – retardation of a relativistic gravity theory is a negligible correction to Newtonian gravity. In the wave zone the tidal forces associated with the (instantaneous) Newtonian field are a negligible correction to the tidal forces of the outgoing radiation field of a relativistic gravity theory. In the transition zone the tidal forces of the outgoing radiation of a relativistic gravity theory and the tidal forces of the (instantaneous) Newtonian field are of the same order and neither is negligible.

2. Solar Oscillations and Gravitational-Wave Detectors

2.1. *Five-Minute Solar Oscillations*

Solar oscillations with periods around five minutes were first discovered by Leighton (1960). Since that time they have received considerable attention, both theoretical and observational, and have become a firmly established solar phenomena (for a review of the evidence for solar oscillations see Hill 1980).

The label "five-minute oscillations" refers to a band of oscillations with periods ranging from four minutes to ten minutes. These oscillations are interpreted as high-order non-radial adiabatic acoustic modes ("p-modes") of the sun, stochastically excited by turbulence (Goldreich and Keeley 1977a; Gough 1980; Grec *et al.* 1983). The p-modes are confined to a region bounded by the rapid change of density near the surface of the sun and the increase of sound speed with depth (Duvall and Harvey 1983).

Observation of the solar oscillations fall into three classes: spectroscopic doppler shift measurements of radial surface velocities (*e.g.*, Grec *et al.* 1980; Claverie *et al.* 1979); high-precision photometric measurements of fluctuations in solar intensity (*e.g.*, Brown and Harrison 1980); and astrometric measurements of periodic diameter fluctuations of the solar disc (*e.g.*, Caudell *et al.* 1980; Keil and Worden 1980). Spectroscopic doppler measurements are the most widely used observation technique.

Solar oscillations in the five-minute band have been identified with spherical harmonic degree ranging from $l = 0$ to $l \gtrsim 1000$ (*e.g.*, Duvall and Harvey 1983; Kuhn and O'Hanlon 1983; Grec *et al.* 1983). As a source of gravitational radiation, even in the transition zone, only the $l = 2$ modes are significant: the wave amplitude from a higher order mode l is suppressed relative to the $l = 2$ mode by a factor of $(\omega R_\odot)^{l-2} \cong (2\times 10^{-2})^{l-2}$.

With a radial surface velocity of 3 cm s^{-1} (Grec *et al.* 1983) the quadrupole moment typical of an $l = 2$ ten-minute p-mode oscillation is

$\sim 3\times10^{12}\,\mathrm{cm}^3$ (in geometrized units) (Johnson *et al.* 1980). In the transition zone (*e.g.*, at $\omega r = 5$, which is the Earth's location for ten-minute oscillations) this quadrupole moment induces a strain of magnitude 3×10^{-26} (*cf.* equations 3.4.5, 3.4.1, 3.2.4). As discussed below, such a strain might be detectable by future space-based optically linked satellites integrating over long periods of time.

2.2. *Detecting Five-Minute Solar Gravitational Radiation*

The quadrupole moment associated with five minute solar oscillations induces a strain of 10^{-26} in the transition zone. Seismic noise rules out an earth-based detector for gravitational radiation of this period and magnitude (*cf.* Weiss 1979).

A space-based system as described by Weiss (1979) or Decher *et al.* (1980) is potentially capable of measuring the gravitational radiation produced by the five minute oscillations. The antenna of such a system might consist of three satellites, corresponding to the three free masses of a ground-based laser-interferometer system (*e.g.*, Drever 1983), in a solar orbit. The orientation of the satellites could be chosen to obtain a right-angle configuration, as in a ground-based interferometer, with near-equal arm lengths to minimize the effects of laser frequency instability. In the system proposed by Decher *et al.* (1980), the arm length is 10^6 km. The central satellite is equipped with a laser transmitter and transmits to the remaining two satellites, equipped with laser transponders. The returned signals are heterodyned to produce an output that shows the presence (or absence) of

gravitational waves. Optical lasers are preferred to minimize solar plasma noise, which is proportional to (frequency)$^{-4}$.

Using drag-free satellites and maintaining equal arm lengths to minimize the effects of laser frequency instability, the antenna might be shot noise limited. In Weiss (1979), equation (42) gives the spectral density of the shot noise:

$$\left[\frac{\Delta l}{l}\right]^2 = \frac{\lambda^4}{d_1^2 d_2^2}\left[\frac{\hbar\,\omega}{\eta P_1} + \frac{\hbar\,\omega}{\eta P_2}\right] \quad . \tag{2.2.1}$$

Here λ is the wavelength of the laser, d_1 and d_2 are the diameters of the optics at the transmitter and transponders, $\hbar$ is the Planck constant divided by 2π, ω is the angular frequency of the laser, η is the quantum efficiency of the detecting optics, and P_1 and P_2 are the powers of the transmitting and transponding lasers. With a 1 watt laser transponder and transmitter operating at 5000 Å, 150 cm optics and a quantum efficiency of ½, the spectral density of the shot noise is $(\Delta l/l)^2 \sim 10^{-44}\,\mathrm{Hz}^{-1}$. For periodic sources such as the solar gravitational waves, the spectral density is related to the time over which the waves are observed (t_{obs}) and the minimum measurable gravitational-wave amplitude (h_{min}) by

$$h_{\mathrm{min}}\sqrt{t_{\mathrm{obs}}} \gtrsim 2\times\left[\frac{\Delta l}{l}\right] \quad . \tag{2.2.2}$$

With an integration time of four months, the minimum measurable gravitational-wave strain is $\sim 10^{-26}$.

Such a space-based laser-interferometer has been proposed by Weiss (1979) or Decher *et al.* (1980) to search for cosmic gravitational waves with periods ranging from 10^{-1} s to 1000 s. As the detector is inherently broad band, it is possible to search parasitically for the narrow-band signal of the highly periodic solar gravitational waves in broad-band data collected for almost any other purpose — thus permitting observation times comparable with the lifetime of the detector.

3. Transition-Zone Radiation Fields

3.1. *Introductory Remarks*

We now turn attention to three approximations that are central to our calculation of the transition zone gravitational field: the Weak-Field approximation, the Newtonian-Source approximation, and the Slow-Motion approximation.

The *Weak-Field approximation* neglects all terms of greater than linear order in the fields. In this approximation the time-dependent and time-independent parts of the sun's gravitational field are separately generated by the time-dependent and time-independent parts of the sun's stress energy. This permits us to write the source of the gravitational waves as the Eulerian perturbation $\delta T^{\mu\nu}$ of the sun's equilibrium stress-energy tensor, with δT^{00} playing the key role. The fractional errors made in the evaluation of gravitational radiation by neglecting non-linearities are in order-of-magnitude the unperturbed

Newtonian gravitational potential of the sun $M_\odot/R_\odot$:

$$\begin{aligned} &\text{Weak-Field Approximation:} && 1 \gg |\Phi_{\text{Newton}}| \quad , \\ &\text{Source of gravitational waves:} && \delta T^{00} = e^{-i\omega t}\delta\rho(x_j) \quad , \\ &\text{Makes fractional errors} && \sim |\Phi_{\text{Newton}}| \lesssim 10^{-5} \quad , \end{aligned} \tag{3.1.1}$$

where $\delta\rho\exp(-i\omega t)$ is the Eulerian perturbation of the Solar mass density. Here and henceforth we will always assume that the real part of all complex expressions is taken.

The *Newtonian-Source approximation* neglects the perturbations δT^{jk} of the stress and δT^{0j} of the energy flux compared to δT^{00}. The velocity of the solar fluid engaged in solar oscillations is typically $v_j \lesssim 10 \text{ cm s}^{-1} \sim 10^{-9}$; consequently, the solar oscillation energy flux is of order

$$\delta T^{0j} \equiv \begin{bmatrix}\text{Eulerian perturbation} \\ \text{of solar energy flux}\end{bmatrix} \sim e^{-i\omega t}\,\delta(\rho v_j) \sim 10^{-9}\delta\rho \quad .$$

The solar oscillations are adiabatic perturbations; thus, the time-dependent stress perturbation is of order

$$\delta T^{jk} \equiv \begin{bmatrix}\text{Eulerian perturbation} \\ \text{of solar stress}\end{bmatrix} \sim \delta p \sim \frac{p_0}{\rho_0}\delta\rho \sim 10^{-5}\delta\rho \quad \text{in the sun} \quad ,$$

where

$$p_0 \equiv \begin{bmatrix}\text{Static, equilibrium} \\ \text{solar pressure}\end{bmatrix} \quad , \quad \delta p \equiv \begin{bmatrix}\text{Eulerian perturbation} \\ \text{of solar pressure}\end{bmatrix} \quad .$$

In neglecting energy flux and stress, the Newtonian-Source

approximation makes errors of order the energy flux and stress:

$$\begin{array}{ll} \text{Newtonian–Source Approximation:} & \delta\rho \equiv \delta T^{00} \gg \delta T^{0j},\ \delta T^{jk} \quad , \\ \text{Makes errors} & \max(\delta T^{0j}, \delta T^{jk}) \sim 10^{-5}\delta\rho \quad . \end{array} \tag{3.1.2}$$

The *Slow-Motion approximation* assumes that in describing the solar gravitational waves retardation across the sun's disc is negligible:

$$\text{Slow–Motion Approximation: } \omega L \ll 1 \quad ,$$

$$\omega \equiv \left[\begin{array}{l}\text{Angular frequency} \\ \text{of radiation}\end{array}\right] = 3\times10^{-13}\ \text{cm}^{-1} \text{ for ten–minute oscillations} \quad ,$$

$$L \equiv \left[\begin{array}{l}\text{Size} \\ \text{of sun}\end{array}\right] = 7\times10^{10}\ \text{cm} \quad ,$$

$$\text{Makes fractional errors } \sim (\omega L)^2 \sim 4\times10^{-4} \quad . \tag{3.1.3}$$

The application of these approximations to field equations and equations of motion will be referred to below as "linearization."

A detector for monitoring the solar gravitational radiation will be nearly stationary with respect to the sun ($v_{\text{orbital}} \sim 10^{-4}$). In this work the detector velocity is neglected, with resulting errors $\sim v^2_{\text{orbital}} \sim 10^{-8}$. Gravitational tidal accelerations then affect the relative distances ξ_i in the detector according to

$$\frac{d^2\xi_j}{dt^2} = -e^{-i\omega t}E_{jk}\xi_k \quad . \tag{3.1.4}$$

For example, in any metric theory of gravity $e^{-i\omega t}E_{jk}$ is, apart from gravitational redshift corrections of order $M_\odot/r$, the electric part of the

Riemann tensor:

$$e^{-i\omega t}E_{jk} = R_{j0k0} \quad . \tag{3.1.5}$$

3.2. *Spin-Zero Theory: Nordstrøm Gravity*

Nordstrøm's Scalar Theory of gravitation (Nordstrøm 1913) offers a reasonable generalization of the Newtonian theory of gravity consistent with the requirements of special relativity. It is a metric theory of gravity; however, its metric is conformally flat and so cannot account for the observed deflection of light by the sun's gravity. Despite this experimental defect, Nordstrøm's theory is a useful "foil" against which to compare general relativity, and it will be a useful tool in our study of the mixed-spin Jordan-Brans-Dicke theory (below).

Nordstrøm's gravitational field Φ is generated by the trace of the matter stress-energy tensor, and the metric is then generated from the field Φ according to (Misner *et al.* 1973, p. 429):

$$\begin{aligned} &\text{Field Equations:} \quad \eta^{\alpha\beta}\Phi_{,\alpha\beta} = -4\pi\Phi\eta_{\alpha\beta}T^{\alpha\beta} \quad , \\ &\text{Metric:} \qquad\qquad\quad g_{\alpha\beta} = \Phi^2\eta_{\alpha\beta} \quad . \end{aligned} \tag{3.2.1a}$$

The correspondence with Newtonian theory in the weak-field limit permits the identification

$$\Phi = 1+\phi \quad where \quad |\phi| \ll 1 \quad . \tag{3.2.2}$$

After linearization, the Nordstrøm theory takes on the trappings of

Newtonian theory:

$$\begin{aligned} &\text{Linearized Field Equations:} \quad \eta^{\alpha\beta}\phi_{,\alpha\beta} = 4\pi\delta\rho e^{-i\omega t} \quad , \\ &\text{Metric:} \qquad\qquad\qquad\quad g_{\alpha\beta} = (1+2\phi)\eta_{\alpha\beta} \quad . \end{aligned} \tag{3.2.1b}$$

Our ϕ is a spin-zero ("scalar") field: it transforms as a rank-zero irreducible representation of the Lorentz group.

Instead of directly solving the dynamical field equation with source, we can use the Slow-Motion approximation at the outset to simplify the solution. In the Slow-Motion approximation, the near-zone field is Newtonian; therefore, in the near zone

$$\nabla^2\phi \approx 4\pi e^{-i\omega t}\delta\rho \quad ,$$

with solution

$$\phi = -e^{-i\omega t}\int d^3\bar{x}\frac{\delta\rho(\bar{\mathbf{x}})}{|\mathbf{x}-\bar{\mathbf{x}}|} = -e^{-i\omega t}\sum_{l=2}^{\infty}\frac{(2l-1)!!}{l!}\frac{\mathcal{I}_{A_l}N_{A_l}}{r^{l+1}} \quad . \tag{3.2.3}$$

Here (and henceforth)

$$\mathcal{I}_{A_l} = \left[\int d^3\bar{x}\,\delta\rho(\bar{\mathbf{x}})\bar{X}_{A_l}\right]^{\mathrm{STF}} \quad . \tag{3.2.4}$$

The $l=0$ (mass monopole) term vanishes because mass is conserved in the Slow-Motion, Weak-Field approximation; the $l=1$ (mass dipole) term vanishes because momentum is conserved.

The general vacuum solution of the linearized field equations for outgoing waves at infinity is

$$\phi = e^{-i\omega t}\sum_{l=0}^{\infty}\mathcal{I}_{A_l}N_{A_l}h^l(\omega r) \quad , \tag{3.2.5}$$

where $h^l(\omega r)$ is the l^{th} spherical Hankel function of the first kind, corresponding to the condition of outgoing waves at infinity. The coefficients $\mathcal{I}_{A_l}$ are determined by matching the near-zone limit of (3.2.5) to the near-zone field (3.2.3). Fix attention on a single value of l and note that

$$\lim_{x\to 0} h^l(x) = -\frac{i(2l-1)!!}{x^{l+1}} \quad . \tag{3.2.6}$$

Then, by equating the expansions (3.2.3) and (3.2.5) in the near zone with the help of (3.2.6), identify term by term the coefficients of $r^{-(l+1)}$. The field ϕ is then found to be

$$\phi = -i\frac{\omega^{l+1}}{l!}\mathcal{I}_{A_l}N_{A_l}h^l(\omega r)e^{-i\omega t} \quad . \tag{3.2.7}$$

Because the Nordström theory is a metric theory of gravity, the tidal forces felt by a detector are given by the tidal tensor (3.1.5), where the electric part of the Riemann tensor R_{j0k0} is evaluated to linear order in the metric perturbation $2\phi\eta_{\alpha\beta}$:

$$e^{-i\omega t}E_{jk} \equiv R_{j0k0} = \frac{\partial^2\phi}{\partial x_j \partial x_k} + \omega^2\phi\delta_{jk} \quad . \tag{3.2.8}$$

Substituting (3.2.7) into (3.2.8) we find the tidal force tensor E_{jk} in terms of the mass multipole moments of the solar oscillations:

$$E_{jk}^{\text{Scalar}} = E_{jk}^{\text{Newton}} - i\frac{\omega^{l+3}}{l!}\mathcal{I}_{A_l}N_{A_l}h^l\delta_{jk} \quad . \tag{3.2.9}$$

Here

$$E_{jk}^{\text{Newton}} = \frac{\partial^2 \phi}{\partial x_j \partial x_k} e^{i\omega t}$$

$$= -i\frac{\omega^{l+3}}{l!} \mathcal{I}_{pqA_{l-2}} N_{A_{l-2}}$$

$$\times \left[\left[\frac{l(l-1)}{(2l-1)(2l+1)} h^{l-2} - \frac{2l(l+1)-1}{(2l-1)(2l+3)} h^{l} \right.\right.$$

$$\left.\left. + \frac{(l+1)(l+2)}{(2l+1)(2l+3)} h^{l+2} \right] n_j n_k n_p n_q \right.$$

$$+ \frac{1}{\omega r} \left[\frac{l}{2l+1} h^{l-1} - \frac{l}{\omega r} h^{l} - \frac{l+1}{2l+1} h^{l+1} \right] \left(\delta_{jk} - n_j n_k \right) n_p n_q$$

$$+ \frac{l}{\omega r} \left[\frac{l}{2l+1} h^{l-1} - \frac{1}{\omega r} h^{l} - \frac{l+1}{2l+1} h^{l+1} \right]$$

$$\times \left[\left(\delta_{jp} - n_j n_p \right) n_k + \left(\delta_{kp} - n_k n_p \right) n_j \right] n_q$$

$$\left. + \frac{l(l-1)}{(\omega r)^2} h^{l} \left(\delta_{jp} - n_j n_p \right) \left(\delta_{kq} - n_k n_q \right) \right] \quad . \tag{3.2.10}$$

In the near zone $E_{jk}^{\text{Newton}} e^{-i\omega t}$ is the Newtonian tidal force. If the h^l are replaced by their near-zone limits (3.2.6), then $E_{jk}^{\text{Newton}} e^{-i\omega t}$ is the Newtonian tidal force everywhere.

3.3. *Spin-One Theory*

A second theory, useful for comparison but disproved experimentally, is a spin-one theory of gravitation analogous to electromagnetism. After replacing charge by mass and charge currents by mass fluxes, this gravitational theory differs from electromagnetism only in the sign of the free-field term in the Lagrangian -- the sign changed so that an attractive force results between bodies of positive mass. This theory is not viable: it gives the wrong answer for the deflection of light in a gravitational field; nevertheless, it is a useful foil against which to measure general relativity and Jordan-Brans-Dicke theory, and the techniques used to solve for the field will prove useful when we investigate general relativity (below).

The gravitational potential **A** (analogous to the electromagnetic potential) transforms as a rank 1 irreducible representation of the Lorentz group: thus, we say that it is a spin one (or "vector") field.

The gravitational potential **A** exists on a Minkowski background spacetime. Restrict attention to the special Lorentz coordinate system in which the sun is at rest. There, the concept of a pure spatial rotation is understood. Under these pure spatial rotations the spatial components of the field A_j transform among themselves as a 3-vector field, and the time component A^0 transforms as a scalar field. Having chosen a specific Lorentz coordinate system to describe the background spacetime upon which **A** exists, it is useful to choose a gauge where the time and space components of the field appear separately in the field equations and are coupled only in the gauge condition. The Lorentz

gauge satisfies this requirement. The field equations of the spin-one gravitation theory in the Lorentz gauge are:

$$\begin{aligned} &\text{Field Equations:} && \eta^{\alpha\beta}A_{k,\alpha\beta} = 4\pi\delta J_k e^{-i\omega t} \quad , \\ & && \eta^{\alpha\beta}A^{\,0}_{\,,\alpha\beta} = 4\pi\delta\rho e^{-i\omega t} \quad , \\ &\text{Lorentz Gauge Condition:} && \frac{\partial A_j}{\partial x_j} + \frac{\partial A^{\,0}}{\partial t} = 0 \quad . \end{aligned} \tag{3.3.1}$$

Here $\delta J_k = \delta(\rho v_k)$ is the "mass current" of the solar fluid generated by the solar oscillations.

The field equation for the "scalar field" $A^{\,0}$ is identical to the field equation for the Nordström scalar field ϕ (3.2.1b), and has the same solution (3.2.7).

The 3-vector potential A_k is the sum of a "potential part," $A_k^{\text{Pot.}} = -\Psi_{,k}$ for some Ψ, and a "solenoidal part," $A_k^{\text{Sol.}} = (\text{curl } \mathbf{C})_k$. The solenoidal part is unconstrained by the Lorentz gauge condition (3.3.1); and in the field equations (3.3.1) it is generated by the solenoidal part of the mass current δJ_k. Because $\delta J_k \sim 10^{-9}\delta\rho$, the solenoidal A_k has magnitude $\sim 10^{-9}A^{\,0}$ and is thus negligible. A brief way to say this is that the solenoidal part of A_k is negligible because of the Newtonian Source approximation (3.1.2). The potential part, by contrast, is not negligible.

The most general curl-free solution of the vacuum field equations for A_k is (*cf.* Thorne 1980 Eq. 2.24, 2.45)

$$\begin{aligned} A_k \;=\; & \mathcal{I}_{kA_{l-1}}N_{A_{l-1}}h^{l-1}(\omega r)e^{-i\omega t} \\ & + \left[n_k\mathcal{K}_{A_l}N_{A_l} - \frac{l}{2l+1}\mathcal{K}_{kA_{l-1}}N_{A_{l-1}}\right]h^{l+1}(\omega r)e^{-i\omega t} \quad . \end{aligned} \tag{3.3.2}$$

The unknown coefficients $\mathcal{I}_{A_l}$ and $\mathcal{K}_{A_l}$ are completely determined by substituting A^0 (3.2.7) and A_k (3.3.2) in the Lorentz gauge condition (3.3.1) and equating the coefficients of the h^l. The complete field **A** in the Newtonian-Source approximation is thereby found to be:

$$\begin{aligned} A^0 &= -i\frac{\omega^{l+1}}{l!}\mathcal{I}_{A_l}N_{A_l}h^l(\omega r)e^{-i\omega t} \quad , \\ A_j &= -\frac{\omega^{l+1}}{l!}\mathcal{I}_{jA_{l-1}}N_{A_{l-1}}h^{l-1}(\omega r)e^{-i\omega t} \quad . \end{aligned} \tag{3.3.3}$$

This spin-one gravity theory is not a metric theory. The motion of test particles is governed by the field tensor $F_{\alpha\beta} = A_{[\beta,\alpha]}$ in analogy with the Lorentz force law of electromagnetism:

$$\nabla_{\mathbf{U}}\mathbf{U} = \mathbf{F}(\cdots,\mathbf{U}) \quad .$$

The equation describing the relative acceleration of neighboring free particles separated by a vector ξ_j is found by acting on the equation of motion with ∇_ξ and noting that ∇_ξ commutes with $\nabla_{\mathbf{U}}$ in flat space, and ξ commutes with **U** always:

$$\begin{aligned} \nabla_{\mathbf{U}}\nabla_{\mathbf{U}}\xi &= \nabla_\xi\nabla_{\mathbf{U}}\mathbf{U} \\ &= \nabla_\xi\mathbf{F}(\cdots,\mathbf{U}) + \mathbf{F}(\cdots,\nabla_{\mathbf{U}}\xi) \quad . \end{aligned}$$

The term $\mathbf{F}(\cdots,\nabla_{\mathbf{U}}\xi)$ couples the internal, relative velocities of the detector's free masses $\nabla_{\mathbf{U}}\xi$ to the field. Consistent with earlier comments, both this term and the velocity of the detector relative to the sun are negligible. The equation of relative motion is thus $\nabla_{\mathbf{U}}\nabla_{\mathbf{U}}\xi = \mathbf{F}(\cdots,\mathbf{U})$ or, in component form,

$$\frac{d^2\xi_j}{dt^2} = F_{j0,k}\xi_k = -e^{-i\omega t}E_{jk}^{\text{Vector}}\xi_k \quad . \tag{3.3.4}$$

The tidal acceleration tensor E_{jk}^{Vector} is therefore

$$E_{jk}^{\text{Vector}} \equiv -e^{i\omega t}F_{j0,k} = -e^{i\omega t}A_{[0,j],k} \quad . \tag{3.3.5}$$

The explicit form of the tidal tensor for the spin-one field theory is computed by combining (3.3.5) for the tidal tensor with (3.3.3) for the vector field:

$$E_{jk}^{\text{Vector}} = E_{jk}^{\text{Newton}} + i\frac{\omega^{l+3}}{l!}\mathcal{I}_{jpA_{l-2}}N_{A_{l-2}} \tag{3.3.6}$$

$$\times\left[n_k n_p\left(\frac{l-1}{2l-1}h^{l-2} - \frac{l}{2l-1}h^l\right) + \frac{1}{\omega r}\left(\delta_{pk} - n_p n_k\right)h^{l-1}\right] \quad .$$

3.4. *Spin-Two Theory: General Relativity*

The tensor field of Linearized General Relativity Theory (LGRT) transforms as a rank-two irreducible representation of the Lorentz group and so is a spin-two field. If one views gravitation as a field acting on a background Minkowski spacetime, then the choice of a specific reference frame (that of the sun's center of mass) defines pure spatial rotations. Under such pure spatial rotations, the time-time part of the trace-reversed metric perturbation transforms as a Cartesian-scalar field; the time-space part transforms as a Cartesian-vector field; and the space-space part transforms as a Cartesian-tensor field. Just as in the case of the spin-one theory of §3.3, it is helpful to choose a gauge

where the field components appear separately in the field equations and are coupled only in the gauge condition. The Lorentz gauge satisfies this condition. The field equations of LGRT in Lorentz gauge are (equation 18.8a of Misner *et al.* 1973)

$$\begin{aligned}
&\text{Linearized Field Equations:} && \eta^{\alpha\beta}\bar{h}_{00,\alpha\beta} = -16\pi T_{00} = -16\pi\rho \quad , \\
&&& \eta^{\alpha\beta}\bar{h}_{0j,\alpha\beta} = -16\pi T_{0j} \quad , \\
&&& \eta^{\alpha\beta}\bar{h}_{jk,\alpha\beta} = -16\pi T_{jk} \quad , \\
&\text{Lorentz Gauge Condition:} && \bar{h}^{\mu\nu}{}_{,\nu} = 0 \quad , \\
&\text{Metric:} && g_{\mu\nu} = \eta_{\mu\nu} + h_{\mu\nu} \quad , \\
&&& h_{\mu\nu} \equiv \bar{h}_{\mu\nu} - \tfrac{1}{2}\eta_{\mu\nu}\bar{h}_{\alpha\beta}\eta^{\alpha\beta} \quad .
\end{aligned} \tag{3.4.1}$$

The field equation for $\bar{h}_{00}$ is equivalent to the field equation for the Nordström scalar field ϕ (when we replace 4ϕ by $-\bar{h}_{00}$) (*cf.* Eq. 3.2.1b) and has the same solution, equation (3.2.7).

The field equation and gauge condition for $\bar{h}_{0j}$ are the same as for the A_j of the spin-one case (when we replace A^0 by $4\bar{h}_{00}$ and A_j by $-4\bar{h}_{0j}$); and they have the same (purely potential) solution, equation (3.3.3).

The field $\bar{h}_{jk}$ can be split into pieces that are "potential" and "solenoidal" on each of its indices; and as for A_j and $\bar{h}_{0j}$, the solenoidal pieces are negligible by the Newtonian Source approximation (3.1.2). Thus, $\bar{h}_{jk}$ can be approximated as curl-free on both indices. This property, together with the relation

$$\bar{h}_{00,00} + \bar{h}_{jk,jk} = 0 \tag{3.4.2}$$

[which follows from an iteration of the gauge condition (3.4.1)],

equation (3.2.5) for $\bar{h}_{00} = -4\phi$, and the most general curl-free solution of the vacuum field equation for $\bar{h}_{jk}$ (*cf.* Thorne 1980 Eq. 2.40, 2.45)

$$\begin{aligned}\bar{h}_{jk} &= \mathcal{A}_{A_l} N_{A_l} \delta_{jk} h^l e^{-i\omega t} + \mathcal{B}_{jkA_{l-2}} N_{A_{l-2}} h^{l-2} e^{-i\omega t} \\ &+ \left[n_{(j}\mathcal{C}_{k)A_{l-1}} N_{A_{l-1}} - \frac{l-1}{2l-1}\mathcal{C}_{jkA_{l-2}} N_{A_{l-2}} - \frac{1}{3}\mathcal{C}_{A_l} N_{A_l} \delta_{jk} \right] h^l e^{-i\omega t} \\ &+ \left[\left(n_j n_k - \frac{1}{2l+3}\delta_{jk} \right) \mathcal{D}_{A_l} N_{A_l} - \frac{2l}{2l+3} n_{(j}\mathcal{D}_{k)A_{l-1}} N_{A_{l-1}} \right. \\ &\left. + \frac{l(l-1)}{(2l+1)(2l+3)} \mathcal{D}_{jkA_{l-2}} N_{A_{l-2}} \right] h^{l-2} e^{-i\omega t} \quad ,\end{aligned} \tag{3.4.3}$$

fully determines $\bar{h}_{jk}$:

$$\bar{h}_{jk} = -i\omega^{l+1} \frac{4}{l!} \mathcal{I}_{A_l} N_{A_l} h^l(\omega r) e^{-i\omega t} \quad . \tag{3.4.4}$$

To summarize, the spin-two field of LGRT is

$$\begin{aligned}\bar{h}_{00} &= i\omega^{l+1} \frac{4}{l!} \mathcal{I}_{A_l} N_{A_l} h^l(\omega r) e^{-i\omega t} \quad , \\ \bar{h}_{0j} &= -\omega^{l+1} \frac{4}{l!} \mathcal{I}_{jA_{l-1}} N_{A_{l-1}} h^{l-1}(\omega r) e^{-i\omega t} \quad , \\ \bar{h}_{jk} &= -i\omega^{l+1} \frac{4}{l!} \mathcal{I}_{jkA_{l-2}} N_{A_{l-2}} h^{l-2}(\omega r) e^{-i\omega t} \quad .\end{aligned} \tag{3.4.5}$$

General relativity is a metric theory of gravity, and so the tidal acceleration tensor is given by (3.1.5). When the Riemann tensor is evaluated to linear order with the metric of LGRT (Eq. 3.4.1, 3.4.5) the tidal tensor is found to be

$$E_{jk}^{\rm GRT} = E_{jk}^{\rm Newton} + i\frac{\omega^{l+3}}{l!} \mathcal{I}_{pqA_{l-2}} N_{A_{l-2}}$$

$$\times \left[2 \left(\frac{l-1}{2l-1} h^{l-2} - \frac{l}{2l-1} h^l \right) \left(\delta_{qk} n_p n_j + \delta_{pj} n_q n_k \right) \right.$$

$$+\delta_{jk}n_p n_q h^{l}-2\delta_{pj}\delta_{qk}h^{l-2}$$

$$+\frac{2}{\omega r}\left[\delta_{qk}(\delta_{pj}-n_p n_j)+\delta_{pj}(\delta_{qk}-n_q n_k)\right]h^{l-1}\Bigg] . \qquad (3.4.6)$$

3.5. *Spin-Two/Spin-Zero Mixture: Jordan-Brans-Dicke Theory*

Next to the General Relativity Theory (GRT), the simplest viable candidate-theory of gravitation is the Jordan-Brans-Dicke Theory (JBDT). In addition to the dynamical metric of GRT, JBDT introduces a spin-zero field generated by the trace of the matter stress-energy tensor. The spin-zero field enters the metric field equations both as the inverse Newton gravitational constant and as an additional source.

In the usual mathematical representation of the JBDT theory (*e.g.*, Misner *et al.* 1973, Box 39.1) test particles move along geodesics of the metric – the scalar field does not couple directly to matter but only indirectly through the metric tensor. In this formulation of JBDT, referred to as the Dicke Representation, the spin-zero source to the metric field equations contains terms linear in derivatives of the scalar field and so enters as a source into the linearized field equations for the metric.

An alternative, but physically equivalent, mathematical representation of JBDT eliminates the source terms linear in the scalar field from the metric-tensor field equations, but at the cost of non-geodesic motion for massive test particles. Dicke (1968) characterizes

this reformulation as a rescaling of the unit of time by the square root of the scalar field, holding Planck's constant and the velocity of light invariant. Expressed in this fashion, the JBDT is said to be in the Einstein Representation. The field equations for the scalar field and the metric in the Einstein Representation are

$$\text{Field Equations:} \quad G^{\mu\nu} = 8\pi S^{\mu\nu} + \frac{2\varpi+3}{2\Phi^2}\left(\Phi_{,\mu}\Phi_{,\nu} - \tfrac{1}{2} f_{\mu\nu}\Phi_{,\alpha}\Phi^{,\alpha}\right) \quad ,$$
$$\Box\Phi = \frac{8\pi\Phi^2}{3+2\varpi} S^{\mu\nu} f_{\mu\nu} \quad , \qquad (3.5.1a)$$

where

$$f_{\mu\nu} \equiv \left[\begin{array}{l}\text{The metric tensor of the}\\ \text{Einstein Representation}\end{array}\right] , \quad G^{\mu\nu} \equiv \left[\begin{array}{l}\text{The Einstein Tensor in}\\ \text{the Einstein Representation}\end{array}\right] ,$$

$$S^{\mu\nu} \equiv \left[\begin{array}{l}\text{The stress-energy}\\ \text{tensor of the matter}\\ \text{fields expressed in the}\\ \text{Einstein Representation}\end{array}\right] , \quad \varpi \equiv \left[\text{The Dicke coupling constant}\right] .$$

The Einstein Representation of the JBDT theory is simply related to the Dicke Representation by the following conformal transformation:

$$g_{\mu\nu} \equiv \left[\begin{array}{l}\text{The metric tensor of the}\\ \text{Dicke Representation}\end{array}\right] = \Phi^{-1} f_{\mu\nu} \quad , \qquad (3.5.2)$$

$$T^{\mu\nu} \equiv \left[\begin{array}{l}\text{The stress-energy tensor in}\\ \text{the Dicke Representation}\end{array}\right] = \Phi^3 S^{\mu\nu} \quad .$$

Note that the field equation (3.5.1a) for the field Φ may be rewritten as a linear equation by replacing $\Phi^2 S^{\mu\nu} f_{\mu\nu}$ by $T^{\mu\nu} g_{\mu\nu}$.

After linearization, the scalar and tensor fields are decoupled in the Einstein Representation:

$$\begin{aligned} &\text{Field Equations:} && \eta^{\alpha\beta}\Phi_{,\alpha\beta} = \frac{8\pi}{3+2\varpi}T^{\alpha\beta}\eta_{\alpha\beta} \quad , \\ & && \eta^{\alpha\beta}\bar{\gamma}^{\mu\nu}_{,\alpha\beta} = 8\pi T^{\mu\nu} \quad , \\ &\text{Metric:} && f_{\mu\nu} = \eta_{\mu\nu}+\gamma_{\mu\nu} \quad , \\ & && \gamma_{\mu\nu} = \bar{\gamma}_{\mu\nu}-\tfrac{1}{2}\eta_{\mu\nu}\bar{\gamma}_{\alpha\beta}\eta^{\alpha\beta} \quad . \end{aligned} \tag{3.5.1b}$$

The field equation for the scalar field Φ is equivalent to (3.2.1a) for the Nordstrøm scalar field if we set $\rho = T^{\alpha\beta}\eta_{\alpha\beta}$, which is in fact true in the Newtonian-Source approximation; and the field equations (3.5.1b) for the metric perturbation $\gamma_{\mu\nu}$ are equivalent to (3.4.1) for the metric perturbation $h_{\mu\nu}$ of LGRT. Consequently, the solution of the field equations for $\bar{\gamma}_{\mu\nu}$ is given by (3.4.5), and the solution of the field equation (3.5.1b) for $-\frac{1}{2}(3+2\varpi)\Phi$ is given by equations (3.2.2) and (3.2.7). Combining (3.4.5), (3.2.2), (3.2.7), and the conformal transformation (3.5.2), yields the metric perturbation in the Dicke Representation:

$$\begin{aligned} g_{\mu\nu} &= \Phi^{-1}f_{\mu\nu} \\ &= \left[1+\frac{2}{3+2\varpi}\phi\right]\left[\eta_{\mu\nu}+h_{\mu\nu}\right] \\ &= \eta_{\mu\nu}+\left[h_{\mu\nu}+\frac{2}{3+2\varpi}\phi\,\eta_{\mu\nu}\right] \quad , \end{aligned} \tag{3.5.3}$$

where ϕ is the scalar field of Nordstrøm theory (eq. 3.2.7) and $h_{\mu\nu}$ is the metric perturbation of LGRT (eq. 3.4.1b, 3.4.5).

In the Dicke representation, test particles travel along geodesics of the metric $g_{\mu\nu}$. The tidal force tensor for JBDT is thus (*cf.* eq. 3.2.9,

3.2.10, 3.4.6)

$$E_{jk}^{\rm JBDT} = E_{jk}^{\rm GRT} + \frac{1}{3+2\varpi} E_{jk}^{\rm Scalar} \quad . \tag{3.5.4}$$

3.6. *Evaluation of Transition-Zone Phase Shifts*

The time-dependent tidal acceleration between two neighboring particles separated by ξ is given by (3.1.4). As all present and planned detectors are sensitive only to the tidal force along the separation ξ, we will restrict attention to the tidal force along ξ:

$$\frac{E_{jk}\xi_j\xi_k}{|\xi|} e^{-i\omega t} \quad . \tag{3.6.1}$$

To aid in defining and interpreting the transition-zone phase shifts, consider a model detector consisting of two masses free to move in response to the gravitational-wave tidal forces, but otherwise fixed in space. This detector differs from the more practical two-arm detector described in §2.2; how that difference affects our results is discussed in §3.7.

There are two types of orientation for our model detector: a longitudinal orientation, $\xi \| \mathbf{n}$, and a transverse orientation, $\xi \perp \mathbf{n}$, where $\mathbf{n}$ is the unit radial vector.

Longitudinal detectors are unique in the sense that they are specified entirely by location – a longitudinal detector is not orientable. The tidal force tensor normalized to unit separation of test masses for a longitudinal detector is found by evaluating (3.6.1) with the tidal

tensors (3.2.9), (3.2.10), (3.3.6), (3.4.6), (3.5.4) and the normalized separation vector for longitudinal detectors $\xi_j/|\xi| = n_j$:

$$E_{jk}^{\text{Scalar}} n_j n_k = E_{jk}^{\text{Newton}} n_j n_k - i\frac{\omega^{l+3}}{l!}\mathcal{I}_{A_l} N_l h^l \quad ,$$

$$E_{jk}^{\text{Vector}} n_j n_k = E_{jk}^{\text{Newton}} n_j n_k + i\frac{\omega^{l+3}}{l!}\mathcal{I}_{A_l} N_{A_l}\left[\frac{l-1}{2l-1}h^{l-2} - \frac{l}{2l-1}h^l\right] \quad ,$$

$$E_{jk}^{\text{GRT}} n_j n_k = E_{jk}^{\text{Newton}} n_j n_k - i\frac{\omega^{l+3}}{l!}\mathcal{I}_{A_l} N_{A_l}\left[\frac{2l+1}{2l-1}h^l + \frac{2}{2l-1}h^{l-2}\right] \quad ,$$

$$E_{jk}^{\text{JBDT}} n_j n_k = E_{jk}^{\text{GRT}} n_j n_k + \frac{1}{3+2\varpi} E_{jk}^{\text{Scalar}} n_j n_k \quad , \tag{3.6.2a}$$

with

$$\begin{aligned} E_{jk}^{\text{Newton}} n_j n_k \;=\; & -i\frac{\omega^{l+3}}{l!}\mathcal{I}_{A_l} N_{A_l}\left[\frac{l(l-1)}{(2l-1)(2l+1)}h^{l-2}\right. \\ & \left. - \frac{2l(l+1)-1}{(2l-1)(2l+3)}h^l + \frac{(l+1)(l+2)}{(2l+1)(2l+3)}h^{l+2}\right] \quad . \end{aligned} \tag{3.6.2b}$$

The complete specification of a transverse detector requires an orientation $\boldsymbol{\xi} \perp \mathbf{n}$. We shall characterize that orientation by the parameter

$$\gamma \equiv \frac{\mathcal{I}_{jkA_{l-2}} \hat{\xi}_j \hat{\xi}_k N_{A_{l-2}}}{\mathcal{I}_{A_l} N_{A_l}} \quad ; \quad \hat{\xi}_j \equiv \frac{\xi_j}{|\xi|} \quad . \tag{3.6.3}$$

In terms of γ the tidal-force normalized to unit length for transverse detectors is found by evaluating (3.6.1) with the tidal tensors (3.2.9), (3.2.10), (3.3.6), (3.4.6), (3.5.4) and the normalized separation vector for

transverse detectors $\hat{\xi} \equiv \xi/|\xi|$:

$$E_{jk}^{\text{Scalar}}\hat{\xi}_j\hat{\xi}_k = E_{jk}^{\text{Newton}}\hat{\xi}_j\hat{\xi}_k - i\frac{\omega^{l+3}}{l!}\mathcal{I}_{A_l}N_{A_l}h^l \quad ,$$

$$E_{jk}^{\text{Vector}}\hat{\xi}_j\hat{\xi}_k = E_{jk}^{\text{Newton}}\hat{\xi}_j\hat{\xi}_k + i\frac{\omega^{l+3}}{l!}\mathcal{I}_{A_l}N_{A_l}\frac{\gamma}{\omega r}h^{l-1} \quad ,$$

$$E_{jk}^{\text{GRT}}\hat{\xi}_j\hat{\xi}_k = E_{jk}^{\text{Newton}}\hat{\xi}_j\hat{\xi}_k + i\frac{\omega^{l+3}}{l!}\mathcal{I}_{A_l}N_{A_l}\left[h^l - 2\gamma h^{l-2} + 4\frac{\gamma}{\omega r}h^{l-1}\right] \quad ,$$

$$E_{jk}^{\text{JBDT}}\hat{\xi}_j\hat{\xi}_k = E_{jk}^{\text{GRT}}\hat{\xi}_j\hat{\xi}_k + \frac{1}{3+2\varpi}E_{jk}^{\text{Scalar}}\hat{\xi}_j\hat{\xi}_k \quad , \tag{3.6.4a}$$

with

$$E_{jk}^{\text{Newton}}\hat{\xi}_j\hat{\xi}_k = -i\frac{\omega^{l+3}}{l!}\mathcal{I}_{A_l}N_{A_l}$$

$$\times\left[\frac{1}{\omega r}\left(\frac{l}{2l+1}h^{l-1} - \frac{l}{\omega r}h^l - \frac{l+1}{2l+1}h^{l+1}\right) + \gamma\frac{l(l-1)}{(\omega r)^2}h^l\right] \tag{3.6.4b}$$

The transition-zone phase may be defined relative to either the near-zone tidal force or the wave-zone tidal force. To evaluate the phase of the tidal force in the wave zone (relative to the instantaneous action-at-a-distance of Newtonian theory), substitute the wave-zone limit

$$\lim_{\omega r \gg 1} h^l(\omega r) = \frac{(-i)^{l+1}e^{i\omega r}}{\omega r}$$

into the tidal force equations (3.6.2) and (3.6.4). Thereby find that in the wave zone, the phase of the tidal force is ωr + constant, the constant a

characteristic of the spin(s) of the theory of interest. (In the full non-linear theory of general relativity, gravitational radiation does not travel along flat-space characteristics; however, that subtlety does not enter at linear order but arises as a logarithmic correction at quadratic and higher order in the field. In the transition zone the error in phase introduced by the use of flat-space characteristics is of order $\omega M_{\odot} \sim 10^{-7}$ and is ignored in this analysis). To evaluate the phase of the tidal force in the near zone (relative to instantaneous action-at-a-distance), substitute the near-zone limit

$$\lim_{\omega r \ll 1} h^l(\omega r) = \frac{(\omega r)^l}{(2l+1)!!} - i\frac{(2l-1)!!}{(\omega r)^{l+1}}$$

into the tidal force equations (3.6.2) and (3.6.4), thereby finding that in the near zone the phase of the tidal force is $\propto (\omega r)^{2l+1}$, independent of the spin of the relativistic theory. In the special case of general relativity, the near-zone phase shift for longitudinal detectors is

$$\frac{(\omega r)^{2l+1}}{(2l-1)!!\,(2l+1)!!} + O((\omega r)^{2l+3}) \quad .$$

The near-zone phase for transverse detectors in general relativity depends on the orientation parameter γ. If γ is neither 0 nor $-1/(l(l-1))$, then the near-zone phase is

$$-(\omega r)^{2l+1}\frac{3\gamma(3l^2-3l-2)}{(1+\gamma l(l-1))\,(2l-1)!!\,(2l+1)!!} + O((\omega r)^{2l+3}) \quad .$$

As the wave-zone phase is not asymptotically constant but varies as ωr, it is preferable to normalize the transition-zone phase shift relative

to the wave-zone phase shift, not to the near-zone phase shift. Thus, we shall define the transition-zone phase shift as

$$\psi \equiv \mathrm{Arg}(-e^{-i\omega r}E_{jk}\xi_j\xi_k) = \tan^{-1}\left[\frac{\mathrm{Im}(-e^{-i\omega r}E_{jk}\xi_j\xi_k)}{\mathrm{Re}(-e^{-i\omega r}E_{jk}\xi_j\xi_k)}\right] . \qquad (3.6.5)$$

This definition leaves a constant phase, characteristic of the spin of the theory, as a wave-zone limit of ψ.

The phase ψ is a function both of the location of the detector $\mathbf{x}$ and the orientation of the detector $\boldsymbol{\xi}$.

3.7. *Discussion*

Beyond the approximations of §3.1, the analysis of §3 does not restrict the structure of the Eulerian density perturbation $\delta\rho$ inside the sun. The transition-zone phase shift for longitudinal detectors is thus entirely independent of the Eulerian density perturbation, while the phase shift for transverse detectors depends only on the ratio γ of two components of the symmetric, trace-free moment $\mathcal{I}_{A_l}$ of $\delta\rho$ ("orientation parameter"). As discussed in §2.1, only the $l = 2$ oscillations generate significant gravitational radiation; so the following discussion is specialized to $l = 2$.

Figure 1 shows the dependence of the amplitude of the tidal force and the phase ψ on the dimensionless radius ωr for a longitudinal detector in a spin 0, 1, or 2 gravitational field. For large r, the amplitude of the tidal acceleration in the longitudinal direction scales as $1/r^2$ for spin 0 and 1, and the amplitude scales as $1/r^3$ for spin two

(note the normalization of the tidal-force amplitude in all the figures – with this normalization, a radiative tidal force would approach a finite, constant amplitude) . The phase asymptotically approaches $\frac{1}{2}\pi$ for spin 0 and 1, but approaches π for spin two. In the transition zone, the phase ψ distinguishes clearly between the three fields.

If the source is idealized as axisymmetric, then the parameter space of transverse detectors admits four particularly interesting subcases. The first case, a transverse detector located on the axis of symmetry, corresponds to $\gamma = -\frac{1}{2}$; the second case, a transverse detector contained entirely in the equatorial plane of the source, corresponds to $\gamma = 1$; the third case, a detector located at the equatorial plane but oriented along the symmetry axis, corresponds to $\gamma = -2$. In the fourth case, a detector is located in the source's equatorial plane, normal to the radius vector and inclined to the equatorial plane by 45°. If we orient our coordinate system so that the symmetry axis is along the z-axis, it is clear that the off-diagonal elements of the quadrupole moment tensor of the axisymmetric source vanish; hence, the tidal acceleration in case 4 is the sum of the tidal forces acting in cases 2 and 3. This is equivalent to setting $\gamma = -\frac{1}{2}$; *i.e.*, case 4 is equivalent to case 1.

Cases two and three investigate the two independent polarization modes of the spin-one field discussed in §3.3; however, they measure the same polarization mode of the spin-two theory described in §3.4.

Figure 2 shows the gravitational wave amplitude $E_{jk}\xi_j\xi_k$ and phase ψ for cases 1 and 4 ($\gamma = -\frac{1}{2}$). Only the spin-zero field is radiative at the

pole (*i.e.*, only for it does the amplitude scale as $1/r$ at large r); the amplitudes of the tidal acceleration for the vector and tensor field both scale as $1/r^2$. In the transition zone, the phase ψ of each field evolves differently, approaching well-distinguished limits of $-\pi$ for the scalar field, $-\frac{1}{2}\pi$ for the vector field, and 0 for the tensor field. Again, the three fields are easily distinguished by ψ in the transition zone.

Figure 3 shows the gravitational-wave amplitude and the phase ψ for case 2 ($\gamma = 1$). While the spin-zero and spin-two fields are radiative for this detector orientation, the spin-one field is not. At large r, the phase ψ approaches $-\pi$ radians for the spin-zero field and 0 radians for the spin-one and spin-two fields. Although the phases of the spin one and spin-two fields approach the same phase in the wave zone, the phase ψ distinguishes clearly between the three fields in the transition zone.

Figure 4 shows the gravitational-wave amplitude and phase for case 3 ($\gamma = -2$). The spin-one field is not radiative for case 3; however the spin-one and spin-two fields do scale as $1/r$ for large r. The phase of the spin-one field approaches $-\frac{1}{2}\pi$ radians at large r, while the phase of the spin-zero and spin-two fields approach π radians in the wave zone. Even though the phase of the spin-zero and spin-two fields approach the same wave-zone limit, the evolution of the phases in the transition-zone is very different, so all three fields are distinguished easily by the phase in the transition zone.

In none of the detector configurations we have described does the spin-one field radiate. The spin-one field does radiate a tidal force;

however, that tidal force is "rotational", *i.e.*, it is a tidal force transverse to the separation between the two test masses, while the detectors we have considered here measure only tidal forces along the separation of the two free masses and so are insensitive to the radiative spin-one tidal force.

The emergence of spin-two phase shifts is vividly displayed by comparing the spin-two phase curves in Figures 3 and 4: at small ωr the field is Newtonian (scalar, instantaneous) in character, while at large ωr the spin-two phase shifts of the radiation field dominate – *i.e.*, $\psi(\gamma=1)$ and $\psi(\gamma=-2)$ differ by π.

To summarize, in the wave zone the spin-zero and spin-two gravitational fields generate a tidal force along a separation normal to the radius vector; the spin-one gravitational field does not. In the wave zone, the scalar-field tidal force is characterized entirely by its trace ("expansion wave"), the vector-field tidal force by its anti-symmetric part ("rotation wave"), and the tensor-field tidal force by its symmetric, trace-free part ("shear wave"). In the transition zone the non-radiative components of the tidal forces for all three fields are of the same magnitude as the radiative components, and generate significant "shear" and "expansion" tidal forces. In the transition zone, the spin of the gravitational field characterizes tidal forces, and the orientation-dependent phase ψ unambiguously distinguishes between the spin 0, 1, and 2 fields.

The two-arm detector described in §2.2 is sensitive to the differences in the amplitude $E_{jk}\xi_j\xi_k$ and the phase ψ acting on each

arm. As shown in Figures 1 through 4, the transition zone tidal-force phase and amplitude are sensitive to orientation for spin-zero, one, and two fields; thus the two-arm detector of §2.2 will be able to distinguish between spin zero, one, and two gravitational fields. The phase shift measured by the two-arm detector may be described in terms of the amplitude and phase measured by the model detector of §3.6:

$$\overline{\psi} = \mathrm{Arg}\left[A_1 e^{i\psi_1} + A_2 e^{i\psi_2}\right] = \tan^{-1}\left[\frac{A_1 \sin\psi_1 + A_2 \sin\psi_2}{A_1 \cos\psi_1 + A_2 \cos\psi_2}\right] , \qquad (3.7.1)$$

Here A_i is the amplitude of the tidal force (eq. 3.6.2 or 3.6.4) and ψ_i is the phase (3.6.5) of the tidal force on arm i ($i = 1, 2$).

The tidal force (3.5.4) shows that a comparison of JBDT and GRT is essentially a comparison of GRT and Nordström's Scalar Theory. The tidal force in the transition zone is the sum of the spin-two field tidal force and the spin-zero field tidal force weighted by $2/(3+2\omega)$, where ω is the Dicke coupling constant. Differences in ψ between GRT and JBDT result from the deviations E_{jk}^{GRT} and E_{jk}^{Scalar} from E_{jk}^{Newton}. In the transition zone, these deviations are of the same magnitude as E_{jk}^{Newton} and differ in phase by approximately π radians (*cf.* Figure 3). This means that the task of measuring large ω reduces to measuring ψ to better than 1 part in 2ω radians.

Solar-system light-deflection and time-delay experiments give a lower bound on the Dicke coupling constant; currently, $\omega \gtrsim 400$ (Will 1981). Thus, to distinguish usefully between JBDT and GRT, a transition-zone phase measurement must be capable of resolving the phase to

better than 1 part in 10^3 radians.

There are several different kinds of transition-zone measurements that can be used to distinguish between JBDT and GRT: comparisons of the phase of solar surface oscillations with the phase of detector excitations; comparisons of phases of detector excitations for detectors with different orientations and positions; and comparisons of amplitudes of detector excitations for detectors with different orientations and positions. Of these measurement strategies, the latter two require multiple detectors and so are less feasible than the first. We will restrict attention to the first measurement strategy: a comparison of the phase of solar surface oscillations with the phase of detector oscillations.

Spectroscopic doppler-shift measurements might be made capable of determining the phase of the $l = 2$ solar surface oscillations. The phase of the detector excitations relative to the surface oscillations may be measured by phase-locking the detector signal to the phase of the optical solar oscillations. The accuracy $\Delta\psi$ with which the phase of the detector signal may be measured is (for small $\Delta\psi$)

$$\Delta\psi = \frac{2}{h}\left[\left(\frac{\Delta l}{l}\right)^2 \frac{1}{t_{obs}}\right]^{1/2} , \qquad (3.7.2)$$

where $(\Delta l/l)^2$ is the spectral density of the detector noise (*cf.* Weiss 1979; or eq. 2.2.1), t_{obs} is the observation time, and h is the amplitude of the metric perturbation. With the proposed detectors discussed in §2.2, a measurement of the phase ψ to 1 part in 1000 does not appear likely;

thus, an improvement in the lower bound on the Dicke coupling constant is not to be expected from such an experiment. Nevertheless, the direct measurement of the spin of the gravitational field that could be achieved by such an experiment, albeit with only modest accuracy, would make it an attractive by-product of future space-based searches for cosmic gravitational waves. It would provide a test of general relativity in a regime heretofore untested: the regime of dynamical fields. The modest accuracy with which it could do this service should be compared to the primitive state of solar-system tests of general relativity in static fields in the 1960's.

If accurate measurements of solar gravitational-wave amplitude can be made, they might also be used together with optical observations of the solar oscillation surface amplitude to test solar models. For instance, the p-mode oscillations of a given solar model may be calculated via the usual perturbation analysis. The amplitude of the oscillations may be determined by optical observations of solar surface velocity. The magnitude of the oscillatory quadrupole moment of the sun may then be calculated from the solar model and compared with the experimental value.

4. Conclusions

Ten-minute-period solar oscillations are a predicted source of gravitational radiation. Earth and the easily accessible inner solar system occupy the transition zone of the radiation field, where the predicted strain is $\sim 10^{-26}$. The time-varying tidal force is expected to

show a phase shift that, in the transition zone, is highly sensitive to the spin of the gravitational field. Proposed space-based searches for cosmic gravitational waves might be used to measure this time-varying tidal force and thereby make a direct determination of the spin of the gravitational field. While the precision of such experiments does not appear to be sufficient to increase the lower bound on the Dicke coupling constant, experiments of this kind do provide a test of general relativity in a regime previously untested: one where the gravitational field is dynamic rather than static.

Acknowledgments

I thank Kip S. Thorne for suggesting this problem, for helpful discussions at several stages of the work, and for a critical reading of the manuscript. I also thank Yekta Gursel for useful discussions on the techniques of multipolar expansions of gravitational radiation. Pawan Kumar and Eric Aslakson provided me with details of solar oscillation research, both theoretical and observational. Part of this work was supported by NSF grant AST82-14126.

References

Brown, T. M., & Harrison, R. L. 1980. **Nonlinear and Nonradial Stellar Pulsation: proceedings of a workshop held at the University of Arizona in Tuscon, March 12-16, 1979,** eds. Hill, H. A., & Dziembowski, W. A., Springer-Verlag, Berlin, pp. 200-203.

Caudell, T. P., Knapp, J., Hill, H. A., & Logan, J. D. 1980. **Nonlinear and Nonradial Stellar Pulsation: proceedings of a workshop held at the University of Arizona in Tuscon, March 12-16, 1979,** eds. Hill, H. A., & Dziembowski, W. A., Springer-Verlag, Berlin, pp. 206-218.

Claverie, A., Isaak, G. R., McLeod, C. P., van der Raay, H. B., & Roca Cortes, T., 1979. *Nature*, **282,** 591.

Decher, R., Randall, J. L., Bender, P. L., & Faller, J. E. 1980. *SPIE Vol.* 228 —*Active Optical Devices and Applications*, 149—153.

Dicke, R. H. 1968. *The Theoretical Significance of Experimental Relativity*, Gordon and Breach, New York, pp. 34-43.

Douglass, D. H. 1979. *A Close-Up of the Sun*, JPL Publication 78-70, Jet Propulsion Laboratory, Pasadena (California), pp. 498—517.

Drever, R. W. P. 1983. *Gravitational Radiation*, eds. Dureulle, N. & Piran, T., North Holland, Amsterdam.

Duvall Jr, T. L. & Harvey, J. W. 1983. *Nature*, **302,** 24.

Eardley, D. M., Lee, D. L., & Lightman, A. P. 1973. *Phys. Rev. D*, **8,** 3308—3321.

Goldreich, P., & Keeley, D. A. 1977a. *Astrophys. J.*, **211,** 934—942.

Goldreich, P., & Keeley, D. A. 1977b. *Astrophys. J.*, **212**, 243–251.

Gough, D. 1980. **Nonlinear and Nonradial Stellar Pulsation: proceedings of a workshop held at the University of Arizona in Tuscon, March 12–16, 1979**, eds. Hill, H. A., & Dziembowski, W. A., Springer-Verlag, Berlin, pp. 274–299.

Grec, G., Fossat, E., & Pomerantz, M. A. 1980. *Nature*, **288**, 541–544.

Grec, G., Fossat, E., & Pomerantz, M. A. 1983. *Solar Physics*, **82**, 55–66.

Hill, H. A. 1980. **Nonlinear and Nonradial Stellar Pulsation: proceedings of a workshop held at the University of Arizona in Tuscon, March 12–16, 1979**, eds. Hill, H. A., & Dziembowski, W. A., Springer-Verlag, Berlin, pp. 174–180.

Johnson, W. W., Winget, D. E., Douglass, D. H., & Van Horn, H. M. 1980. **Nonlinear and Nonradial Stellar Pulsation: proceedings of a workshop held at the University of Arizona in Tuscon, March 12–16, 1979**, eds. Hill, H. A., & Dziembowski, W. A., Springer-Verlag, Berlin, pp. 357–368.

Keil, S. L., & Worden, S., P. 1980. **Nonlinear and Nonradial Stellar Pulsation: proceedings of a workshop held at the University of Arizona in Tuscon, March 12–16, 1979**, eds. Hill, H. A., & Dziembowski, W. A., Springer-Verlag, Berlin, pp. 220–236.

Kuhn, J. R., & O'Hanlon, M. 1983. *Solar Physics*, **87**, 207–219.

Leighton, R. B., Noyes, R. W., & Simon, G. W. 1960. *Astrophys. J.*, **135**, 474.

Misner, C., Thorne, K. S., & Wheeler, J. A. 1973. *Gravitation*, Freeman, San Francisco.

Nordström, G. 1913. *Ann. Phys.* (*Germany*), **42**, pp. 533–554.

Taylor, J. H., Fowler, L. A., & McCulloch, P. M. 1979. *Nature*, **277**, 437–40,

Thorne, K. S. 1980. *Rev. Mod. Phys.*, **52**, 299–339.

Weiss, R. 1979. *Sources of Gravitational Radiation*, ed. Smarr, L., Cambridge University Press, Cambridge, pp. 24–27.

Will, C. M. 1981. *Theory and Experiment in Gravitational Physics*, Cambridge University Press, Cambridge, pp. 173–175.

Figure Captions.

Figure 1. Phases (Eq. 3.6.5) and scaled amplitudes of the $l=2$ spin zero, one, and two gravitational-wave tidal forces measured along the radius vector. The spin-zero theory represented is the linearized version of Nordström (1913), where the metric is conformally flat and the conformal factor is a scalar field that satisfies the Klein-Gordon equation with the mass-density Eulerian perturbation of the Sun as the source (for more detail, see §3.2). The spin-one theory is analogous to electromagnetism, with the electric current replaced by a mass current, and the sign of the free-field term of the Lagrangian changed to allow for an attractive force (§3.3; problem 7.2 of MTW). The spin-two theory is linearized general relativity (§3.4). The phase ψ at r is measured relative to the ωr phase shift of a plane wave traversing the same distance, and the amplitude $E_{jk}\xi_j\xi_k$ of the tidal force is scaled so that a radiative tidal force (i.e., one that scales as $1/r$ for large ωr) will asymptotically approach a finite constant. Note that the phase distinguishes clearly between the three fields, and that none of the fields are radiative. The locations of the inner solar-system planets are shown for ten-minute period oscillations. For more detail, see the discussion of §3.7.

Figure 2. Phases and scaled amplitudes of the $l=2$ spin zero, one, and two gravitational-wave tidal forces. The component depicted is that measured at the pole of an axisymmetric source along a direction

transverse to the symmetry axis (case 1 of §3.7; orientation parameter $\gamma=-\frac{1}{2}$). The phase and scaled amplitude depicted in this figure are also those of the component of the tidal force measured at the source's equator and in the transverse direction inclined by 45 to the symmetry axis (case 4 of §3.7). The spin-zero, one, and two theories, as well as the normalization of the phase and amplitude, are described in the text and more briefly in the caption of Figure 1. Note that the phase distinguishes clearly between the three fields, and that only the scalar field is radiative off the pole.

Figure 3. Phases and scaled amplitudes of the $l=2$ spin zero, one, and two gravitational-wave tidal forces. The component depicted is that measured at the equator of an axisymmetric source along a direction perpendicular to the radius vector and the axis of symmetry (case 2 of §3.7; orientation parameter $\gamma=1$). The normalization of the phase and amplitude is discussed in the caption to Figure 1. In the wave zone ($\omega r \gtrsim 7$ the tidal force of the spin-zero and spin-two fields are radiative, but the tidal force of the spin-one field is not. In the transition zone ($1 \lesssim \omega r \lesssim 7$) measurements of the phase and amplitude of the gravitational tidal force can be used to distinguish between the spin zero, one, and two fields.

Figure 4. Phases and scaled amplitudes of the $l=2$ spin-zero, one, and two gravitational-wave tidal forces. The component depicted is that measured at the equator of an axisymmetric source along the direction

parallel to the axis of symmetry (case 3 of §3.7; orientation parameter $\gamma=-2$). The normalization of the phase and amplitude is discussed in the caption to Figure 1. In the wave zone the tidal force of the spin-zero and spin-two fields are radiative, but the tidal force of the spin-one field is not. In the transition zone the phases and amplitudes distinguish between the tidal forces of the different fields. The emergence of the spin-two phase shifts (polarization) can be seen by comparing the spin-two curves of Figures 3 and 4: in the transition zone, the phases evolve so that in the wave zone the phases of these two components of the tidal force differ by π radians.

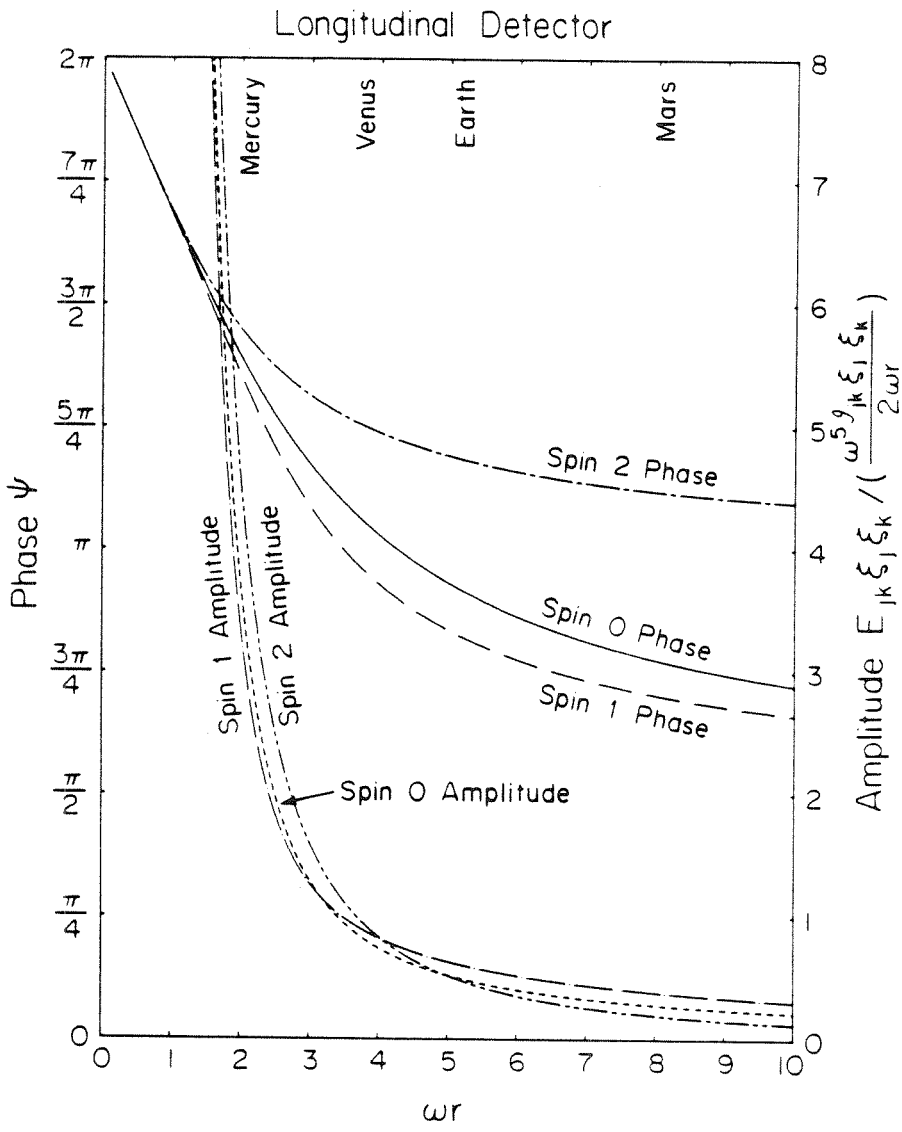
Longitudinal Detector
Mercury
Venus
Earth
Mars
Spin 2 Phase
Spin 0 Phase
Spin 1 Phase
Spin 1 Amplitude
Spin 2 Amplitude
Spin 0 Amplitude
Phase ψ
Amplitude $E_{jk}\xi_j\xi_k / (\frac{\omega^5 g_{jk}\xi_j\xi_k}{2\omega r})$
ωr
0
π/4
π/2
3π/4
π
5π/4
3π/2
7π/4
2π
0 1 2 3 4 5 6 7 8 9 10
0 1 2 3 4 5 6 7 8

Figure 1

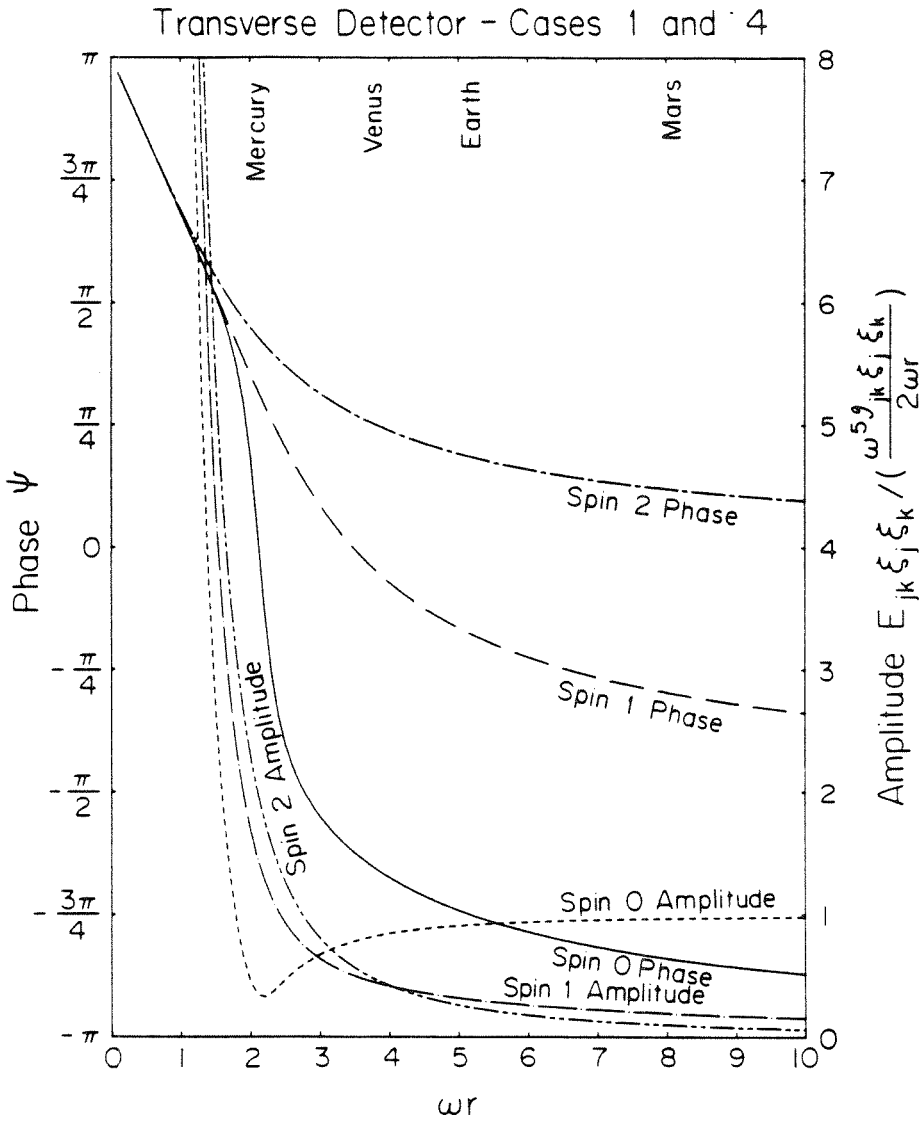
Transverse Detector - Cases 1 and 4
Mercury
Venus
Earth
Mars
Spin 2 Phase
Spin 1 Phase
Spin 2 Amplitude
Spin 0 Amplitude
Spin 0 Phase
Spin 1 Amplitude
Phase ψ
Amplitude $E_{jk}\xi_j\xi_k / (\frac{\omega^5 g_{jk}\xi_j\xi_k}{2\omega r})$
ωr
π
3π/4
π/2
π/4
0
-π/4
-π/2
-3π/4
-π
0 1 2 3 4 5 6 7 8 9 10
8 7 6 5 4 3 2 1 0

Figure 2

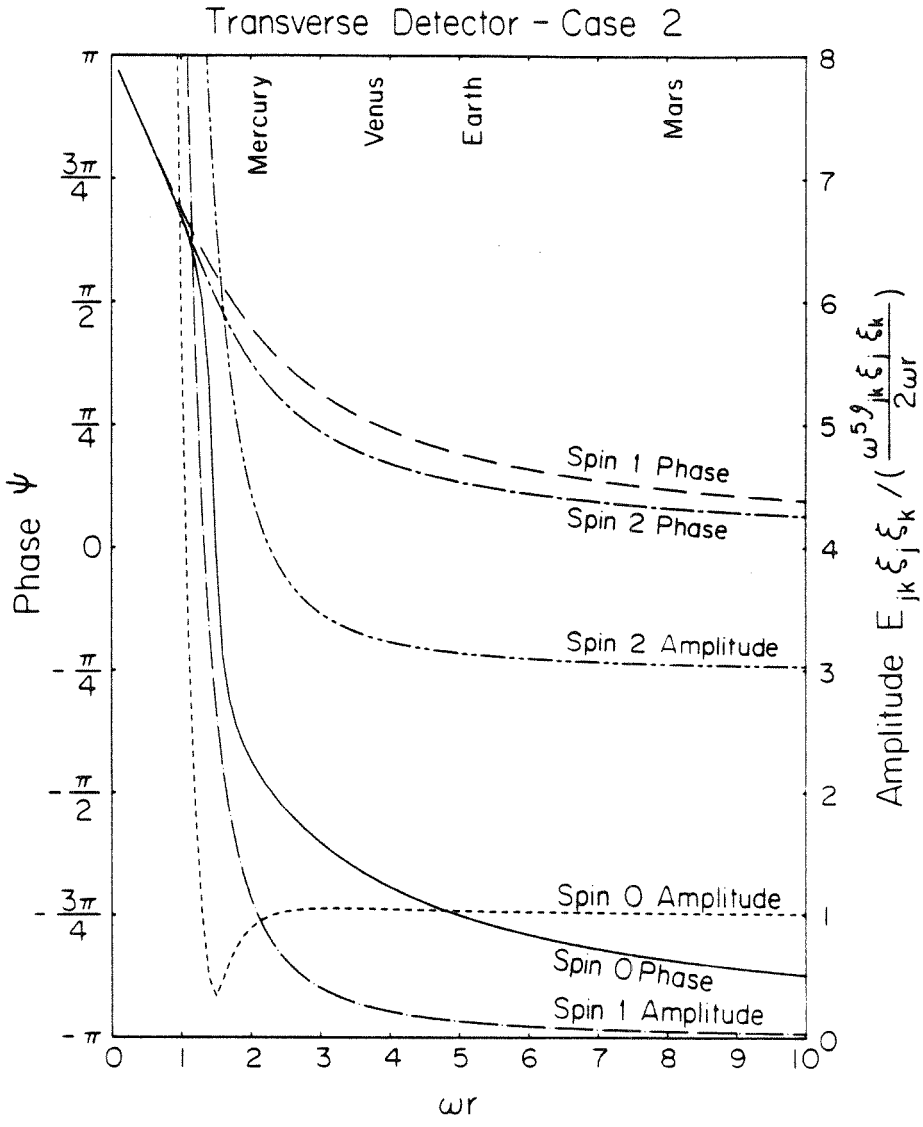
Transverse Detector - Case 2
Mercury
Venus
Earth
Mars
Spin 1 Phase
Spin 2 Phase
Spin 2 Amplitude
Spin 0 Amplitude
Spin 0 Phase
Spin 1 Amplitude
Phase ψ
Amplitude $E_{jk}\xi_j\xi_k / (\frac{\omega^5 g_{jk}\xi_j\xi_k}{2\omega r})$
ωr
π
3π/4
π/2
π/4
0
-π/4
-π/2
-3π/4
-π
0 1 2 3 4 5 6 7 8 9 10
0 1 2 3 4 5 6 7 8

Figure 3

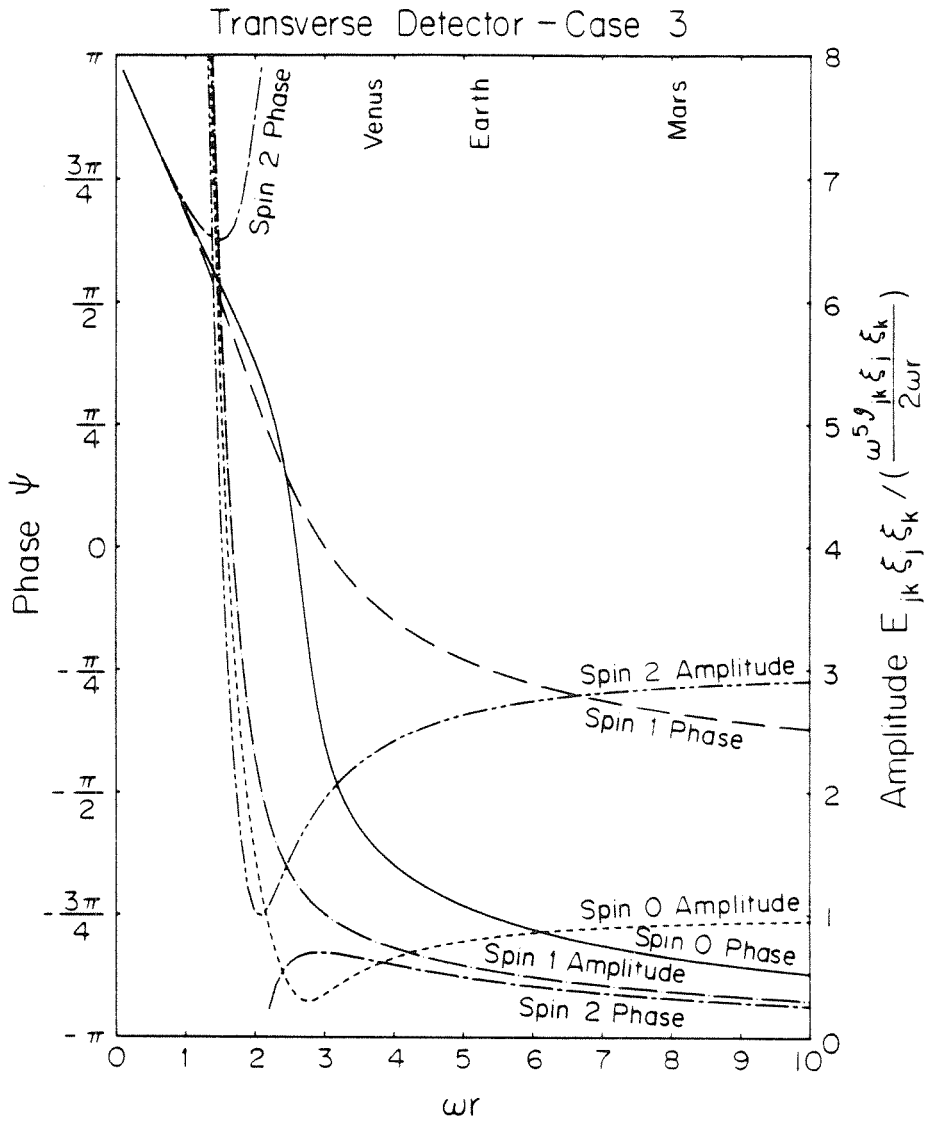
Transverse Detector – Case 3
Phase ψ
Amplitude $E_{jk}\xi_j\xi_k / \left(\frac{\omega^5 g_{jk}\xi_j\xi_k}{2\omega r}\right)$
ωr
Venus
Earth
Mars
Spin 2 Phase
Spin 2 Amplitude
Spin 1 Phase
Spin 0 Amplitude
Spin 0 Phase
Spin 1 Amplitude
Spin 2 Phase
π
3π/4
π/2
π/4
0
-π/4
-π/2
-3π/4
-π
0 1 2 3 4 5 6 7 8 9 10
0 1 2 3 4 5 6 7 8

Figure 4